WIND RESOURCE ASSESSMENT AND WIND FARM MODELING IN COMPLEX TERRAIN: BODRUM PENINSULA CASE STUDY USING COMPUTATIONAL FLUID DYNAMICS

A THESIS SUBMITTED TO
THE GRADUATE SCHOOL OF NATURAL AND APPLIED SCIENCES
OF
MIDDLE EAST TECHNICAL UNIVERSITY

BY

SEMİH ÖZDEDE

IN PARTIAL FULFILLMENT OF THE REQUIREMENTS
FOR
THE DEGREE OF MASTER OF SCIENCE
IN
AEROSPACE ENGINEERING

SEPTEMBER 2013

Approval of the thesis:

WIND RESOURCE ASSESSMENT AND WIND FARM MODELING IN COMPLEX TERRAIN: BODRUM PENINSULA CASE STUDY USING COMPUTATIONAL FLUID DYNAMICS

submitted by **SEMİH ÖZDEDE** in partial fulfillment of the requirements for the degree of **Master of Science in Aerospace Engineering Department, Middle East Technical University** by,

Prof. Dr. Canan Özgen
Dean, Graduate School of **Natural and Applied Sciences** _____

Prof. Dr. Ozan Tekinalp
Head of Department, **Aerospace Engineering** _____

Assoc. Prof. Dr. Dilek Funda Kurtuluş
Supervisor, **Aerospace Engineering Dept., METU** _____

Examining Committee Members:

Prof. Dr. İbrahim Sinan Akmandor
Aerospace Engineering, METU _____

Assoc. Prof. Dr. Dilek Funda Kurtuluş
Aerospace Engineering, METU _____

Assoc. Prof. Dr. Oğuz Uzol
Aerospace Engineering, METU _____

Prof. Dr. Altan Kayran
Aerospace Engineering, METU _____

Erman Terciyanlı, M.Sc.
Project Manager, TÜBİTAK MAM _____

Date: 04.09.2013

I hereby declare that all information in this document has been obtained and presented in accordance with academic rules and ethical conduct. I also declare that, as required by these rules and conduct, I have fully cited and referenced all material and results that are not original to this work.

Name, Last Name: **SEMİH ÖZDEDE**

Signature :

ABSTRACT

WIND RESOURCE ASSESSMENT AND WIND FARM MODELING
IN COMPLEX TERRAIN: BODRUM PENINSULA CASE STUDY
USING COMPUTATIONAL FLUID DYNAMICS

Özdede, Semih
M.S., Department of Aerospace Engineering
Supervisor : Assoc. Prof. Dr. Dilek Funda Kurtuluş

September 2013, 132 pages

Wind Resource Assessment studies have become remarkable research tool to determine the possible Wind Farm locations in last two decades. Wind Farm Modeling is essential to pinpoint the wind turbines in selected region by simulating the possible layout designs of Wind Farm in advance. These studies provide improvements in cost efficiency and Annual Energy Production with the aid of Computational Fluid Dynamics (CFD). In this study, the methodologies of Wind Resource Assessment and Wind Farm Modeling are examined with a case study. The methodologies are applied to Bodrum Peninsula which is defined as a complex terrain. This topography is composed of urban, suburban, hills, different shape of islands and coastal areas. Besides these, it has various roughness classes and very high energy potential according to previous researches. WindSim program which is one of the developed research tools for this topic is utilized to perform all the necessary steps. Embedded CFD program in WindSim computes Reynolds Averaged Navier Stokes equations by using finite volume methods. Sector-wise steady state simulations are performed to predict the flow over the terrain. Annual Energy Production and wake losses are investigated for Onshore and Offshore Wind Farms. Parametric study is conducted for the variations of crosswind and downwind spacing between the wind turbines in the wind farm layouts. In parallel, AEROWIND, in-house code, is developed to perform data analysis of site information, aerodynamics of wind turbine, energy and economy analysis. This theoretical research program reduces the wind farm layout design time.

Keywords: Wind Energy, Wind Farm, Computational Fluid Dynamics, Jensen Wake Model, AEROWIND.

ÖZ

KOMPLEKS ARAZİDE RÜZGÂR KAYNAKLARININ ARAŞTIRILMASI VE RÜZGÂR TARLASININ MODELLENMESİ: HESAPLAMALI AKIŞKANLAR DİNAMİĞİ KULLANARAK BODRUM YARIMADASI ÖRNEK ÇALIŞMASI

Özdede, Semih
Yüksek Lisans, Havacılık ve Uzay Mühendisliği Bölümü
Tez Yöneticisi : Doç. Dr. Dilek Funda Kurtuluş

Eylül 2013, 132 sayfa

Rüzgâr Kaynakları Değerlendirilmesi çalışmaları, rüzgâr tarlalarının muhtemel yerlerinin belirlenmesinde geçtiğimiz yirmi yıldır kayda değer bir araştırma aracı olmuştur. Rüzgâr Tarlası Modellemesi, muhtemel rüzgâr tarlası plan tasarımlarını önceden simüle ederek rüzgâr türbinlerinin seçilen alanda tam yerlerinin belirlenmesinde gereklidir. Bu çalışmalar, Hesaplamalı Akışkanlar Dinamiği (HAD) yardımıyla maliyet verimliliğinde ve Yıllık Enerji Üretiminde gelişimler sağlamaktadır. Bu çalışmada, Rüzgâr Kaynakları Değerlendirilmesi ve Rüzgâr Tarlası Modellemesi yöntemleri örnek bir çalışma ile incelenmektedir. Kompleks bir arazi olarak tanımlanan Bodrum Yarımadasına bu yöntemler uygulanmaktadır. Bu topografyayı; şehir içi, şehrin çevresindeki yerleşimler, dağlar, farklı boyutlardaki adalar ve kıyı kesimleri oluşturmaktadır. Bunların yanında, daha önceki çalışmalara göre çeşitli pürüzlülük sınıflarına ve çok yüksek enerji potansiyeline sahiptir. Bu konu için geliştirilmiş araştırma araçlarından bir olan WindSim programı, gerekli tüm aşamaları yürütmesi için kullanılmaktadır. WindSim içine gömülmüş HAD programı RANS denklemlerini sonlu hacimler yöntemi kullanarak hesaplamaktadır. Arazi üzerindeki akışı tahmin edebilmek için sektör bazında ve durağan simülasyonlar yürütülmüştür. Kara ve Deniz Üstü Rüzgâr Tarlaları için Yıllık Enerji Üretimi ve iz kayıpları araştırılmıştır. Rüzgâr tarlası düzenlerinde, rüzgâr türbinlerinin arasındaki hem rüzgâra karşı hem de rüzgâr yönündeki uzaklıkların değişimleri için parametrik çalışma yürütülmüştür. Paralel olarak; arazi bilgisinin veri analizi, rüzgâr türbini aerodinamiği, enerji ve ekonomi analizi hesaplamak için AEROWIND, kurum içi kodu, geliştirilmiştir. Bu teorik araştırma programı rüzgâr tarlası düzenin tasarım zamanını azaltmaktadır.

Anahtar Kelimeler: Rüzgâr Enerjisi, Rüzgâr Tarlası, Hesaplamalı Akışkanlar Dinamiği, Jensen İz Modeli, AEROWIND.

To my family…

ACKNOWLEDGMENTS

I would like to express my profound gratitude and deep regards to my supervisor Assoc.Prof.Dr. Dilek Funda Kurtuluş for her patience, exemplary guidance and constant encouragement throughout this thesis. I would like to thank her valuable and constructive suggestions during the planning and development of this thesis. I have been amazingly fortunate to have an advisor who gave me the freedom to explore on my own and at the same time the guidance to recover when my steps faltered. I owe a very important debt to her.

I also would like to mention my sincere thanks to all my friends for their friendship and understandings during this process. My thanks and appreciations go to Ceren Büyük, Bora Atak, İzzet Seferbeyoğlu, Murat Aliravcı, Halil İbrahim Aktay, Cengiz Özdemir, Mete Çoşkun, Leyla Çelebioğlu, Erdal Bozkurt and Emre Sazak.

I owe my profound gratitude to Dr. Ali Ruhşen Çete for the encouragement to enroll this program. I am indebted to Erman Terciyanlı for his very valuable comments and guidance about technical issues. I also want to thank to Asst. Prof. Dr. Bedri Kurtuluş for providing the necessary data about Bodrum Peninsula. Besides, I am grateful to Gökhan Ahmet for his technical advices in the early stage of thesis.

I would like to thank to METU WIND organization for providing WindSim program package which is needed for this type of research.

Lastly, my deepest appreciation goes to my family for their moral support and unceasing encouragement in every stage of this process. Without their thrust and understanding this thesis would not have been possible.

TABLE OF CONTENTS

LIST OF TABLES

TABLES

LIST OF FIGURES

FIGURES

LIST OF SYMBOLS

LATIN SYMBOLS

A	Rotor area
A_{shadow}	Shadowed rotor area due to wake expansion
AR	Aspect Ratio
a	Axial induction factor
a'	Tangential induction factor
B	Number of blades
B_A	Benefit costs
C_A	Total cost of the project
C_d	Two dimensional drag coefficient
C_F	Capacity factor
C_I	Initial investment for a wind project
C_l	Two dimensional lift coefficient
C_{LD}	Design lift drag ratio
C_m	Pitching moment ratio
C_n	Normal dimensionless force element
C_{OM}	Operation and maintenance costs
C_p	Power coefficient
C_T	Thrust coefficient
C_t	Tangential dimensionless force element
$C_{\varepsilon 1}, C_{\varepsilon 2}$	Constants of k-epsilon turbulence model
C_μ	Constant determined from a shear layer in local equilibrium
c	(i) Scale factor
c	(ii)Chord length
D	(i) Diameter of Rotor
D	(ii)Drag Force
d	Distance between two rotors in x direction
E_{IR}	Energy production between cut-in and rated speed
E_{IO}	Energy production between rated and cut-out speed

E_T	Total energy production
e	Escalation rate
e_a	Apparent rate of escalation
F	Total loss factor
F_{hub}	Hub loss factor
F_N	Normal force
F_T	Tangential force
F_{tip}	Tip loss factor
f	Frequency of occurrence
f_{hub}	Hub loss coefficient
f_{tip}	Tip loss coefficient
I	Interest (discount) rate
I_{real}	Real rate of discount
K	Turbulent kinetic energy
KE	Isotropic kinetic energy
k	(i) Shape factor
k	(ii) Wake decay coefficient
L	Lift Force
m	Ratio of operation and maintenance to initial investment cost
$\dot{m}$	Mass flow rate of air
N	Number of variables
$n_{payback}$	Payback time
P	Wind Power
$\overline{P}/A$	Average wind power density
$P_{available}$	Available power in the wind
P_{curve}	Power curve of wind turbine
P_{rated}	Rated power of wind turbine
P_k	Turbulent Production Term
p	Pressure
Q'	Sectional torque
R	Blade radius
R_{Design}	Design blade radius
R_{hub}	Hub radius
Re	Reynolds number

r	Local blade radius
T	(i) Temperature
T	(ii)Thrust force
T'	Sectional thrust force
TI	Turbulent intensity
$Time$	Operation time
U	(i) Characteristic velocity
U	(ii)Velocity component in x direction
$\overline{U}$	Long term average wind speed
U_{cut-in}	Cut-in wind speed
$U_{cut-out}$	Cut-out wind speed
U_{hub}	Wind speed at hub height
$U_{reference}$	Wind speed at reference height
U_{rel}	Relative wind speed
U_T	Wind speed behind the rotor
U_{tip}	Wind speed at the tip of the blade
$\overline{u_i u_j}$	Reynolds stresses
V	Velocity component in y direction
W	Velocity component in z direction
x	X - distance (linear) in Cartesian coordinates
y	Y - distance (linear) in Cartesian coordinates
z	(i) Height above from ground
z	(ii) Z - distance (linear) in Cartesian coordinates
z_{hub}	Hub height above from ground
$z_{reference}$	Reference height
z_o	Surface roughness

GREEK SYMBOLS

α	(i) Power law exponent
α	(ii) Angle of attack
α_{Design}	Design angle of attack
α_{stall}	Stall angle of airfoil
Δa	Difference between new and old axial induction factor
$\Delta a'$	Difference between new and old tangential induction factor
δU	Velocity deficit
ε	Turbulent dissipation rate
$\eta_{aerodynamic}$	Aerodynamic efficiency
$\eta_{gearbox}$	Gearbox efficiency
$\eta_{generator}$	Generator efficiency
η_{other}	Efficiency of other factors
η_{total}	Total efficiency
θ_p	Section pitch angle
$\theta_{p,0}$	Blade pitch angle
θ_T	Section twist angle
κ	Von Karman constant
λ	Tip speed ratio
λ_{Design}	Design tip speed ratio
λ_r	Local tip speed ratio
μ	Dynamic viscosity
ν	Kinematic viscosity
ν_T	Turbulent viscosity
ρ	Air density
σ'	Local solidity
σ_K	Diffusion constant
σ_U	Standard deviation of individual wind speed averages
σ_ε	Diffusion constant
τ	Shear stress
φ	Angle of relative wind
ω	Induced tangential angular speed
Ω	Angular speed of blades

SUBSCRIPTS

i, j, k	Indices
max	Maximum value
mean	Mean value
new	New value of variable
old	Old value of variable
w	Wall
τ	Friction
∞	Free-stream conditions

LIST OF ABBREVIATIONS

ABBREVIATIONS

ABL	Atmospheric Boundary Layer
AEP	Annual Energy Production
AOA	Angle of Attack
BCR	Benefit cost ratio
BEMT	Blade Element Momentum Theory
CFD	Computational Fluid Dynamics
CLC	CORINE Land Cover
COE	Cost of Generated Electricity
CORINE	Coordination of Information on the Environment
CWE	Computational Wind Engineering
DTM	Digital Terrain Model
HAWT	Horizontal Axis Wind Turbine
HGK	General Command of Mapping
IEC	International Electrotechnical Commission
IR	Inflation Rate
IRR	Internal Rate of Return
LS	Linear Superposition
MEASNET	International Network For Harmonized and Recognized Measurements in Wind Energy
NPV	Net Present Value
NREL	National Renewable Energy Laboratory (USA)
RANS	Reynolds Averaged Navier Stokes
REPA	Wind Energy Potential Map of Turkey Project
RNG	Re-Normalization Group
RPM	Rotations Per Minute
RSS	Root Square of Sum of Square
WAsP	Wind Atlas Analysis and Application Program
WRA	Wind Resource Assessment
WS	WindSim
YEGM	General Directorate of Renewable Energy

CHAPTER 1

INTRODUCTION

The population of the world increases over years inevitably. Therefore, energy demand mounts up simultaneously. However, world has limited energy resources. The consumption is high and it will be higher upcoming decades. The investigation of new energy sources has been popular topic in last decades. The reason is that fossil fuel reserves of earth are not infinite and they have adverse effects on environmental life. Polluting air, water and soil are the consequences of using fossil fuels. One of the releasing gases is carbon-dioxide which is categorized in greenhouse gases advances radiation forcing and causes to global warming and increases in average surface temperature on Earth. The vast majority of scientists all agreed that it gives the major adverse effects. Renewable energy sources are the remedy to overcome these issues, because it has minor effects on environment. Renewable energy is generated from resources which are present in nature such as wind, sunlight, rain, waves, tides, geothermal and biomass [1].

Wind energy and wind turbine technology has developed rapidly among these energy resources since 1950s. Wind energy is clean, plentiful, widely distributed. Its huge potential spreads all over the world. Harnessing of the wind energy has become an important topic for engineers. Thus, interest in this field grows up. Lots of articles and academic dissertations were published about wind energy in the last decade [2].

1.1. History of Modern Wind Turbines

Firstly, converting the wind power into mechanical energy is applied by windmills. With the passing years, it is undisputable that generating electrical power has become the priority of all nations due to energy demand. Therefore, the purpose of wind driven machines changed and they has evolved to wind turbine technology gradually. Wind turbines which are multi-disciplinary machines first convert the kinetic energy of the wind into mechanical energy by aerodynamically designed blades. Afterwards, shafts and gearbox transmit the mechanical energy to generators. Consequently, mechanical energy is transformed to electric energy by generator. The efficiency of this machine is limited due to physical laws. This physical law explanation is proved by the Betz Limit Theory. However, today’s engineers continue to study on innovations and expense breakdown in every stage of this sophisticated machine [3].

Mobility of rotating object that was invented with the discovery of wheel in 3000 B.C. by Sumerians found an application area in wind turbines later on. First known windmill is used by Hero of Alexandria. It was estimated that Hero lived in first century of B.C. or A.D. In his work, Pneumatics is the equipment that supplies air to an organ by using a windmill ([1], [4]). On future dates, Persians were utilized for mechanical purposes in ninth century A.D. This windmill type is oriented vertically which is categorized in drag-based devices. This type of windmill was inherently inefficient and vulnerable to damages from severe wind conditions. The main purpose of this device was to grind grain simply [3]. It was predicted that the horizontal axis windmills were first invented in Europe. In the year of 1180 the origins of horizontal axis windmills was appeared in the Duchy of Normandy. In Holland, many development was made in windmills and it became a new type of device which was known as Dutch-windmill around 16^{th} century. During Middle Ages, these windmills were improved and they were utilized for mechanical works such as water pumping, sawing wood, grinding grain and other powering devices [5].

In nineteenth century, almost 2500 wind turbines were utilized such as to pump water for irrigation or to grind grain in Denmark. Foremost, the windmills were evolved to wind turbines in the United States by Charles Brush in 1888 when the rotor system was linked to an electric generator. This idea has brought about the usage of small electrical generators and Marcellus Jacobs worked on the small turbine designs. The most impressive thing about these small wind turbines is that they had three blades with airfoil shapes. They really look alike today's turbines. He also achieved battery storage and this turbine can be considered as the forerunner of modern small wind turbines. In Figure 1.1, Jacobs's turbine can be observed [5]. In 1930s, modern Danish wind turbines were erected from the developers. During those dates, the largest wind turbine ever was developed in the United States. It was two-bladed with a diameter of 53.3 m and output power of 1.25 MW. However, there was no enough knowledge to perform this machine healthy and properly. This turbine can be qualified as the predecessor for the wind turbines which were built by United States Department of Energy in the 1970s [5].

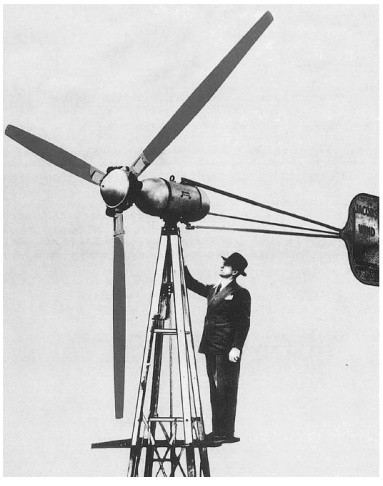

Figure 1.1: Jacobs Turbine in 1961 [5]

After 1970s, innovations in the wind turbine energy and technology have advanced rapidly. Grants of government have increased for the researches of this field due to booming in petroleum prices since 1970. Research and Development studies in Europe changed the view from the intended use of wind turbines to generate high amount of electric energy. With the years passing and with the advances in technology more aerodynamic and economic turbines have manufactured. The size of the Horizontal Axis Wind Turbine (HAWT) ranged from 25kW to 6MW over years as illustrated in Figure 1.2 [1]. Comparison was made with Washington Monument which is located in Washington DC. The largest commercial wind turbine which was designed by wind turbine manufacturer Enercon was erected in Emden Germany in 2007. This turbine has a hub height of 135 m and rotor diameter of 126 m. Firstly, it was designed to generate 6MW, but after technical modifications its capacity was scaled up to 7.58MW per turbine in 2009. Besides, many companies are working on a design of 10MW wind turbine [1].

This clean energy source contributes to the decrease of carbon dioxide emission with countries awareness. Design standards and certification procedures have been declared, thus the reliability and performance of the wind turbines have developed year by year. Wind turbine designers and manufacturers agreed with International Standards IEC 61400-series. The cost of energy per kW for wind turbine has dropped to reasonable numbers in order to compete with other conventional sources without incentives. Many countries which give various incentives are ambitious to grow the rate of wind energy in their lands rapidly.

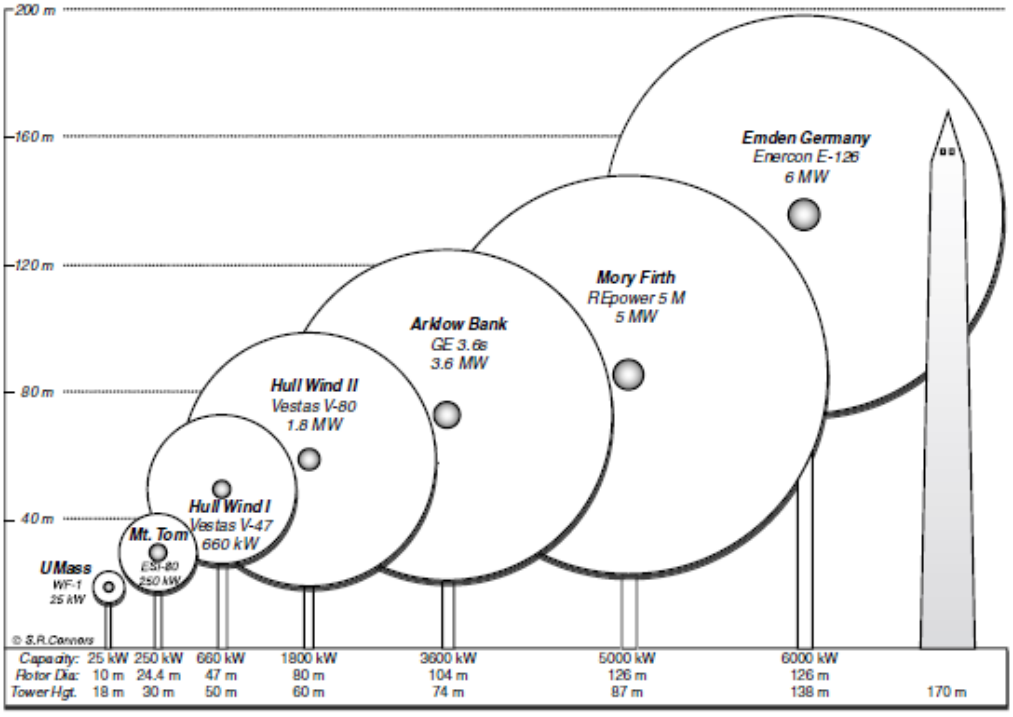

Figure 1.2: Representative Size, Height, and Diameter of Wind Turbines [1]

It should be emphasized that the wind power is related to some important parameters in scientific evaluation. As the Englishman John Smeaton contributed this evaluation with windmill testing apparatus by obtaining the basic variables in 1759 [5]. After years, other scientists used these inferences and innovations in this field. Eventually, they put the essential variables into equation. This equation is stated below.

$$P = \frac{1}{2}\rho A U_{\infty}^{3} C_{p} \tag{1.1}$$

The rules of this equation indicate that, the variables are density of air (ρ), rotor swept area (A), free stream wind speed (U) and power coefficient (Cp). The main important variable is the speed of wind cubed undoubtedly.

Wind Turbines are categorized by many types but they are distinguished from each other generally by axis orientation. The orientations are horizontal axis and vertical axis. Vertical Axis Wind Turbines are not efficient inherently and while vertical ones get larger, they are not feasible anymore. On the other hand, Horizontal Axis Wind Turbines are feasible and efficient ones. Therefore, the vast majority of installed wind turbines in the world are Modern Multi Mega Watt Horizontal Axis types. In Figure 1.3, Siemens Bonus Wind Turbine is illustrated. In recent years, new design which is called Offshore Wind Turbine has developed to get high electricity production more efficiently. This type is installed on offshore places where the sea depth is reasonable. However, it is relatively expensive [1].

Figure 1.3: Multi Mega Watt HAWT (Rotor Diameter: 107m and Rated Power 3.6MW) [3]

State of the art in wind turbine design has evolved in last 40 years. Wind Turbines have become more reliable, more cost effective and quitter. In order to reduce the cost of energy the innovations still continues especially in lower wind speeds. Intermittency, transmission and storage technologies will be developed to increase the wind energy probably. For offshore turbines, it is predicted that there will be many opportunities in this field on future dates ([1], [5]).

A Wind Farm which consists of wind turbines in the same region have covered hundreds of square kilometers. They can be located onshore or offshore places. The biggest onshore Wind Farms were established in United States and China. The Gansu Wind Farm in China has 5.16 GW installed power and the goal of this project is to reach 20 GW installed capacity by 2020. The Alta Wind Energy Center, United States has approximately 400 Horizontal Axis Wind Turbines in Kern County, California. Most of these turbines have rated power of 3 MW. Total installed capacity of this wind farm is 1.32 GW. The biggest offshore Wind Farms were located in UK. These are London Array (630 MW) and Greater Gabbard Wind Farm (504 MW). Moreover, many others are under construction all over the world [6]. Onshore and Offshore Wind Farms are illustrated in Figure 1.4 and 1.5, respectively.

Figure 1.4: Onshore Wind Farm, Bozcaada, Turkey [7]

Figure 1.5: Offshore Wind Farm in Baltic Sea of Copenhagen, Denmark [7]

1.2. Wind Energy in the World

While the technology of wind turbines has improved over years, the output power increases considerably. Besides, wind farms get popular with the passing years. Therefore, the total installed capacity in the world increased by 44.8 GW in 2012. Eventually, the capacity attained to 282.6 GW which corresponds to 18.7 % increase according to previous year. Apart from Europe North America and China has shown impressive improvement since 2006. China has increased the total installed capacity from 25.8 GW to 75.3 GW during 2009-2012 period. Besides, many countries have installed a considerable amount of installed power during 2011-2012 period such as USA, India, Germany, Spain, UK, Italy and Brazil. Nowadays, many countries have also started to generate electricity from wind turbines in their lands [7]. Total installed capacity in the world was shown in Figure 1.6. In Table 1.1, the total installed capacity for top eight countries and Turkey were presented.

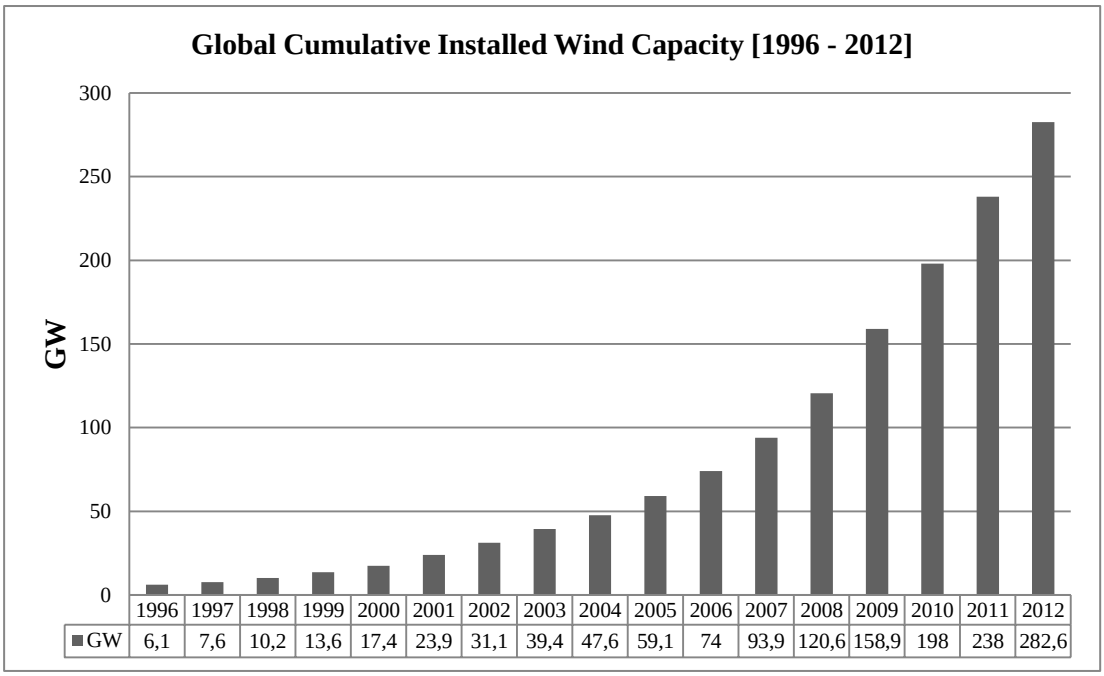

	1996	1997	1998	1999	2000	2001	2002	2003	2004	2005	2006	2007	2008	2009	2010	2011	2012
GW	6,1	7,6	10,2	13,6	17,4	23,9	31,1	39,4	47,6	59,1	74	93,9	120,6	158,9	198	238	282,6

Figure 1.6: Total Installed Capacity in the World (Replotted based on data in Ref. [7])

Table 1.1: Total Installed Capacity for Countries (Re-tabulated based on data in Ref. [7])

	Country	Total Capacity in MW (end of 2012)
1	China	75324
2	United States	60007
3	Germany	31308
4	Spain	22796
5	India	18421
6	United Kingdom	8445
7	Italy	8144
8	France	7564
18	**Turkey**	**2312**
Total		**282587**

1.3. Wind Energy in Turkey

The history of the usage of wind turbine in Turkey has started since 2000. Installed power was 50MW in 2006. The wind resource assessment was investigated by Wind Energy Potential Map of Turkey Project (REPA) in 2007. It was attained to 2312MW in 2012 with the guide of experts and incentives of the government. Generally, most of them are located in Marmara and Aegean regions. There are 157 licensed wind farms in Turkey at the end of 2011 [8]. The total installed capacity of Turkey is shown in Figure 1.7.

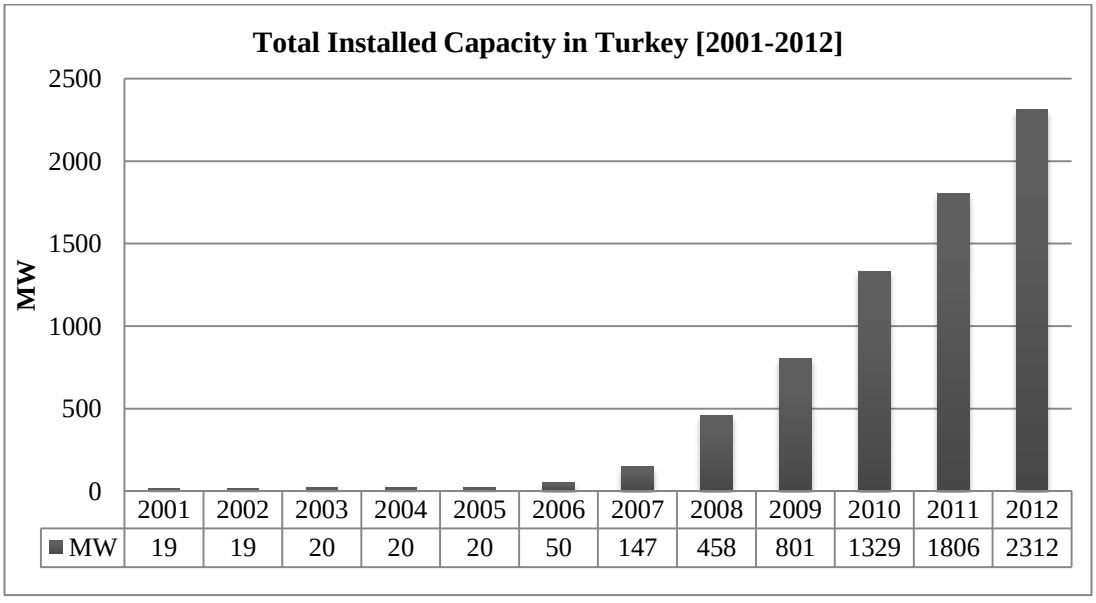

Figure 1.7: Total Installed Capacity in Turkey (Replotted based on data in Ref. [8])

The recent published laws and the regulations give the investors confident to install wind turbines and wind farms in Turkey. The objective of the government in wind power source is determined to attain 20GW installed power next 10 years in Turkey. Another motivation for the renewable energy systems like wind power should be considered as the strict global standpoint for less carbon emissions and clean futures.

1.4. Brief Information of Bodrum Peninsula

In ancient times, Bodrum was called as Halicarnassus of Caria. Bodrum Peninsula where is chosen as case study for this investigation is located in Aegean region of Turkey. This region has huge wind energy potential according to previous researches. The reason of choosing the Bodrum Peninsula for this research is that it can be defined as complex terrain. Besides, it has various roughness lengths. Therefore, it is suitable to investigate with non-linearized approaches. In this study, computational area has 26.5x26.5 km projection and different altitudes in regional. This topography is composed of urban, suburban, hills, different shape of islands and coastal areas. Geographical location of Bodrum Peninsula in Turkey can be observed in Figure 1.8. The wind potential in this region should be researched to determine wind farm location in advance.

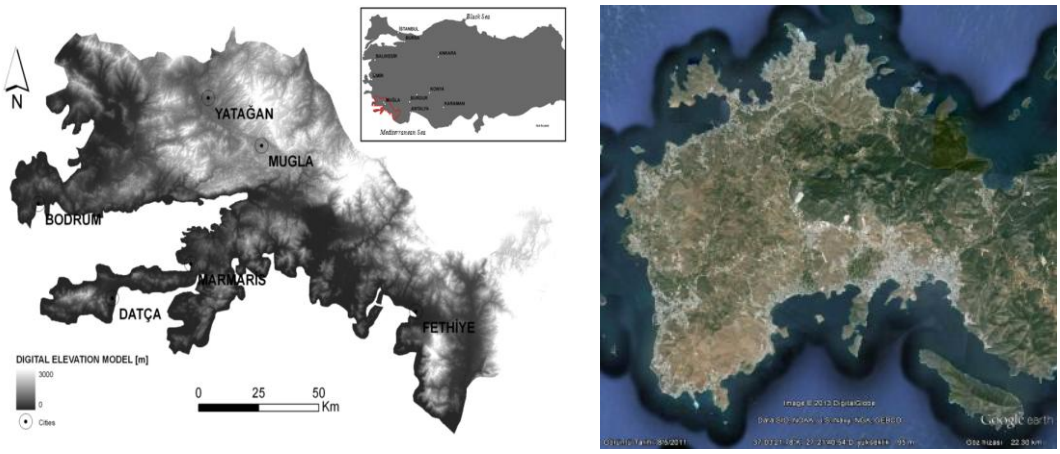

Figure 1.8: Geographical Location (left) and Map (right) of Bodrum Peninsula

1.5. Objective and Scope of the Study

In this research, the main objective is to examine the methodologies of Wind Resource Assessment and Wind Farm Modeling. Computational Fluid Dynamics has been widely used tool to investigate this type of researches in recent years. Therefore, WindSim program, which is one of the research tools for complex terrain analysis in wind engineering, is performed in the current thesis to perform CFD analyses, Wind Resource Assessment and Wind Farm Modeling. Moreover, parametric study is conducted for the wind farm layout designs considering wake interactions. High AEP, minimum wake interactions and minimum land cover are investigated to determine the optimal wind farm layout at the end of the parametric study.

In parallel, AEROWIND in-house code is developed to compute many important parameters of wind farm by using theoretical approaches. The main objectives are to make the initial calculations and to reduce the wind farm layout design time. This program can be coupled with research tools (WindSim, WAsP, WindPRO, Meteodyn WT, openWind, WindFarmer and etc.) or can be performed alone. It consists of four tabs which are site information, aerodynamics, energy and economy. It is written in MATLAB numerical computing environment. Many validation cases are conducted to test the functionality of the code.

Moreover, the case study is carried out in Bodrum Peninsula which has various roughness classes over the terrain. This region can be defined as complex terrain because of a great variety of topographical shapes. At the end of the study, different layouts of Offshore and Onshore Wind Farms are investigated in WindSim.

The thesis is divided into six chapters to cover the objectives sufficiently.

In Chapter 1, some background information about modern wind turbines are given. The progress of wind power in the world and Turkey is clarified with the numerical representation. Furthermore, the brief information about Bodrum Peninsula is presented. Lastly, the objective and scope of the work are mentioned.

In Chapter 2, many previous works about WRA and Wind Farm Modeling are reviewed extensively. The history of the usage of CFD is also given for these research areas. Many dissertations about WindSim are explained elaborately.

In Chapter 3, method of Wind Resource Assessment is explained. The preparation of grids, numerical model, CFD methodology of the program, roughness map arrangement and boundary conditions are disclosed. Moreover, wind data analysis is conducted to arrange necessary information for analyses.

In Chapter 4, theoretical background of AEROWIND in-house code is explained. The necessary algorithm is also given for BEMT, Jensen wake model and present worth approach.

In Chapter 5, the CFD simulations are carried out and original mesh is determined according to grid dependency study. Computation times of different cases are compared. The effect of turbulence models is investigated. Furthermore, wind resource map is obtained at selected altitudes above from the terrain. Wind farm sites are determined according to objectives of thesis. In the second part of the chapter, economic analysis is conducted to examine the important economic parameters. After that, validation cases are investigated with AEROWIND code. Lastly, different wind farm layouts are examined in order to obtain AEP and wake losses in WindSim program.

In Chapter 6, the general conclusions of the study and future work are declared.

CHAPTER 2

LITERATURE REVIEW

This chapter is devoted to the literature survey of Wind Resource Assessment (WRA) and Wind Farm Modeling. In the first section of this chapter, background information about WRA is addressed broadly. Furthermore, the progress in this field is presented. Previous studies about WRA are numerous and they were conducted with different approaches in particular locations all over the world. Numerical and experimental approaches are commonly performed to research the wind resource assessment. In the second section, Wind Farm modeling including micro siting and wake modeling are pointed out in detail. The studies of this field are essential to review in order to understand the usage of the current methods. Thus, relevant studies in WindSim program are given to exemplify this approach.

2.1. Wind Resource Assessment (WRA)

Wind is mainly caused by the differences in atmospheric pressure. Thermal and density differences in various regions can be occurred because of the solar radiation. The equator absorbed solar radiation more than the poles. The spatial temperature variation causes convective air motion in the lower stratifications of the atmosphere which is called as troposphere. The heat transfer mechanism forces the air to move from high pressure to low pressure. Other effects can be added as follows:

a. Earth's rotation (Air is deflected by Coriolis Effect)
b. Surface Friction
c. Seasonal Variations
d. Gravity
e. Inertia of air
f. Obstacles, Roughness and Orography

These effects result in various speeds of wind [1]. The rotation of earth influences the circulation of the atmosphere greatly. The pressure gradient force in vertical direction is balanced by gravitational forces. This concludes that wind can be assumed as the result of the horizontal pressure gradients. In addition to these, gravitational forces, inertia of air, friction and terrain properties determine the distribution of the wind direction all over the world [9].

The Coriolis Effect causes a deflection on moving objects when they are observed from a rotation reference frame. The rotation reference frame is Earth in this study. It influences the air to move towards the poles by deflecting to the east direction, and at the same time the air moves towards the equator by deflecting to the west direction. The wind never reaches the low pressure region but it makes circulation around this region with constant pressure. This force is the consequence of the rotation of the earth, inertial forces due to large scale circular motion and the frictional forces due to terrain [10].

Spera [11] noted that atmospheric movement can change in both time and space. The extents of the some events including wind turbine design and wind farm site selection can be observed in Figure 2.1. The variations of wind speed in time can be specified in four categorized. These are inter-annual, annual, diurnal and short term variations in speed. Inter annual variation is based on long-term data. Meteorologists take 30 years data into account to obtain reliable inspection about climate or weather assessment. Annual variation is related to seasonal and monthly averaged wind speeds. It is important to determine site selection due to the seasonal variations. Diurnal variation indicates recordings of the time of day due to daily radiation cycle. Short term recordings can show the turbulence and gusts. Generally this period is 10 minutes or less. These variations affect the consideration of the wind turbine design about load and fatigue estimation, control, system operation, and power quality [1].

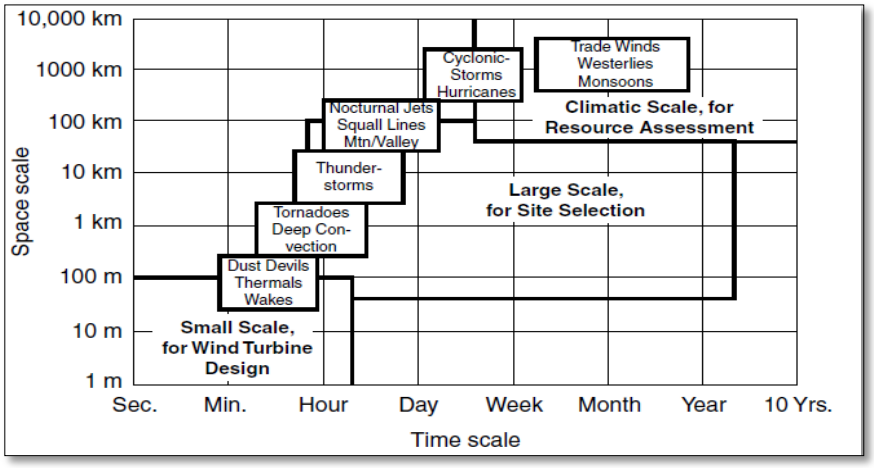

Figure 2.1: Time and Space Scales of Atmospheric Motion [11]

Met stations which are erected for a region close the desired area collect meteorological wind speed data. The sensors have to conform to IAC and IEC standards. Data Logger system sends the whole collected data to main system via GPRS. Furthermore, these devices are calibrated and tested in particular conditions. The instrumentation on the met stations is specially designed to measure many essential parameters for wind energy. These instruments and their measurement purpose are stated below;

- Anemometers for wind speed (turbulence, gusts can be captured)
- Wind Vanes for wind direction
- Thermometers for ambient air temperature
- Barometers for air pressure
- Humidity sensor for atmospheric humidity

Humidity sensor is important measurement component for Wind Resource Assesment studies, especially in humid regions. Water vapour concentration in air is as a function of temperature and pressure. Wet bulb temperature, dewpoint temperature and relative humidity have effects on the accuracy and uncertainty of the humidity sensor. In general, it is coupled with temperature sensor. The instruments should be well operated and maintained. They cooperate with each other in order to compute air density, assessing atmospheric stability and detecting icing conditions.

Ten minutes average wind speed, direction and standard deviation are recorded from the anemometer and wind vane generally. Besides, met stations have many anemometers and other equipments which are located at different heights such as 10, 20, 30, 50, 70, and 100 meters. According to standards, the tallest anemometer should be two thirds of the hub height of the wind turbine. Met stations should be erected close to planned wind turbine locations. They can be distributed inside 2-10 km radius of region ([1], [5], [10]). The wind speed, wind power density, wind roses, Weibull parameters, pressure, temperature, elevation and roughness can be recorded for each system of met station eventually.

Wind Resources Assessment (WRA) can be observed preliminary by wind atlas. The wind atlas has been constituted to determine the wind energy potential of the country, to aid the policy makers for defining the strategy, to guide the potential wind energy investors for finding the most suitable windy regions. The information is based on meteorological station recordings, wind measurements, land topography, field surveys and advanced numerical techniques [5]. Although the wind farms have welcomed in every region of Turkey yet, the amount of these union of utilized wind power stations have increased year by year. WRA investigation is the key factor to harvest the potential wind energy efficiently in realistic predictions in the territories. Commonly, there are three types of WRA regarding to resolution range. First one is macro-scale WRA and it aims to constitute wind atlas including wide areas (50-200km). Second one is meso-scale WRA and it covers the national wind map (5km). Therefore, it is important to review meso-scale studies for pre-feasibility of WRA. Last one is micro scale WRA and it ranges from 10m to 100m [10]. Thus, microscale studies are detailed investigations for site selection. WRA and Wind Farm Modeling can be investigated mainly by three methods;

1. Numerical Weather Research and Forecasting Methods (e.g. MM5)
2. Linearized methods (e.g. WAsP, WindPRO programs)
3. Non-linearized methods (e.g. WindSim, Meteodyn WT programs)

First one is that Numerical Weather Research and Forecasting Methods (WRF) are carried out for meso-scale WRA. This method is based on previous or current weather data to parameterizations for solar radiation, moist processes, heat exchange, soil, vegetation, surface water, and the effects of terrain. This analysis is utilized to constitute wind atlas considering maximum 1 km resolution [12].

The other two methods are for micro-siting investigation. Micro siting is conducted with high resolution flow field analysis. The determination of the best location of each wind turbine for maximum annual power production is investigated by numerical computation including wake models. Maximizing the power helps to reduce the payback time for investors. In present academic studies, CFD models are utilized to determine the exact location of wind turbine by implementing wake models and genetic algorithms [1].

Linear and non-linear code based programs are widely utilized as research tool to obtain power output predictions for wind turbines and wind farms while focusing on huge regions [13]. The linear flow modeling gives accurate results in very smooth lands, because of the fact that it just computes the flow by extrapolating of available wind data for every direction. Therefore, linearized based codes only give necessary information about the global wind atlas. They solve the flow model so fast. However, more complex areas are difficult to solve with linear based programs [14]. For more accurate results non-linear programs are used especially based on Computational Fluid Dynamics (CFD). WindSim software which is utilized CFD methods in this research that it solves Reynolds Averaged Navier Stokes (RANS) equations by using finite volume method. Direct Numerical Simulation (DNS), Large Eddy Simulation (LES), Detached Eddy Simulation (DES) are the other methods to handle Navier Stokes equations. However, these approaches are not implemented into WindSim Program [15].

Apart from WindSim program; WAsP (Wind Atlas Analysis and Application Program), GH WindFarmer, WindPRO and etc. softwares are utilized to predict wind resource assessment studies in offshores and normal lands. These programs are validated with the data of various meteorological stations. For example, the blind comparison of flow models which provides data sets of validation models in selected complex terrain was applied to validate these codes. Askervein Hill [16] and Bolund Experiment ([17], [18]) which are collected real data from met stations are two unique challenging validation cases for the codes. WindSim program is validated by both experiments and the results are satisfied with the recorded data [19].

In Turkey, wind resource assessment studies were not very well known procedure until the wind potential atlas of Turkey which is called REPA have been constituted in order to provide coherent numerical assumptions by the collected data from met stations. However, its principle is based on linear approximations. Mesoscale Numerical Weather Forecast Model is utilized to obtain the information roughly about countries, cities, etc. This model is based on the satellite observations made over the last 20 years. The resolution of this simulation depends on simulation area. It is approximately 2.5 or 5 km for Turkey region.

The nature of turbulent flow which can be defined as phenomenon for engineers is computed by using the turbulent modeling. State-of-art of solving this phenomenon has been researched for years. The latest popular method is Computational Fluid Dynamics and it has been widely applied to solve many fluid dynamics problems since 1960s. However, the scientists should overcome long computational time. The important criterion is to solve the physical event. The methodologies of unsteady and steady computations are different to each other. Mesh refinement study and turbulence mathematical modeling type are essential procedures to achieve the right solution of the problem for both computation types. Moreover, the adaptive meshing techniques or the usage of coarser mesh can be reduced the computation time. The selection of turbulence mathematical modeling should be investigated properly. However, the most applied method is to solve Reynolds Averaged Navier Stokes equations with the standard k-epsilon turbulence model [20].

The important issues before starting analyses are the meshing procedures and turbulence modeling for the preparation of this engineering problem. There are many ways to construct the solution domain. Structured mesh and unstructured mesh are two main options. Unstructured mesh with solution adaptive mesh refinement approach is efficient way to reduce computational time. It allows making finer meshes close to the topography. Besides, the applied turbulence modeling can give different values region to region [21]. The flow field can be defined as complex terrain which can consist of urban, suburban, hills, different shape of islands, coastal areas and so on. All of these terrain features should be considered as roughness effects and their influences can be assigned according to roughness classes. Interactions of wind velocity and various topographic features generate a unique Atmospheric Boundary Layer (ABL) which should be taken into account in wind resource assessment and wind climate problems. The solution of ABL for smooth areas is amenable whereas the urban flows are not consistent and needed the micro scale analyses. Referring from mesoscale analyses, the microscale analyses can be performed with vertical wind profile by logarithmic law or power law [22].

Atmospheric Boundary Layer is a part of troposphere and it is the lowermost of layer. Approximately 75% mass of atmosphere presents in this layer. It has a height of 2 km that depends on time of day, roughness and orography. ABL have been studied for years by scientists. They suggested some attitudes towards the problem in order to solve the Navier Stokes Equations. As flow characteristics vary with time, mechanisms of the whole system have started mixing and interacting each other by given inputs. In background of the flow solver programs, there are several turbulence models such as standard k-ε, standard k-w, Large Eddy Simulations (LES), Reynolds Averaged Navier Stokes (RANS), other commercial CFD codes and special programs for this purpose [15]. Flow over the flat and frictionless wall is assumed in the calculations. Unique velocity profiles are occurred because of various roughness lengths [23]. Flow over a hill causes different characteristics of air motion. The flow encounters with a hill and the natural characteristics are shown in Figure 2.2. These characteristics can be observed in low altitudes and they are flow separation, circulation, wake of windmill, recirculation and so on [14].

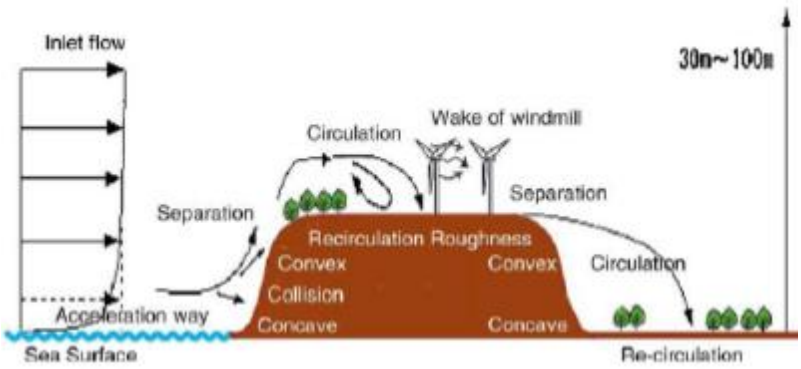

Figure 2.2: Flow Characteristics over a Hill [14]

If wind has turbulence and unsteady regime, wind shear forces will increase on wind turbines. This event decreases efficiency and life time of components of wind turbines. Therefore, vertical wind speed is essential to be predicted. Since vertical velocity profile is homogenous and stable, Monin-Obukhov theory can be used to estimate correctly the velocity profile especially close to coastal areas. However, WRA problems have complex terrain generally ([24], [25]). Complex areas should be examined with CFD analyses in order to capture flow characteristics properly.

Özdede et al. [26] showed that features of the complex terrain cause to form different flow characteristics remarkably. In this respect, WindSim, CFD tool, is utilized to obtain the wind map over Bodrum Peninsula considering the effects of complex terrain. It is also possible to investigate the wind speed distribution at selected altitude from the ground by using the post processing modules of the program. After all, wind maps have different mean wind speeds in regional due to the effects of orography and roughness. It is also stated that this region has huge wind energy potential at the end of the study.

To better focusing on the wind resource assessment and wind climate changes for various applications, previous and current state of art should be researched. The strong way to achieve better predictions, Computational Fluid Dynamics (CFD) is the most popular tool to model the flow problems in recent years. Murakami [20] and Stathopoulos [27] stated in 1997 that Computational Wind Engineering (CWE) definition is used for wind modeling with the aid of CFD. As discussed in the study of Murakami [20], wind engineering applications which are very much dependent to aerodynamics and structural dynamics disciplines have some various concerns such as air pollution for population, wind loads and wind fluctuations on structures (buildings, bridges, and towers), wind comfort close to buildings, wind climate for wind energy. The concentrated topic name is called CWE which has been initiated to research two decades ago. The related atmospheric cases are impingement, separation, reattachment, circulation, vortices and etc. These cause extremely anisotropic turbulent regions in flow field and it is hard to resolve in fluid dynamics.

In the year of 1999, Gosman [28] showed that the developments in CFD field are enriched with modeling of turbulence, heat and mass transfer, mesh generation and parallel computing. Moreover, CFD code developers had many improvements in ease of use and computation speed with new advanced computers. However, CFD codes needed to be better to resolve the physics of wind modeling. However, Gosman noted that RANS model can capture limited knowledge for unsteady flows. LES which is different modeling for turbulence can be the remedy for the limitations and deficiencies of Reynolds averaging. LES can surpass the limitations of RANS by using computational grid spacing and considering the small scale grid effects. LES is expensive than RANS because of the long integration time, computing unsteady motions and temporal resolution.

Kim and Boysan [21] studied the success of the usage of CFD in environmental flows in 1999. Particularly, the environmental flows can be related to urban climatology. Solution-adaptive unstructured mesh refinement was utilized to obtain the velocity profile properly. Building aerodynamics was studied with economically meshed over complex geometries. Strouhal number, pressure distribution and skin friction distribution were recorded. Standard k-epsilon is not matched with the experimental results for blunt cube model. Other turbulence models agree with the experimental results.

In 2008, Ayotte [29] discussed linear modeling and nonlinear modeling of the atmospheric flow. The comparisons were made with wind tunnel experimental results. Slope of the hill and roughness values are selected as different values and the results of nonlinear modeling agree well with the measurements. However, the cases with linear modeling are not satisfied and the errors increase with the increment of slope of the hill and roughness values.

Especially, the validation experiments give important knowledge about the insight of the atmospheric boundary layer. These experiments are named as blind comparison studies. It is unique experience to evaluate the accuracy of the flow models. Many scientists, researchers and numerical code developers from industry attended these events in order to understand the flow physics better. Taylor et al. [15] reported the real measurements from Askervein Hill, Scotland in 1982. This study can be described as flow over a low hill that is alike many existing Wind Farm region in those years. 50 towers were employed to collect wind speed, wind direction and turbulence in three components. Another experiment was reported by Berg et al and Bechmann et al. ([17], [18]). The measurements were collected with ten masts from Bolund Peninsula, Denmark in 2010. The masts were equipped with high frequency cup anemometers. This research can be depicted as atmospheric flow over complex terrain. Since wind turbines were erected in complex orography, estimation of the wind potential in these areas has become important topic. Therefore, data from Askervein Hill and Bolund Peninsula experiments can be validated with numerical and wind tunnel tests. In Figure 2.3, Bolund Peninsula and locations of ten masts are illustrated.

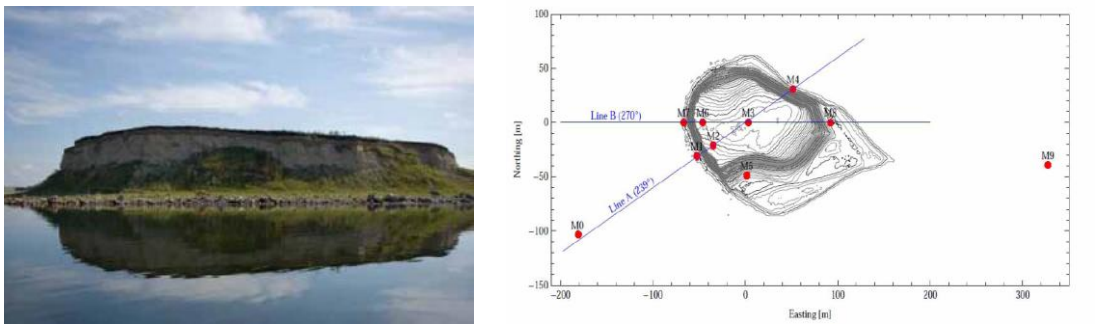

Figure 2.3: Bolund Peninsula and Location of Ten Masts [19]

2.2. Wind Farm Modeling

In present study, WindSim program will be performed to investigate the WRA. The engineering approach of this investigation can be comprehended by this section. Thus, the current available literature about the method of WindSim analysis is quite important to review. Leroy [30] tested the WindSim program with the experimental data of Askervein Hill in 1999. Leroy pointed out that results were changed significantly with the grid spacing and grid refinement study. Besides, the first cells close to terrain are needed to capture the flow physics literally. Another thing is that too refinement in z direction leads to construct long thin cells which cause numerical instabilities. The separation region is questionable according to results and this flow characteristic affects the solution domain. In separated regions, average velocity could not be predicted well. The reason is that measurements were taken in large time scale and neighbouring hills could affect the Askervein Hill. The implementation of low roughness values gave good results over the hill. At last, the results are accurate with measurements. However, the code found lower velocities than the measured ones in downwind region if the terrain is assumed as flat plain.

Weir and Gravdahl [19] presented the validation study of Bolund Experiment with WindSim program in 2011. Terrain and roughness data were taken into account in the analyses. As mentioned earlier, steady state simulation is modeled in WindSim program by incompressible RANS equations. CFD simulations matched very well with the measurements although the terrain is complex. The quality of the findings is related to terrain and roughness data obviously. Wind speed and turbulence kinetic energy are quite similar especially near the terrain, lee of the hill and escarpment. The option of smoothing the terrain in WindSim can be used to reach convergence in complex cases. Moreover, the resolution and suitable turbulence modeling are the key points for resolving the complex flows. Analyses with RANS k-epsilon which is stated as the best one in that study were tested according to international blind comparison results. The error is in the order of 5-6% at 5 meters.

Wallbank [15] investigated the difference between linear modeling WAsP and non-linear modeling WindSim program in 2007. In order to achieve the validation, the measurements collected from erected masts in complex terrain were utilized. The location information is not given because of the commercial sensitivity. The best combination of the parameters were searched including cell number, grid nesting, turbulence model, solver settings, and so on. Changing grid nesting is almost no difference for maximum resolution in accuracy. The grid resolution which affects cell number was limited because of the available RAM in hardware. Therefore, some errors occurred due to no refinement in steep terrain. Non-linear (CFD) and linear models are showed similar trends for errors in order of the magnitude. Delta RIX formula helps WAsP to obtain sensible values for complex terrains. Turbulent intensity and inflow angle values are over predicted by linear and non-linear models.

Gravdahl [31] studied the parameter sensitivity on numerical field modeling and the AEP in 2007. The lower estimation for AEP was experienced by wind farm owners beforehand. To avoid this conflict, CFD gets accurate results. Smooth and complex terrains were selected in that study. Besides, Gravdahl et al. [32] carried out the blind test validations for optimized micro siting. Several wind farm sites in Europe were investigated according to different grid resolutions. Wake modeling was considered to determine the wind turbines to be erected properly. Improvement in AEP was observed remarkably. Simisiroglou [33] researched AEP value of one wind farm where was installed in complex terrain in Greece. AEP estimation and wake effects were investigated with WindSim program. Wake models were utilized to compare the energy losses of wind farm. Fallo [14] also carried out WRA study in a region of Central Italy. The validation of WindSim was made by 2D simulation. Wind Farm layout design was prepared by using two year wind measurements. Castellani and Franceschini [34] researched the AEP estimation in Fossato di Vico, Italy. The errors were below 10% for energy production in the complex terrain.

Gravdahl et al. [35] used different analytical wake models which are proposed by Jensen [36], Larsen [37] and Ishihara et al. [38]. Actuator Disc Concept enables to capture wake-wake, wake-terrain interactions and thermal effects in complex terrain. Horns Rev and Lillgrund Offshore Wind Farms were validated with this approach. Wake modeling helps to optimize energy production and reduce wind turbine fatigue. Meissner [39] indicated that Park Optimizer program examines WindSim results according to IEC 61400-1 standard. Turbulence, flow inclination, speed and severe wind conditions are considered to determine the appropriate turbine type. This program uses a heuristic algorithm to design Wind Farm on desired location. However, it gives good results but not accurate. More sophisticated algorithm works better to estimate pinpoint wind turbine spots. Wind Farm layout design can be investigated with techno-economical optimization which will gain maximum profit from the project. 60 Wind Farm Site which has highly complex terrain was tested and analyzed to validate this code [39].

CHAPTER 3

WIND RESOURCE ASSESSMENT METHOD

In this chapter, WindSim program is utilized to investigate the WRA studies in complex terrain. Bodrum Peninsula is selected as a case study. The terrain occupies 26.5x26.5km in normal projection. For this research, terrain map from HGK (General Command of Mapping) and error-free wind data from YEGM (General Directorate of Renewable Energy) are used. One year measurements which are based on one hour averaged data were collected from 01.01.2003 to 31.12.2003 via one met station. Additionally, the roughness map from CORINE (Coordination of information on the environment) Land Cover Project is used to consider the surface roughness in the area.

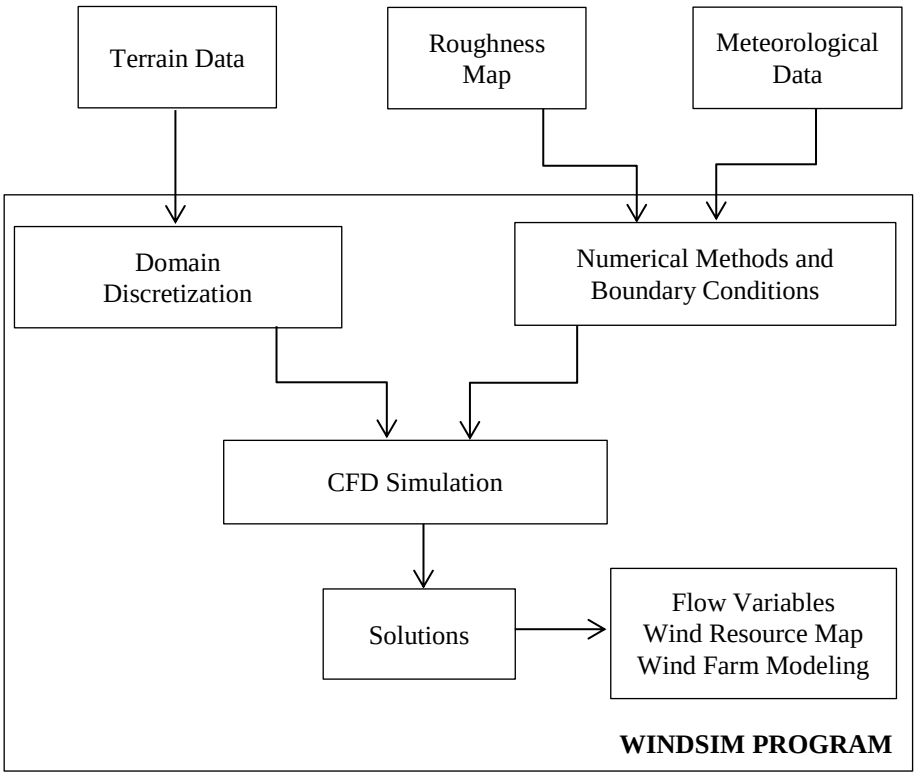

Figure 3.1: Basic Flowchart of Wind Resource Assessment Study

The basic flowchart of this process is presented in Figure 3.1. Preliminary research is based on meso-scale WRA studies in order to obtain wind map in Bodrum Peninsula. WindSim program facilitates this assessment in complex terrain. The candidate zones of Wind Energy Power Plant can be determined from the resource map acquired from this study. After the determination of Wind Farm location, the layout of wind turbines can be investigated.

3.1. Computational Fluid Dynamics Method

Computational Fluid Dynamics or CFD is the simulation of the systems including fluid flow, heat transfer and mass transfer with the aid of computer modeling. CFD helps to examine not only the insight of the model but also foresight for possible designs. Moreover, the design cycles can be reduced and more economic researches can be performed. The interfaces of all commercial CFD codes generally are equipped with three parts: Pre-processor, solver, post-processor [40].

As mentioned in previous section, this method is preferred to ease the WRA studies. WindSim program is utilized as CFD solver tool in this research. It is commercial software and developed specially for this purpose by WindSim AS of Norway. The numerical method is based on solving incompressible Reynolds Averaged Navier Stokes (RANS) equations using Finite Volume Method by PHOENICS CFD software. Sector wise steady state simulations are performed to predict the flow over the terrain.

WindSim program is one of the popular Wind Farm design tools. Micro siting and AEP can be researched within the acceptable limits of wind turbine fatigue. Pinpointing the turbines in desired locations is iterative process and three wake models can be used ([14], [15], [19]). There are six modules to follow the steps in the program hierarchically. The modules are listed below and a view of the modules is given in Figure 3.2 ([41], [42]).

1. Terrain
2. Wind Fields
3. Objects
4. Results
5. Wind Resources
6. Energy

Figure 3.2: Modules of WindSim

In first module, terrain and roughness data is inserted into program. Moreover, the domain discretization is constructed by meshing options. In second module, the numerical calculation is performed by defining the necessary options. These are boundary and initial conditions, physical models, calculation parameters, the location of convergence monitoring. Once 3D solution domain is constructed, the CFD simulations of the wind fields can initiate. The RANS equations are solved with the determined turbulence model. RANS equations are discretized and integrated by using finite volume method. The initial conditions which are guessed values are assigned according to boundary conditions. The solution is computed iteratively until the converged solution is achieved. Three possible methods are available to solve RANS equations in WindSim: Segregated Solver (SIMPLEST), Algebraic Coupled Multi-grid Solver (MIGAL) and Parallel Solver [41].

In third module, the location of climatologies, transferred climatologies and wind turbines are identified. In fourth module, results of parameters are obtained in 2D horizontal planes from ground. In fifth module, wind resource maps are presented. In last module, AEP values per wind turbine are determined including wake losses by using the results of the finished simulation [42].

3.2. Reynolds Averaged Navier Stokes Equations

CFD code PHOENICS employs three dimensional RANS equations to simulate the flow field. It is indicated that the RANS equations models solve the turbulence fairly good. This method obtains high accuracy solutions with statistical approach. The initial boundary conditions are used to converge a steady state solution iteratively. The result has one wind and one turbulence distribution in the solution domain. Since the neutral boundary layer is analyzed, the energy equation will not be computed because of any thermal effect. Therefore, mass and momentum parts of the Navier Stokes equations are stated below as given in Cartesian tensor form [43]:

$$\frac{\partial U_i}{\partial x_i} = 0 \tag{3.1}$$

$$U_j \frac{\partial U_i}{\partial x_j} = -\frac{1}{\rho}\frac{\partial p}{\partial x_i} + \frac{\partial}{\partial x_j}\left(\nu \left(\frac{\partial U_i}{\partial x_j} + \frac{\partial U_j}{\partial x_i} \right) - \left(\overline{u_i u_j} \right) \right) \tag{3.2}$$

where U is the velocity, x is the location component, p is the pressure, ρ is the density, υ is the kinematic viscosity and the subscripts i and j are the unit vectors. The $\left(\overline{u_i u_j}\right)$ term is known as Reynolds stresses and it is evaluated from the Boussinesq assumption:

$$\left(\overline{u_i u_j}\right) = -\nu_T \left(\frac{\partial U_i}{\partial x_j} + \frac{\partial U_j}{\partial x_i} \right) + \frac{2}{3}\delta_{ij} K \tag{3.3}$$

where ν_T is the turbulent viscosity and K is the turbulent kinetic energy [43]. For instance, the standard k-epsilon model is the default turbulence model to link the turbulent viscosity to k and epsilon. The turbulent kinetic energy (K) and its dissipation rate (ε) can be expressed below.

$$\nu_T = c_\mu \frac{K^2}{\varepsilon} \tag{3.4}$$

$$\frac{\partial}{\partial x_i}\left(U_i K\right) = \frac{\partial}{\partial x_i}\left(\frac{\nu_T}{\sigma_k} \frac{\partial k}{\partial x_i} \right) + P_k - \varepsilon \tag{3.5}$$

$$\frac{\partial}{\partial x_i}\left(U_i \varepsilon\right) = \frac{\partial}{\partial x_i}\left(\frac{\nu_T}{\sigma_\varepsilon} \frac{\partial \varepsilon}{\partial x_i} \right) + c_{\varepsilon 1} \frac{\varepsilon}{K} P_k - c_{\varepsilon 2} \frac{\varepsilon^2}{K} \tag{3.6}$$

P_k is the turbulent production term:

$$P_k = \nu_T \left(\frac{\partial U_i}{\partial x_j} + \frac{\partial U_j}{\partial x_i} \right) \frac{\partial U_i}{\partial x_j} \tag{3.7}$$

The model constants of k-epsilon model are:

$$c_\mu = 0.09,\ \sigma_k = 1.0,\ \sigma_\varepsilon = 1.3,\ \mathrm{c}_{\varepsilon 1} = 1.44,\ \mathrm{c}_{\varepsilon 2} = 1.92 \tag{3.8}$$

σ_k is the diffusion constant, c_μ is determined from the shear layer in the local equilibrium, $c_{\varepsilon 2}$ is determined from the experiments of the decaying grid turbulence. In the case of neutral ABL, the standard k-epsilon model overpredicts the turbulent viscosity in the weak shear layer far away from the terrain. This model can be adjusted to achieve better results in this region by these constants. The constants can be managed where the logarithmic law is valid:

$$c_\mu = \left(\frac{\overline{u_i u_j}}{K} \right)^2 \tag{3.9}$$

$$c_{\varepsilon 1} = c_{\varepsilon 2} - \frac{\kappa^2}{\sqrt{c_\mu}\sigma_\varepsilon} \tag{3.10}$$

The model constants of modified k-epsilon model are [39]:

$$c_\mu = 0.0324,\ \sigma_k = 1.0,\ \sigma_\varepsilon = 1.85,\ \mathrm{c}_{\varepsilon 1} = 1.44,\ \mathrm{c}_{\varepsilon 2} = 1.92 \tag{3.11}$$

Other modifications of k-epsilon turbulence model are the Yap correction and the RNG (ReNormalization Group). For further information, Refs. [44] and [45] can be examined respectively. As mentioned previously, there are several turbulence models installed in the WindSim program. In general, the standard k-epsilon consistently gives accurate results according to the last experiences. Noting that, the measurement masts generally erect on top hills. However, the effect of turbulence model is not significant in this specific place. The important thing is to resolve the flow separation areas in the flow domain and this phenomenon usually occurs behind the hills [42].

If the turbulence models are examined briefly, the general expectation can be followed. The modified k-epsilon model is the modification of the k-epsilon to obtain better solutions in the neutral ABL. The difference can be ignored. Another model, the Yap correction [44] consists of a modification of the epsilon equation in the form of an extra source term which is added to the right hand side of the epsilon equation. This model augments a turbulent source close to ground. It is better way to compute recirculation and stagnation in complex cases. The flow similarity between this model and standard k-epsilon model can be observed far away from the terrain. Lastly, the RNG k-epsilon model does not give better results than other models. Additionally, this model can obtain worse results than standard k-epsilon model [42].

3.3. Initial and Boundary Conditions

The height of the ABL, free stream velocity magnitude and direction form the vertical profile of the wind. As referred to chapter 1, the log law helps to predict the ABL. The steady state calculations are performed for every wind direction which is selected for this study as 12 directions. The resolution is chosen as 30 degrees and the data is taken from the climatology data. In Figure 3.3, example for a wind rose is taken from the Ref. [5]. It is divided by 16 directions and the notations are given for every 22.5 degrees.

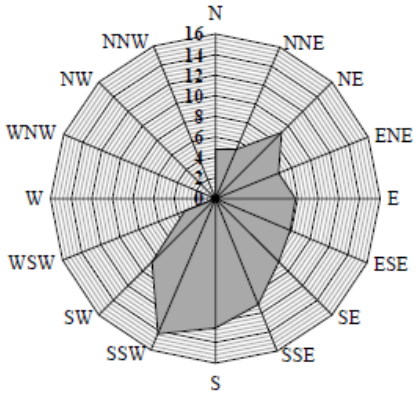

Figure 3.3: Example for a Wind Rose Showing Distribution of Frequency in Different Directions [5]

To complete the analyses, 12 CFD simulations are carried out in order. The geometry of the solution domain resembles to a flow through a wind tunnel. One inlet and one outlet section are identified for the domain which is rotated according to wind direction. The bottom side of the tunnel can be considered as the terrain. The top side of the tunnel is selected as fixed pressure condition as recommended for complex terrain case [42]. The height of the ABL is chosen as 500 m that is most used in reference to many scientists [14]. In order to avoid convergence problem in WindSim, the velocity above ABL is selected as 10 m/s. Air density is selected as 1.225 kg/m^3. Wall functions are applied over the terrain. The ABL can be defined with this mathematical equation which is called as Monin-Obukhov similarity. The mean velocity vertical profile can be computed as follows considering wind speed and roughness lengths:

$$\frac{U(z)}{U_\tau} = \frac{1}{\kappa} In\left(\frac{z}{z_o}\right) \tag{3.12}$$

where U is the wind speed, U_τ [m/s] is the friction velocity, $\kappa = 0.435$ is the Von Karman constant, z_o [m] is the roughness height and z is the coordinate in vertical direction. The friction velocity is computed by this equation:

$$U_\tau = \sqrt{\frac{\tau_w}{\rho}} \tag{3.13}$$

where τ_w [N/m^2] is the shear stress at the wall boundary and ρ [kg/m^3] is the air density.

The neutrally stratified atmosphere is valid to assume average annual conditions approximately. A neutral stratification indicates the vertical temperature distribution which is the consequence of the buoyancy forces. The default setting is selected as disregard temperature. It is recommended unless temperature measurements are available. The model is resolved with a neutral stratification at the inlet section. No force on the volume of the air will occur because of the density or pressure differences. Thus, no transient phenomena problem is present [42].

Furthermore, Coriolis Effect is not included in the computations. It is emphasized that special algorithm should be added to CFD solver of WindSim. Numerical instabilities can occur without knowledge of this CFD solver algorithm. The reason is that it is difficult to balance the pressure forces at the boundaries accurately in order to obtain the natural phenomena. It is also not recommended to use on the scale of the models around 20 km, because the effect of Coriolis force is negligible in this margin [40]. Another important thing is that high computer storage is needed for large cell numbers in the domain. When the cell number increases, the elliptic nature of pressure field gives errors. Thus, the convergence time goes up at the same time. Coupled solver handles the velocity-pressure coupling strategy in WindSim. An algebraic multi-grid solver computes the hydrodynamic variables in whole domain simultaneously and it splits the solution domain into sub domains to solve separately. Thus, this method speeds up the simulations [42].

3.4. Terrain Descriptions and Domain Discretization

Bodrum Peninsula is selected as the case study. The reason is that this complex terrain is composed of urban, suburban, hills, different shape of islands and coastal areas. Area of raw terrain data has 26.5x26.5 km in normal projection and different altitudes vary in regional. Firstly, the data is arranged in Global Mapper program [46]. In WRA studies, the high resolution is needed especially in micro siting cases. Specifically, the preferred resolution is 10x10 meters. However, the available horizontal resolution is 91x91 meters for this study.

The data was taken from HGK. The descriptions of the terrain are stated in Table 3.1. The terrain data is inserted into Global Mapper Program in order to arrange. Top and perspective view of the terrain can be observed in Figure 3.4 and 3.5, respectively.

Table 3.1: Terrain Descriptions in Global Mapper

	Value
X Resolution	91 m
Y Resolution	91 m
Z Resolution	Not available
X Range	26.45 km
Y Range	26.45 km
Maximum Z	672 m
Minimum Z	- 6 m
Latitude (WGS 84)	27º 12’ 10’’ - 27º 30’ 3’’E
Longitude (WGS 84)	36º 56’ 35’’ - 37º 10’ 52’’N
UTM Region	35th
Latitude (NAD 83)	518099.26 – 544549.26
Longitude (NAD 83)	4088648.652 – 4115098.652

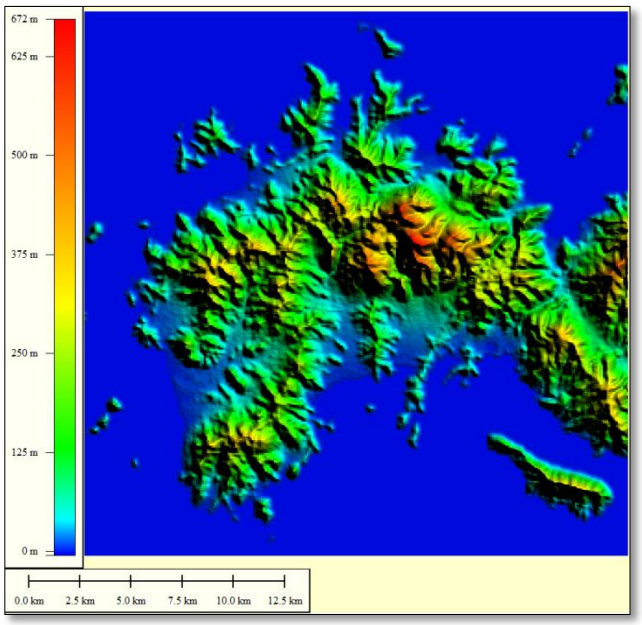

Figure 3.4: Top View of Bodrum Peninsula in Global Mapper Program

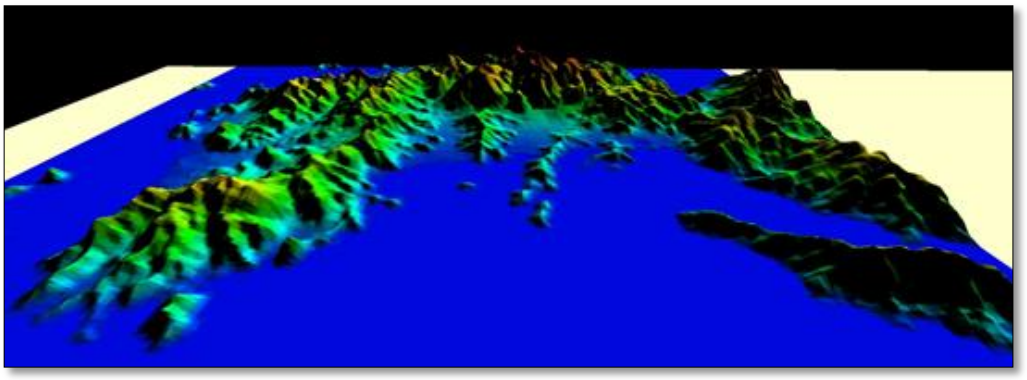

Figure 3.5: Perspective View of Bodrum Peninsula in Global Mapper Program

Afterwards, the terrain is identified in WindSim program before the domain discretization. Inclination angle is also important parameter to review regarding to skewed cells in structured meshing. Making the grid orthogonal is a way to avoid from divergence in simulations. If the inclination angle is higher than 50 degrees, orthogonalization is recommended to active in the WindSim manual [42]. The orography and inclination angle of the Digital Terrain Model (DTM) can be observed in Figure 3.6. Therefore, the default setting can be remained as no orthogonalization. The terrain specifications in WindSim are given in Table 3.2. Artificial resolution which is 13x13m was created in order to reach finer mesh in WindSim program by interpolation method.

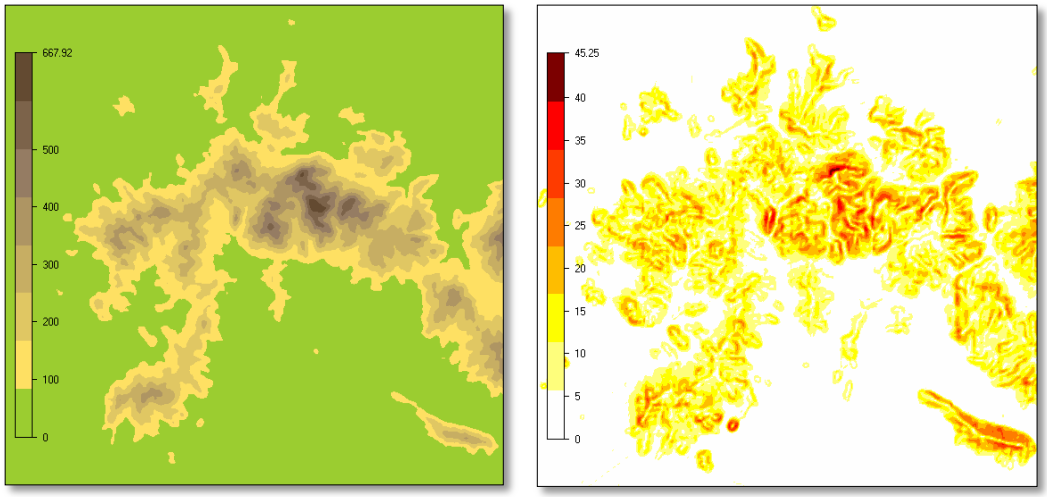

Figure 3.6: Orography (left) and Inclination Angle (right) of the Digital Terrain Model in WindSim

Table 3.2: Terrain Descriptions in WindSim

	Value
X-Direction Resolution	13 m
Y-Direction Resolution	13 m
X Range	25.896 km
Y Range	24.934 km
Latitude	518100 - 543996
Longitude	4089465 - 4114399
Points (X-Y)	1992 - 1918

Computational time and cost should be addressed thoughtfully when the numerical study is conducted. Structured meshing technique is used to construct the domain discretization in WindSim. Domain discretization is crucial to capture the flow characteristics especially in ABL. Therefore, fine mesh is constructed in the region where is close to ground. Apart from this, the growth rate is essential to be determined to have coarser mesh far away from the ground. Thanks to this setting, it reduces computational time remarkably. Eventually, the volume of the computational domain is discretized hexahedral cells that are called mesh or grid.

The DTM in *.gws* format comprises data about the orography and roughness. The boundary layer height, height distribution factor, cell number in z direction, the model height, mesh refinement area and total cell number can be defined. No mesh refinement, no smoothing and no 3D orthogonalization are needed for all cases. The grid dependency study is carried out with four different mesh types. The specifications of these cases are given in Table 3.3. Exception is done for last case where mesh refinement operation which is almost applied to the entire domain is utilized to achieve high cell number over the domain in fourth case. The domain discretization in X-Y direction is given for all mesh types sequentially in Figure 3.7.

Table 3.3: The Specifications of Domain Discretization for All Cases

CASES	**Mesh 1**	**Mesh 2**	**Mesh 3**	**Mesh 4**
Total Cell Number	1412190	2723560	4236320	6493800
X-Direction Resolution	117 m	91 m	78 m	63 m
Y-Direction Resolution	117 m	91 m	78 m	63 m
X-Direction Cell Number	221	284	332	411
Y-Direction Cell Number	213	274	319	395
Z-Direction Cell Number	30	35	40	40
Height Distribution Ratio for Z Direction	0.1	0.1	0.1	0.1
Height Above Terrain (Z)	3662 m	3662 m	3658m	3658m

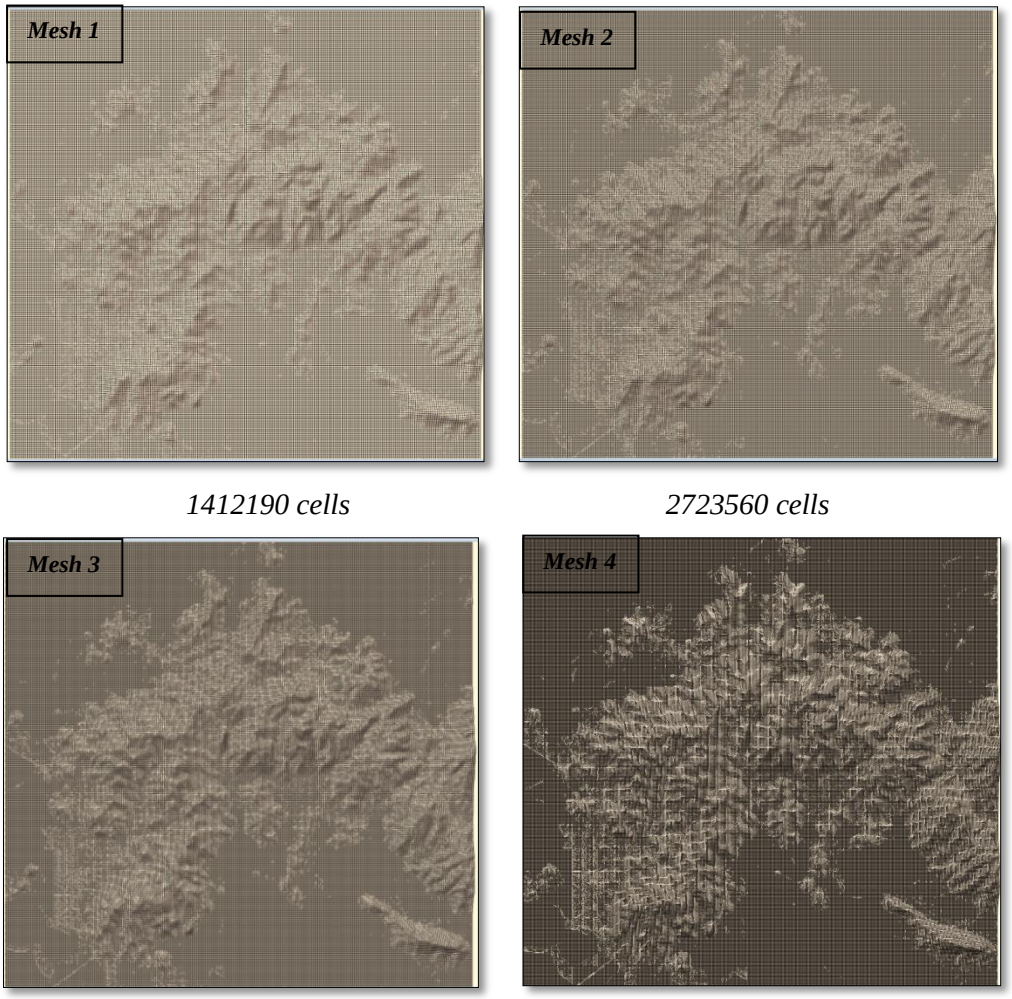

Figure 3.7: Domain Discretization in X-Y direction

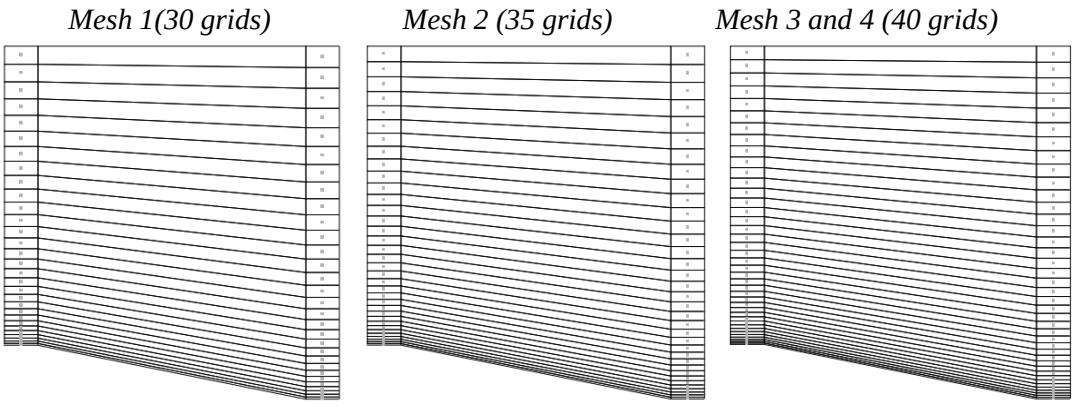

Figure 3.8: Domain Discretization in Vertical Direction (Z)

The nodes which are the center of the hexahedral cells are indicated by dots in the schematic figure. The domain discretization in vertical direction is also presented for the different mesh types in Figure 3.8. The left and right columns show the maximum and minimum elevations respectively. The distribution of the first 10 nodes in z direction is given at the position with maximum and minimum elevations in Table 3.4.

Table 3.4: Distribution of the First 10 Nodes in Z Direction from the Terrain at the Position with Maximum and Minimum Elevation

		1	**2**	**3**	**4**	**5**	**6**	**7**	**8**	**9**	**10**
Mesh 1	Z max [m]	11.1	36.7	69.3	108.7	155.0	208.2	268.2	335.2	409.1	489.8
	Z min [m]	13.1	43.4	81.7	128.3	182.9	245.7	316.6	395.6	482.8	578.1
Mesh 2	Z max [m]	9.5	31.1	57.6	89.2	125.9	167.6	214.3	266	322.8	384.7
	Z min [m]	11.2	36.6	68	105.3	148.6	197.8	252.9	314	381	454
Mesh 3	Z max [m]	8.3	26.9	49.2	75.5	105.5	139.4	177.1	218.7	264.1	313.4
	Z min [m]	9.8	31.8	58.2	89.2	124.8	164.9	209.5	258.6	312.3	370.6
Mesh 4	Z max [m]	8.7	28.2	51.7	79.2	110.7	146.3	185.9	229.5	277.2	328.9
	Z min [m]	10.2	33.1	60.6	92.9	130	171.7	218.2	269.4	325.3	385.9

Since the program does not give any feedback for the quality of the mesh, pre-checking procedure is applied to all the meshes. Largest dimension in a cell is divided by the smallest dimension to determine the aspect ratio. The recommended fraction for aspect ratio is below 10 for the cells closest to the terrain. The convergence might be reached quickly for the aspect ratio around 1. Noting that, two times by node elevation equals the cell height. The evaluation is presented for all meshes in Table 3.5. The maximum cell heights are 117, 91, 78 and 63 m in sequence. The range of x and y resolution shows that the aspect ratio of fourth mesh is better than the others for the cells closest to the terrain.

Table 3.5: Aspect Ratio Evaluation for the Mesh Types

		1	**2**	**3**	**4**	**5**	**6**	**7**	**8**	**9**	**10**
Mesh 1	Cell height [m]	22.2	29.0	36.2	42.6	50.0	56.4	63.6	70.4	77.4	84.0
	Aspect ratio	5.3	4.0	3.2	2.7	2.3	2.1	1.8	1.7	1.5	1.4
Mesh 2	Cell height [m]	19.0	24.2	28.8	34.4	39.0	44.4	49.0	54.4	59.2	64.6
	Aspect ratio	4.8	3.8	3.2	2.6	2.3	2.0	1.9	1.7	1.5	1.4
Mesh 3	Cell height [m]	16.6	20.6	24.0	28.6	31.4	36.4	39.0	44.2	46.6	52.0
	Aspect ratio	4.7	3.8	3.3	2.7	2.5	2.1	2.0	1.8	1.7	1.5
Mesh 4	Cell height [m]	17.4	21.6	25.4	29.6	33.4	37.8	41.4	45.8	49.6	53.8
	Aspect ratio	3.6	2.9	2.5	2.1	1.9	1.7	1.5	1.4	1.3	1.2

Height above terrain is defined as the vertical distance between the highest elevation point in terrain and the top boundary section of the domain. It is set up as automatic in order to obey the rule of thumb. It is about the fraction between the minimum and maximum open area ranging from the terrain to the upper boundary in this cross section. Maximum open area is shown as black rectangles. Red line indicates the upper border of the minimum open area. This computation is based on west-east and south-north direction and the fraction should be larger than 0.95. This provides no blocking effects in the solution domain [42]. In Figure 3.9, the fraction can be observed in west-east and south-north direction of mesh. For example, open area data of prepared mesh 3 is presented in Table 3.6. Therefore, the height of the domain is selected as approximately 3.66 km from the smallest altitude.

$$\frac{\text{Open Area Minimum}}{\text{Open Area Maximum}} > 0.95 \tag{3.14}$$

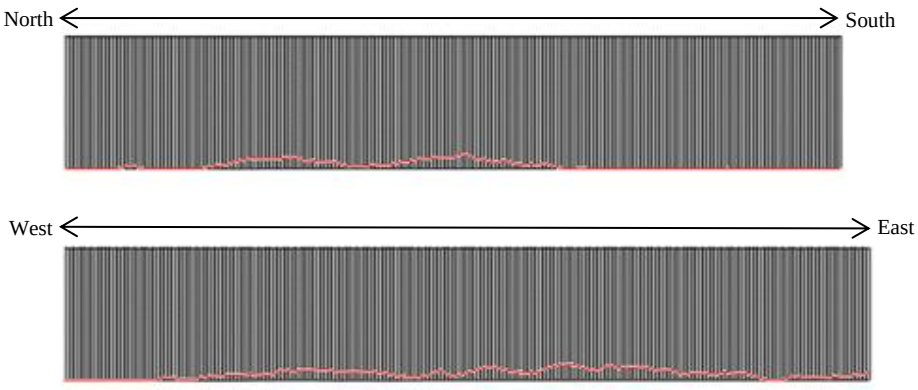

Figure 3.9: View from North-South (Top) and West-East (Bottom) Direction of DTM

Table 3.6: Open Area Data

	Min [m^2]	Max [m^2]	Min/Max
West-East Direction	106142832	107527928	0.9871
South-North Direction	105804992	111490800	0.9490

3.5. Roughness Map Arrangement

Roughness length values are assigned over the terrain by using WAsP Map Editor 10 and Google Earth Programs. WAsP Map Editor Program can create and edit the topographical inputs [47]. The earth scale orography data and geo-referenced data of land cover have become available for every location all over the world. The Corine Land Cover (CLC) project which was funded by the European Commission Program is another step for this process. The land occupation and features of all European countries were searched and obtained in 2000. The researchers categorized different CLC land definitions. The classifications based on wide range study of CLC methodology and roughness length theory were utilized to obtain European Wind Atlas. Furthermore, the CLC cartography was adapted for WAsP program. The usage of roughness length cartography was tested in three different locations in Portugal. Regarding to particular terrain types, 44 CLC Classes were categorized by 14 roughness classes [48]. The roughness lengths are presented corresponding to land features in Table 3.7. In this study, this classification is used to constitute roughness map of Bodrum Peninsula.

The roughness map should be validated with Google Earth program by two consecutive methods. Firstly, the differences in roughness map are inspected and modified neatly by zooming the terrain. Secondly, dislocations of the geo-referenced map are found and arranged by overlapping image method. More precisely, three geo-referenced points are selected in order to match the terrain data in Google Map and the roughness map in WAsP Map Editor. The orography and roughness map in WAsP Map Editor are presented in Figure 3.10. Three arbitrary geo-referenced points (A, B, C) in Google Map and overlapping procedure in WAsP Map Editor are shown in Figure 3.11.

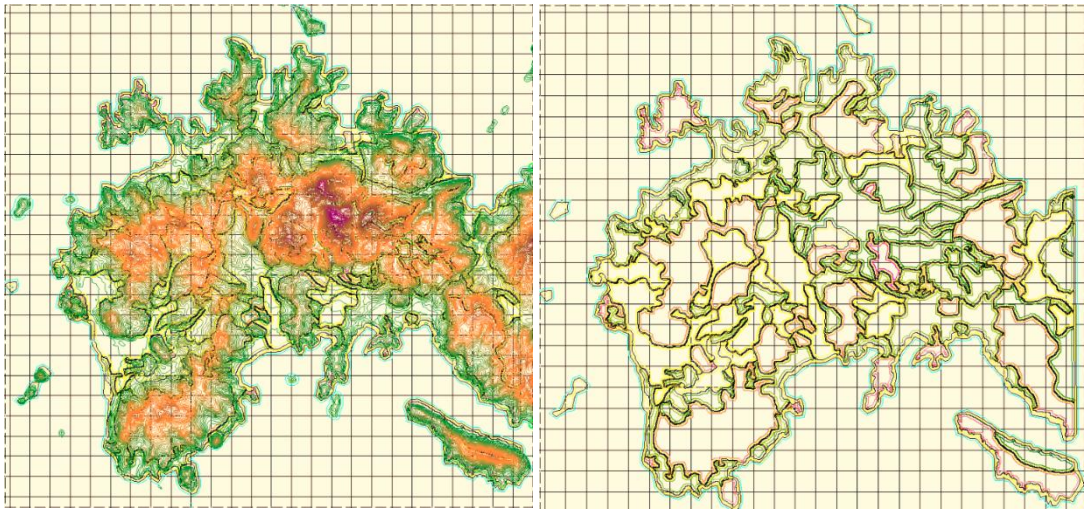

Figure 3.10: The Orography Map (left) and Roughness Map (right) in WAsP Map Editor

Table 3.7: CLC Roughness Length Scale Table (Tabulated from Ref. [48])

		Roughness [m]	
No	**Description of Land**	**Value Range**	**Most Likely Value**
1	Continuous Urban Fabric	1.1 – 1.3	1.2
2	Broad-leaved Forest; Coniferous Forest; Mixed Forest	0.6 – 1.2	0.75
3	Green Urban Areas; Transitional Woodland/shrub; Burnt Areas	0.5 – 0.6	0.6
4	Discontinuous Urban Fabric; Construction Sites; Industrial or Commercial Units; Sport and Leisure Facilities; Port Areas	0.3 – 0.5	0.5
5	Agro-forestry Areas; Complex Cultivation Patterns; Land principally occupied by agriculture, with significant areas of natural vegetation	0.1 – 0.5	0.3
6	Annual Crops associated with permanent crops; Fruit Trees and Berry Plantations; Vineyard; Olive Groves	0.1 – 0.3	0.1
7	Road and Rail Networks and associated land	0.05 – 0.1	0.075
8	Non-irrigated arable land; Permanently irrigated land; Rice fields; Salt Marshes		0.05
9	Sclerophylous vegetation; Moors and heathland; Natural grassland; Pastures	0.03 – 0.1	0.03
10	Dump sites; Mineral extraction sites; Airports; Bare rock; Sparsely vegetated areas		0.005
11	Glaciers and Perpetual Snow		0.001
12	Peatbogs; Salines; Intertidal Flats		0.0005
13	Beaches, Dunes, and Sand Plains		0.0003
14	Water Courses; Water Bodies; Coastal Lagoons; Estuaries; Sea and Ocean		0

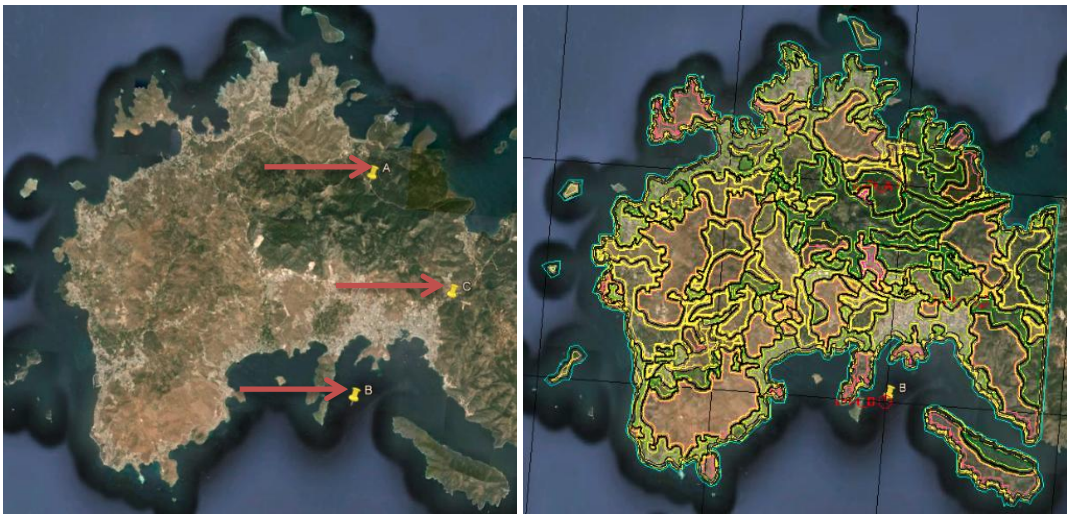

Figure 3.11: Three Arbitrary Geo-Referenced Points (left) and Overlapping Procedure (right)

Eventually, arranged roughness heights over the terrain are read from the *grid.gws* file in WindSim Terrain Editor. Besides, the roughness length of water bodies is assigned as 0.0001 automatically. The roughness height over the terrain is presented according to normal scale in Figure 3.12.

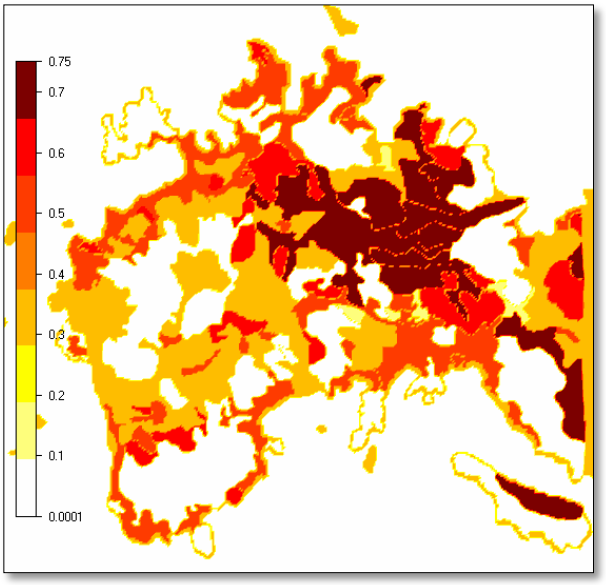

Figure 3.12: Roughness Length in Normal Scale

3.6. Wind Data Analysis

Error-free wind data was acquired from YEGM throughout the year of 2003. This is the only available measured wind data in Bodrum Peninsula for wind resource assessment studies. Unfortunately, there are no temperature recordings and there is also no standard deviation data for wind direction. Recommended mast height should be at least 2/3 hub height. However, the available met station height is 10 m and planned hub height is 100 m.

Wind speed, its standard deviation and wind direction were recorded one hour averaged data to the data logger system in Yalıkavak region by NRG brand measurement system. Cup anemometer and wind direction vane are the sensors of this device. This qualified anemometer has international MEASNET calibration certificate [49]. The met station was erected over the top of the hill at 10 meter high. The components of NRG measurement system are shown in Figure 3.13. The specifications of the met station and wind data are presented in Table 3.8. The met station location is indicated in WindSim in Figure 3.14.

Figure 3.13: Cup Anemometer (top) and Wind Direction Vane (bottom) Components of NRG Measurement System [49]

Table 3.8: Met Station and Wind Data Specifications

Location (NAD 83): [x-y]	528618.2 – 4104861.0
Altitude	255.1
Record Dates:	01.01.2003 – 31.12.2003
Record Numbers	8760
Mast Height:	10 m
Mean Velocity:	5.83 m/s
Mean Standard Deviation:	1.7 m/s
Maximum Velocity:	28.45 m/s

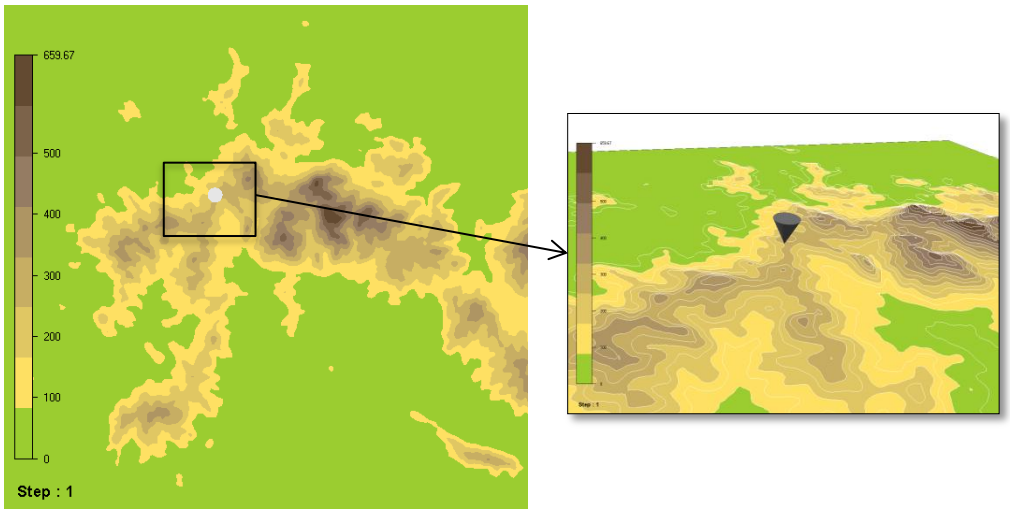

Figure 3.14: Top View (left) and Closer View (right) of Mast Location

Wind data arrangement and analysis operations were carried out by Windographer Demo version 3 Program. This program read the data and converts it into a WindSim climatology file format. Besides, many post-processing features of this program help the data analysis extensively [50]. Monthly averaged wind direction and velocity are plotted in Figure 3.15. Likewise, the mean diurnal wind velocity according to hour of a day is plotted in Figure 3.16.

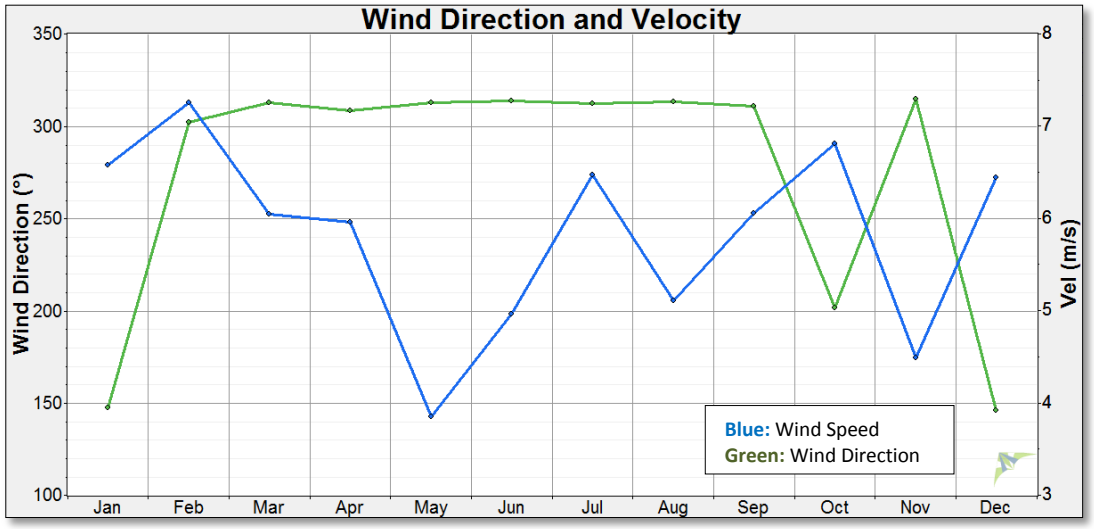

Figure 3.15: Mean Monthly Wind Direction and Velocity

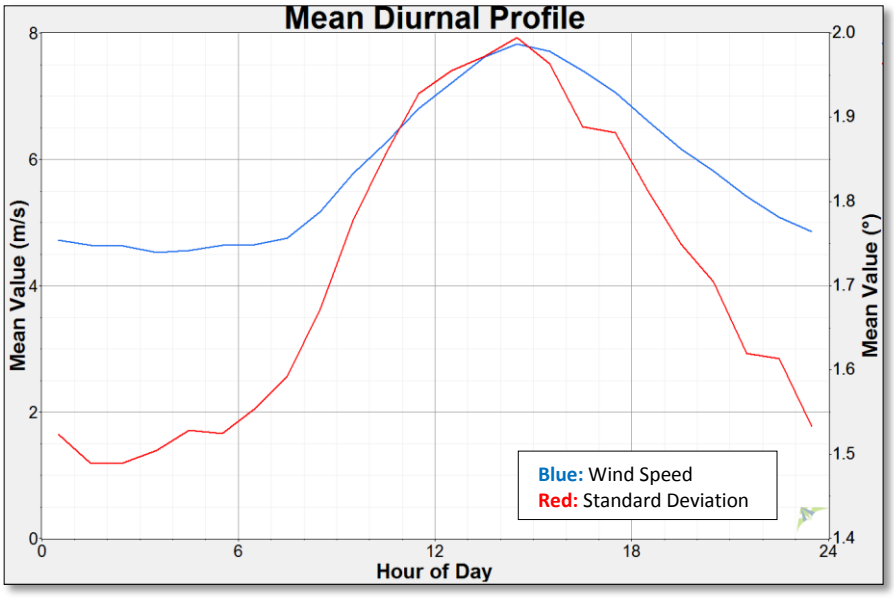

Figure 3.16: Mean Diurnal Wind Velocity for Hour of a Day

The probability density function (PDF) describes the likelihood of wind speed magnitude. According to experiences, the wind speed tends to be below the mean speed predominantly [1]. Different algorithms can describe PDF to obtain the frequency (%). The long term average wind speed can be calculated as follows:

$$\overline{U} = \frac{1}{N}\sum_{i=1}^{N} U_i \tag{3.15}$$

The standard deviation of the individual wind speed averages, σ_U is,

$$\sigma_U = \sqrt{\frac{1}{N-1}\sum_{i=1}^{N}\left(U_i - \overline{U}\right)^2} = \sqrt{\frac{1}{N-1}\left[\sum_{i=1}^{N} U_i^2 - N\overline{U}^2\right]} \tag{3.16}$$

The average wind power density is the average available wind power per area and it is calculated by the formula (3.17). Air density varies with temperature and altitude, it should be calculated with the formula (3.18) to obtain more realistic results [5].

$$\overline{P}/A = \frac{1}{2}\rho\frac{1}{N}\sum_{i=1}^{N}U_i^3 \tag{3.17}$$

$$\rho = \frac{353.049}{T}e^{\left(-0.034\frac{z}{T}\right)} \tag{3.18}$$

The Weibull distribution approach is considered for the energy computations. This method is accepted by Wind Energy IEC 61400 Standards. Wind distribution determines the wind characteristics on the selected site. Many computer codes can calculate this distribution with different statistical algorithms. The objective is to fit a Weibull distribution to wind speed data. The resulting curve shows the frequency histogram of the collected wind data. Three Weibull algorithms are used in Windographer such as Maximum likelihood, least squares and WAsP. Especially, Maximum likelihood method is the default one to plot the PDF graphs in Windographer [46]. The explanation of this algorithm can be found in Ref. [5]. Algorithm of Maximum likelihood is also proposed by Türkyılmaz [51]. The data taken from met station can be examined with this algorithm. It is also added to AEROWIND code. The frequency distribution of wind speeds is defined with two Weibull parameter k (shape factor) and c (scale factor). The frequency of occurrence is computed by the formula:

$$f(U) = \left(\frac{k}{c}\right)\left(\frac{U}{c}\right)^{k-1}e^{-\left(\frac{U}{c}\right)^{k}} \tag{3.19}$$

According to this function, mean velocities are expressed as:

$$U_{mean} = \int_0^{\infty} U\, f(U)\, dU \tag{3.20}$$

If Weibull parameters are known, it is possible to estimate Wind Farm energy density and energy output. Met station data can be collected wind data at particular height. Wind speed at hub height of wind turbine should be found to obtain AEP. Therefore, power law can be used in this estimation. Power law exponent (α) can be taken as 0.2 [51].

$$\frac{U_{hub}}{U_{reference}} = \left(\frac{z_{hub}}{z_{reference}} \right)^{\alpha} \tag{3.21}$$

Shape factor can be calculated iteratively with this formula:

$$k = \left[\frac{\sum_{i=1}^{N} U_i^k In(U_i)}{\sum_{i=1}^{n} U_i^k} - \frac{\sum_{i=1}^{N} In(U_i)}{N} \right]^{-1} \tag{3.22}$$

After the determination of shape factor, scale factor is calculated by this formula:

$$c = \left[\frac{1}{N} \sum_{i=1}^{N} U_i^k \right]^{1/k} \qquad [m/s] \tag{3.23}$$

Many modifications are also made to this algorithm explained in Ref. [51]. The current algorithm is given as follows according to data analysis and maximum likelihood method:

1. Insert orography, roughness length, air density and the wind data to the program,
2. Extrapolate wind speeds to hub height values by using power law,
3. Divide into sectors, constitute wind rose and compute frequency per sector
4. Guess initial value for shape factor (k=1.0),
5. Iterate for optimum shape factor (k),
6. Calculate scale factor (c),
7. Calculate Weibull mean wind speed.

Wind speed frequency distributions are plotted according to different algorithms in Figure 3.17. Weibull constants and other important parameters are tabulated in Table 3.9. The results of other algorithms are taken from Windographer program. Climatology Characteristics including Weibull, frequency and mean wind speed versus sector were tabulated with AEROWIND code in Table 3.10. Explanations of other statistical algorithms can be found in Ref. [50].

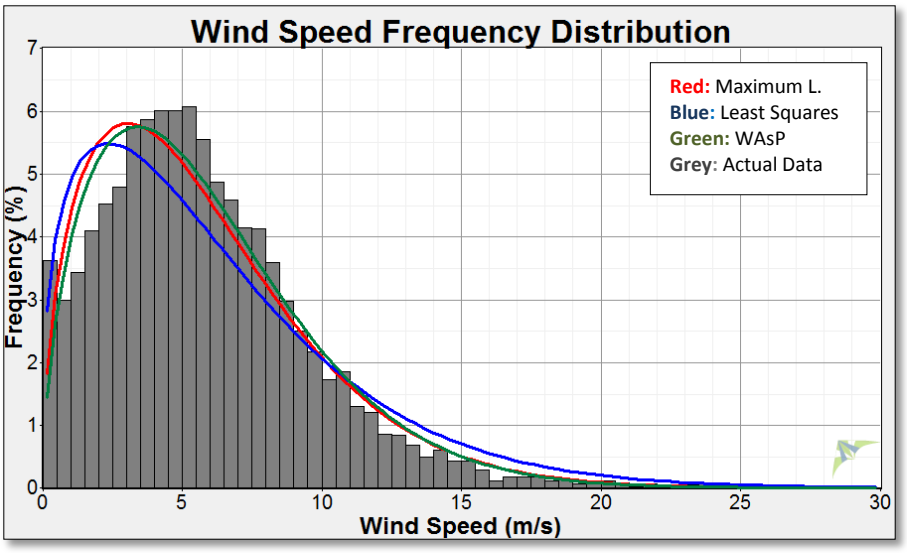

Figure 3.17: Wind Speed Distribution for Different Algorithms

Table 3.9: Wind Speed Distribution Analysis with Different Algorithms

Computation Algorithms	Weibull k	Weibull c [m/s]	Mean [m/s]	Power Density [W/m^2]
AEROWIND	1.486	6.402	5.796	321.9
Maximum likehood	1.495	6.412	5.791	325.1
Least Squares	1.331	6.700	6.159	471.5
WAsP	1.560	6.557	5.893	322.1
Actual Data	8760 Time Steps		5.829	322.1

Table 3.10: Climatology Characteristics including Weibull (k, c), Frequency (% related to all sectors) and Mean Wind Speed (m/s) versus Sector with AEROWIND

Sector Midpoint	0°	30°	60°	90°	120°	150°	180°	210°	240°	270°	300°	330°
k	1.05	0.98	0.97	1.22	1.22	1.55	1.27	0.90	1.33	0.99	2.10	1.89
c	1.14	0.85	0.92	2.58	5.48	8.96	2.75	1.88	2.05	2.01	7.50	5.35
frequency	1.95	1.14	0.61	1.06	7.12	15.38	1.58	0.99	0.50	0.24	40.39	29.14
mean	1.11	0.85	0.92	2.43	5.11	8.05	2.58	1.94	1.90	2.01	6.63	4.75

Frequency of velocity versus wind direction is given as a wind rose in Figure 3.18. The wind rose was divided by 16 sectors. The main dominant sectors can be observed from this figure and they are 150, 300 and 330 degrees. Mean wind speeds can be also seen in Figure 3.18.

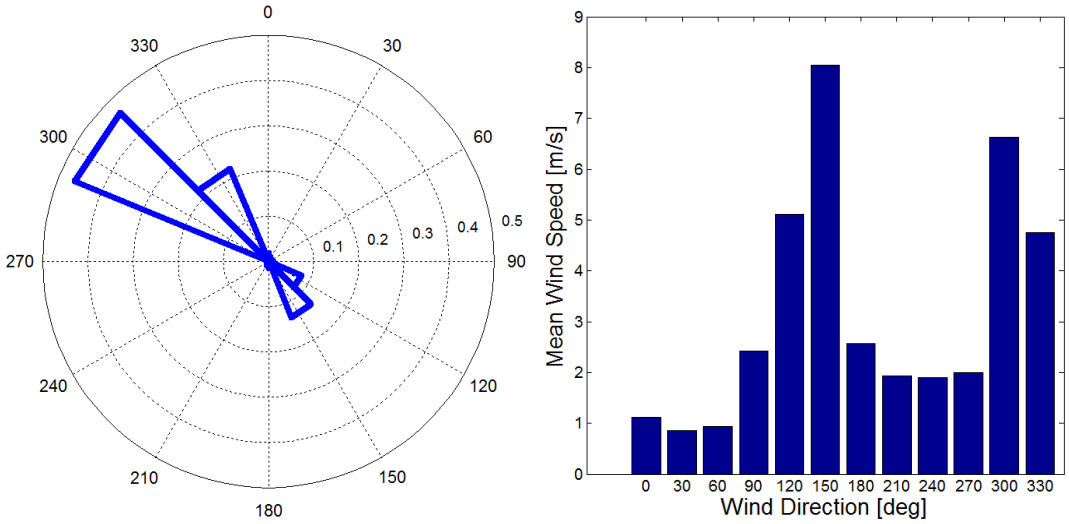

Figure 3.18: Frequency of Wind Directions as a Wind Rose and Mean Wind Speeds for Sectors

3.7. Calculations of Variables

In WindSim, simulations are performed in Wind Field Module. The simulations are based on steady state CFD calculations for every wind sectors. Therefore, 12 simulations are needed to complete the Wind Field Module. The flow variables which are solved by CFD code are stated below [42]:

1. Speed Scalar X: Wind speed scalar in East-West direction (U) - [m/s]
2. Speed Scalar Y: Wind speed scalar in South-North direction (V) - [m/s]
3. Speed Scalar Z: Wind speed scalar in vertical direction (W) - [m/s]
4. Pressure: Relative pressure to fixed zero at zero at sea level [Pa]
5. Turbulent Kinetic Energy (K) : $[m^2/s^2]$
6. Turbulent Dissipation Rate: $[m^2/s^3]$

With these variables, following parameters can be calculated with the formulas [42]:

7. Speed Scalar XY: Wind speed scalar in horizontal plane [m/s]:

$$\text{Speed Scalar XY} = \sqrt{U^2 + V^2} \tag{3.24}$$

8. Speed Scalar XYZ: Wind speed scalar in 3D space [m/s]:

$$\text{Speed Scalar XYZ} = \sqrt{U^2 + V^2 + W^2} \tag{3.25}$$

9. Velocity Vector XY: Wind speed vector in horizontal plane (U,V,0) - [m/s]
10. Velocity Vector XYZ: Wind speed vector in 3D space (U,V,W) - [m/s]
11. Turbulent Intensity: with the assumption of isotropic Kinetic Energy (KE) [%]:

$$\text{TI} = 100 \times \frac{\sqrt{\frac{4}{3} \times KE}}{\sqrt{U^2 + V^2}} \tag{3.26}$$

12. Wind Shear Exponent: The wind shear power exponent of a power law tangent to the calculated wind speed profile [-]

$$\text{Wind Shear Exponent} = \frac{\text{Shear}}{\frac{\text{Speed Scalar XY}}{z}} \tag{3.27}$$

13. Inflow Angle: Angle respect to the horizontal plane [degrees]

$$\text{Inflow Angle} = \tan^{-1}\left(\frac{W}{\text{Speed Scalar XY}}\right) \tag{3.28}$$

Further information about these calculations can be found in the Ref. [42].

CHAPTER 4

ANNUAL ENERGY PRODUCTION CALCULATION METHOD

In this chapter, the theoretical background of the AEROWIND code is expressed. Main purpose is to predict total capital cost, cost of generated wind electricity and payback time in concentrated area. Wind data, topographical conditions and wind turbine specifications should be known to perform the calculations. It is written in MATLAB numerical computing environment. It consists of four main parts. These are stated below:

1. Site Information (based on wind data analysis and maximum likelihood method)
2. Aerodynamics (based on Blade Element Momentum Theory)
3. Wind Farm Energy Analysis (based on Jensen Wake Model)
4. Economics (based on Present Worth approach)

In the first part, site information is examined with maximum likelihood method as mentioned in Chapter 3. Orography and roughness length variations over the terrain should be known. This data provides the necessary coordinates and surface roughness in the selected area. Moreover, wind data and air density are utilized to determine Weibull parameters and mean velocities in sector wise. Once wind rose and Weibull distribution are found, mean wind speed at hub height of wind turbine is obtained in sector wise by power law assumption.

The second part of the code is related to BEMT algorithm. The main idea is to use this method in order to compute power output and thrust coefficient of a wind turbine theoretically. Both parameters are obtained and listed according to different wind speeds. Pitch and stall regulated wind turbines can be computed if the blade geometry, design parameters and aerodynamic data are available. Otherwise, arbitrary wind turbine can be designed with the theoretical assumptions. These are elaborated in following sections.

The third part of the code is essential tool to pinpoint the wind turbines theoretically. Jensen wake model is oldest and simplest analytical method to obtain wake losses in wind farm configurations. Power and thrust coefficient curves are inserted to program. Wake deficits are computed by using Jensen wake model algorithm. Weibull distribution approach is utilized to compute the AEP and Capacity Factor of a wind turbine. In the last part of code, Present Worth approach is utilized to predict total capital cost, cost of wind energy and repayment period. In Figure 4.1, the flowchart of AEROWIND code is presented. The algorithms are explained in following sections.

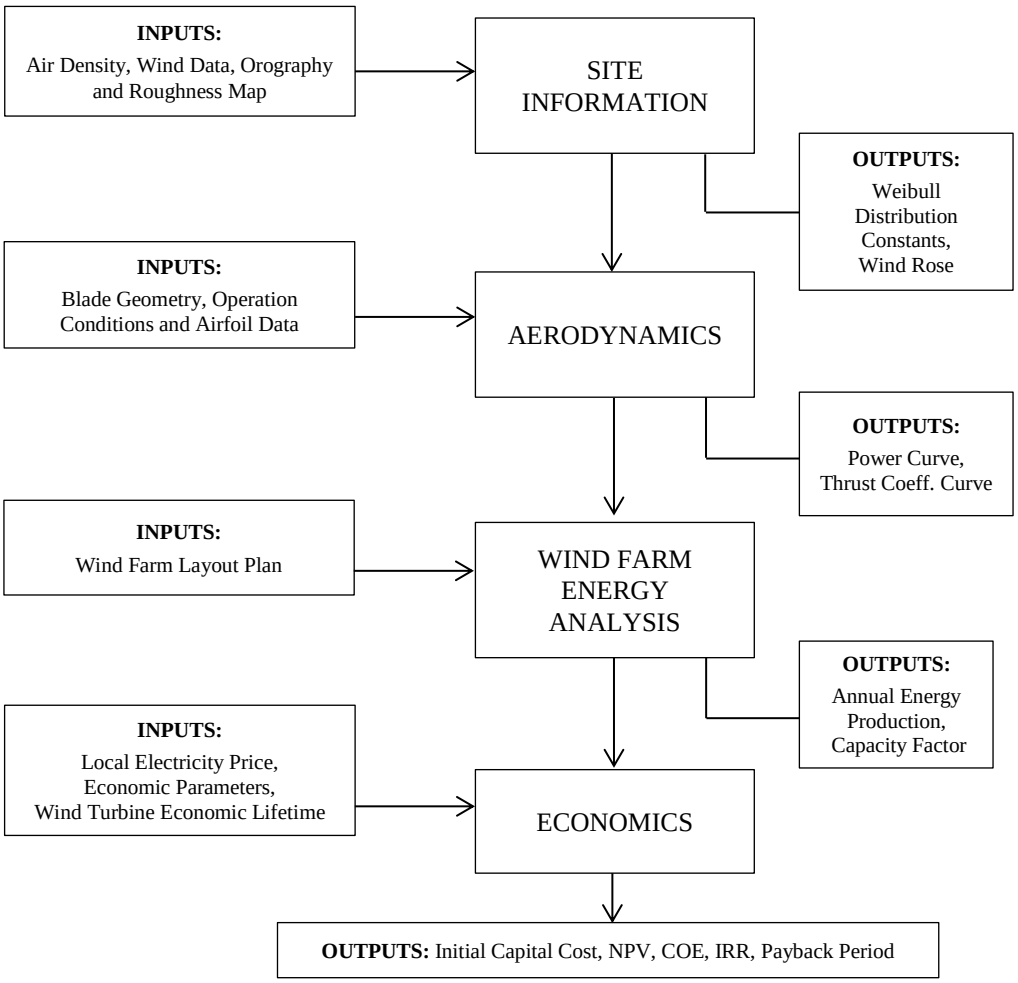

Figure 4.1: Flowchart of AEROWIND Code

4.1. Blade Element Momentum Theory

BEMT is developed by Betz and Glauert in the 1930s [1]. It is the combination of blade element theory and momentum theory. Blade element theory is associated with momentum theory to reduce the difficulties in computing the induced velocities at the rotor. It is a mathematical calculation process to understand and determine the behavior of the rotors. It is possible to compute not only the steady loads but also thrust and power according to various combination of wind speed, rotational speed and pitch angle [2]. Thus, this method is crucial to determine wind turbine performance. In this respect, this method is utilized to obtain the power and thrust coefficient curves of existing wind turbine in this research. The values of power and thrust coefficient can be tabulated according to different velocity magnitudes. Aerodynamics Tab of AEROWIND is arranged according to the theory.

Thrust coefficient is essential parameter to predict the wake losses in Wind Farm configurations. The force that is exerted from the wind in axial direction is proportional to swept area of wind turbine. Many turbine specifications which can be only provided from the wind turbine manufactures are limited in WindSim program. However, BEMT can give essential information about the wind turbine performance theoretically.

The validation process of this code is carried out with three cases. NREL Phase II and III Wind Turbines which reference data are available in literature will be used for validation. Afterwards, NREL 5MW Baseline Wind Turbine will be examined with this theoretical code to place in Wind Farm region. The results are all presented in Chapter 5.

4.1.1. Maximum Power in the Wind

Power in the wind should be researched beforehand. The interaction between the wind and rotor results in power generation. Wind turbine blades are the devices to extract the kinetic energy in the wind and they convert this energy into mechanical energy. The maximum available power for the rotor of Horizontal Axis Wind Turbines can be calculated as follows:

$$P_{\max} = \frac{1}{2}\dot{m}U_{\infty}^{2} = \frac{1}{2}\rho A U_{\infty}^{3} \tag{4.1}$$

As observed in the equation, power is proportional to the cube of wind speed, air density and rotor swept area. Power coefficient (C_p) is an important design parameter which was defined in Rankine-Froude actuator disk model [51]. Power coefficient is the ratio between the maximum available power and the observed power. This dimensionless parameter is computed as follows:

$$C_p = \frac{2P_{available}}{\rho A U_{\infty}^{3}} = \frac{2P_{available}}{\rho \pi R^{2} U_{\infty}^{3}} \tag{4.2}$$

Theoretically, this value can attain particular value and this is defined as Betz Limit [2]. This is derived from BEMT method for one dimensional model of an ideal rotor. Many assumptions are considered to examine this problem. Further explanations can be found in Refs. ([1], [2]). Betz limit indicates the maximum efficiency:

$$C_{P\max} = \frac{16}{27} = 0.593 \tag{4.3}$$

This value is only related to aerodynamic efficiency. However; other important parameters should be considered to obtain the efficiency of the whole system. These are generator, gearbox and other auxiliary devices. Their production will give power coefficient of the wind turbine. It is simply presented below;

$$\eta_{Total} = \eta_{Aerodynamic} \times \eta_{Generator} \times \eta_{Gearbox} \tag{4.4}$$

Now, it is known from Betz Limit, the maximum theoretical limit for aerodynamic efficiency of wind turbines is 0.593. The determination of tip speed ratio can give predicted power coefficients empirically by the following formula. This formula is derived in 1976 by Wilson et al. [1].

$$C_p = \frac{16}{27} \frac{\lambda}{\lambda + \dfrac{1.32 + (\dfrac{\lambda - 8}{20})^2}{B^{2/3}}} - \frac{\lambda^2}{\dfrac{C_l}{C_d}(\lambda + \dfrac{1}{2B})} \tag{4.5}$$

Noting that, three-bladed horizontal axis wind turbines are used in this study. In Figure 4.2, the trend varies according to different Lift-Drag ratio of used airfoil. It can be deduced that drag should be minimized. For the best case in the figure, the tip speed ratio can be chosen as 8. Maximum power coefficient is found as 0.51; however, in reality it drops to around 0.45 due to tip, stall and drag losses. To express the tip speed ratio, it is the ratio of tip speed velocity to free stream velocity. Speaking physically, the spanwise velocity where is perpendicular to blade rotation plane is lower than the streamwise component. Streamwise component is the result of tip speed ratio [2]. The tip speed ratio (λ) is presented below:

$$\lambda = \frac{U_{tip}}{U_\infty} = \frac{\Omega R}{U_\infty} \tag{4.6}$$

In addition to these, according to application type for high RPM speeds tip speed ratios can be selected $4<\lambda<10$ and for greater torque values tip speed ratios can be selected $1<\lambda<3$. Wake losses are dominant at low tip speed ratios and very high tip speed ratios for HAWT.

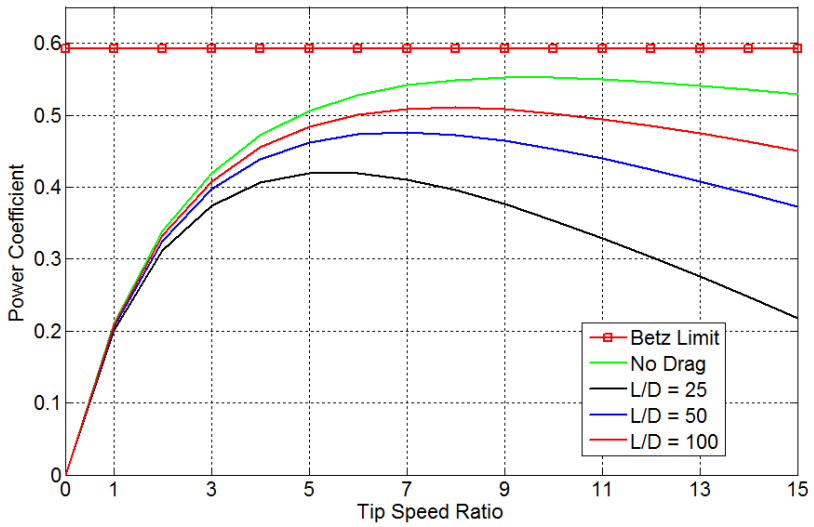

Figure 4.2: Power Coefficient versus Tip Speed Ratio for different L/D Ratios

4.1.2. Calculation of Power and Thrust Coefficient

Wind turbine blades have twisted and variable cross section areas along the length. Both effects have contributions for lift and drag forces. The cross section of the blades has airfoil shapes which are aerodynamically efficient. The pressure differences between the upper and lower surface of the blade cause lift forces dominantly. Besides that, the drag force is the main result of the wall friction forces over the blade.

Momentum theory is related to control volume analysis considering the conservation of linear and angular momentum. Wind turbine blade is divided into equivalent sections in order to determine the lift and drag forces for each element. Each blade section have own airfoil shape and chord length. Illustration of this process is presented in Figure 4.3. Many assumptions are made in this study and they are stated below ([1], [2], [51]):

- No aerodynamic interaction between the sections,
- The forces over each blade are constant,
- Wake rotation is included,
- Drag effect is included,
- Prandtl root and tip effects are included,
- Turbulent Wake State (Glauert or Buhl) is included,
- 3D effects are not included.

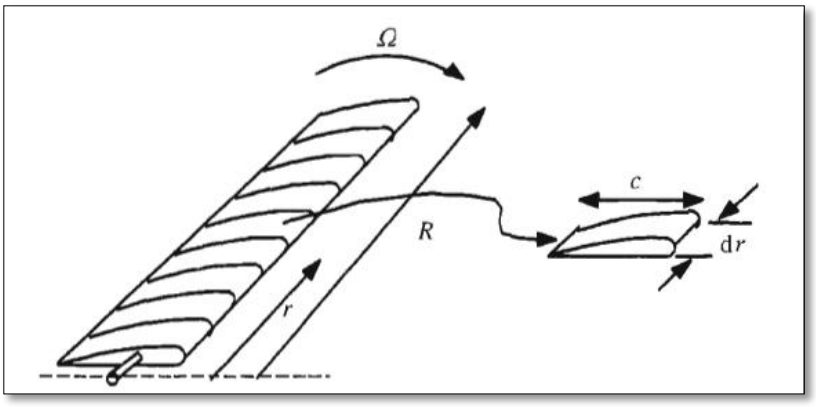

Figure 4.3: N Sections of Wind Turbine Blade [1]

Besides, the aerodynamic characteristics of airfoil are only related to its shape and Reynolds number at each section. Aerodynamic characteristics also depend on airfoil selection and it is the crucial point in the design to attain the suitable lift values and low bending moments. These features yield a wind turbine to become more power productive and low fatigues. There are criterions which should be taken into account in selecting right airfoil for wind turbines and these are stated below [1]:

- Operation Reynolds number (Re)
- Angle of attack (α)
- Lift and Drag coefficients (C_l, C_d) from polar tables
- Pitching moment (C_m)
- Maximum L/D ratio

Reynolds number can be calculated locally as follows;

$$\mathrm{Re} = \frac{\rho U c}{\mu} = \frac{\rho U_\infty \lambda_r \, c}{\mu} \tag{4.7}$$

Stream tube of a wind turbine is presented in Figure 4.4. Two important design parameters are defined in this theory:

1. Axial induction factor (a),
2. Tangential induction factor (a').

$$U_{\text{wind velocity at the rotor disc}} = U_{\text{upstream wind velocity}} \times (1 - a) \tag{4.8}$$

$$U_{\text{wind velocity at the rotor disc}} = U_{\text{downstream wind velocity}} \times (2 - a) \tag{4.9}$$

$$a' = \frac{\omega}{2\Omega} \tag{4.10}$$

In this equation, ω is induced tangential angular speed and Ω is the angular speed of the blade.

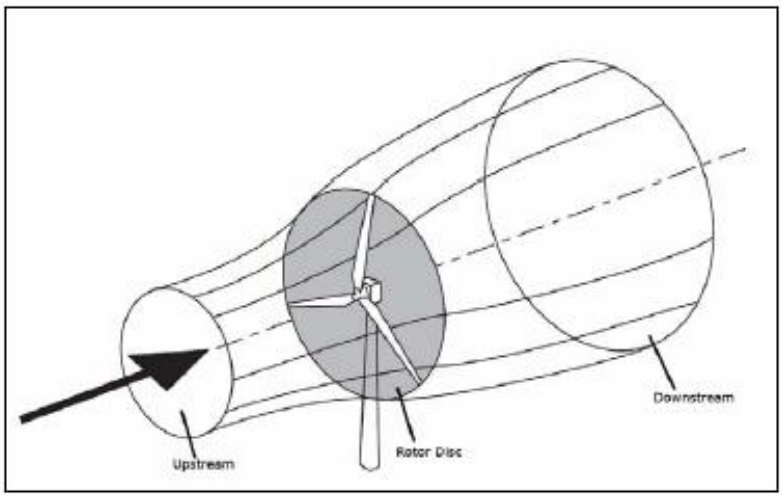

Figure 4.4: Stream Tube of a Wind Turbine [1]

These parameters are computed to obtain the rotor performance iteratively. The resulting parameters are power, thrust force, torque and blade loadings. In Figure 4.5, blade loadings can be observed over an upwind type of HAWT. As observed, thrust and driving torque are the consequences of wind speed and rotor shape. In BEMT, tangential force distribution and axial force distribution are computed for each blade element and the integration of the forces gives torque and thrust.

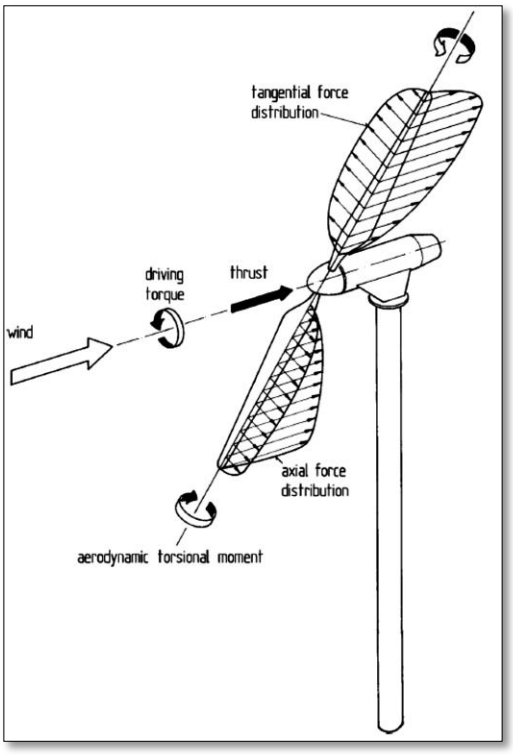

Figure 4.5: Blade Loadings on Upwind Wind Turbine [3]

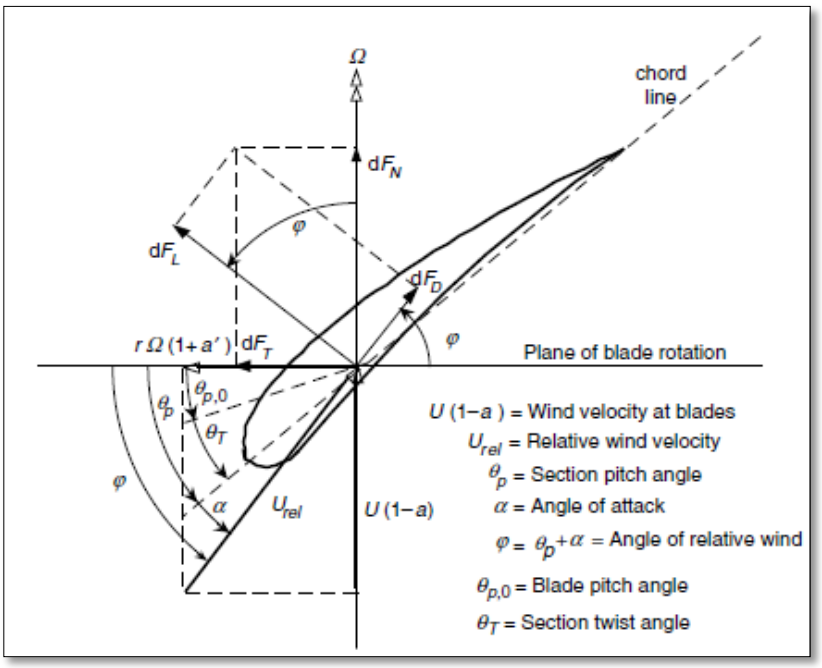

Figure 4.6: Representation of the Parameters over an Infinitesimal Airfoil [1]

In Figure 4.6, important parameters over an infinitesimal airfoil are presented. The sum of angle of attack (α) and section pitch angle (θ_p) is the angle of relative wind (φ).

$$\varphi = \alpha + \theta_p \tag{4.11}$$

$$\theta_p = \theta_T + \theta_{p,0} \tag{4.12}$$

Angle of relative wind from geometrical relations:

$$\varphi = \tan^{-1} \frac{U_\infty (1-a)}{U_{tip}(1+a')} \tag{4.13}$$

Tip speed can be computed as follows:

$$U_{tip} = \Omega R \tag{4.14}$$

With the equations (4.6) and (4.13), we can get another relation:

$$\tan\varphi = \frac{(1-a)}{\lambda_r (1+a')} \tag{4.15}$$

Local tip speed ratio is computed by this equation:

$$\lambda_r = \lambda \frac{r}{R} \tag{4.16}$$

Relative wind speed is calculated below:

$$U_{rel} = \sqrt{U_\infty{}^2 + U_{tip}{}^2} = \sqrt{U_\infty{}^2 + (\Omega R)^2} \tag{4.17}$$

Lift force and drag force over an airfoil are calculated per each blade element as:

$$L = \frac{1}{2}\rho U_{rel}^2 c C_l \tag{4.18}$$

$$D = \frac{1}{2}\rho U_{rel}^2 c C_d \tag{4.19}$$

The normal and tangential forces are computed as follows:

$$F_N = L\cos\varphi + D\sin\varphi \tag{4.20}$$

$$F_T = L\sin\varphi - D\cos\varphi \tag{4.21}$$

Local solidity is used to simplify the equations:

$$\sigma' = \frac{Bc(r)}{2\pi r} \tag{4.22}$$

B is denoted as blade number, c(r) is the local chord length and r is the radial position of midpoint of each blade element. The dimensionless force elements can be computed:

$$C_n = C_l\cos\varphi + C_d\sin\varphi \tag{4.23}$$

$$C_t = C_l\sin\varphi - C_d\cos\varphi \tag{4.24}$$

To compute axial and tangential induction factor (a), following expression are used. The local solidity expression is applied to equations.

$$a = \frac{1}{\frac{4F\sin^2\varphi}{\sigma' C_n} + 1} \tag{4.25}$$

$$a' = \frac{1}{\frac{4F\sin\varphi\cos\varphi}{\sigma' C_t} - 1} \tag{4.26}$$

The tip and root losses should be considered to predict the rotor performance accurately. Vortices can occur at tip and root region of wind turbine. The method is developed to estimate these losses by Prandtl. Tip and root losses are defined as:

$$F_{tip} = \frac{2}{\pi}\arccos e^{-f_{tip}} \tag{4.27}$$

$$f_{tip} = \frac{B}{2}\frac{R-r}{r\sin\varphi} \tag{4.28}$$

$$F_{hub} = \frac{2}{\pi}\arccos e^{-f_{hub}} \tag{4.29}$$

$$f_{hub} = \frac{B}{2}\frac{r-r_{hub}}{r_{hub}\sin\varphi} \tag{4.30}$$

Maximum chord length should be assigned at particular span of the wind turbine blade. This location is defined r_{hub} in this study. The computation is not performed between this span to root. Finally, total loss factor is computed as:

$$F = F_{hub}F_{tip} \tag{4.31}$$

Sectional thrust and torque can be calculated as follows:

$$T' = \frac{1}{2}\rho U_{rel}^2 c C_n \tag{4.32}$$

$$Q' = \frac{1}{2}\rho U_{rel}^2 c C_t \tag{4.33}$$

Trapezoidal rule is applied to find the loads of the blade sections at midpoint. Finally, total thrust force, power and power coefficient are found as follows:

$$T = B\int_{1}^{N-1} T'(r)dr \tag{4.34}$$

$$P = \Omega\, B\int_{1}^{N-1} r\; Q'(r)dr \tag{4.35}$$

$$\mathrm{C_P} = \frac{P}{\frac{1}{2}\rho U_{\infty}^3 \pi R^2} \tag{4.36}$$

Alternatively, the rotor performance can be computed from the equation [1]:

$$\mathrm{C_P} = \frac{8}{\lambda N}\sum_{1}^{N} F\sin^2\varphi(\cos\varphi - \lambda_r \sin\varphi)(\sin\varphi + \lambda_r \cos\varphi)\left[1 - \frac{C_d}{C_l}\cot\varphi\right]\lambda_r{}^2 \tag{4.37}$$

If the axial induction factor exceeds 0.4, the momentum theory is no longer applicable. This state is called as ‘‘Turbulent Wake State’’ for wind turbine operation. Thrust coefficient is calculated with axial induction factor. Empirical relations are utilized to ease the calculation of the axial induction by Glauert or Buhl. Equations (4.38) and (4.39) are based on the corrections of Glauert and Buhl, respectively. The axial induction factor is computed with

equation (4.40) below 0.4 from the annular control volume approach of momentum theory. These are stated below [52]:

$$C_T = 0.889 - \frac{0.0203 - (a - 0.143)^2}{0.6427} \qquad a \geq 0.4 \tag{4.38}$$

$$C_T = \frac{8}{9} + \left(4F - \frac{40}{9}\right)a + \left(\frac{50}{9} - 4F\right)a^2 \qquad a \geq 0.4 \tag{4.39}$$

$$C_T = \frac{2dT}{\rho U_\infty^2 2\pi r dr} = \frac{(1-a)^2 \sigma C_n}{\sin^2 \varphi} \qquad a < 0.4 \tag{4.40}$$

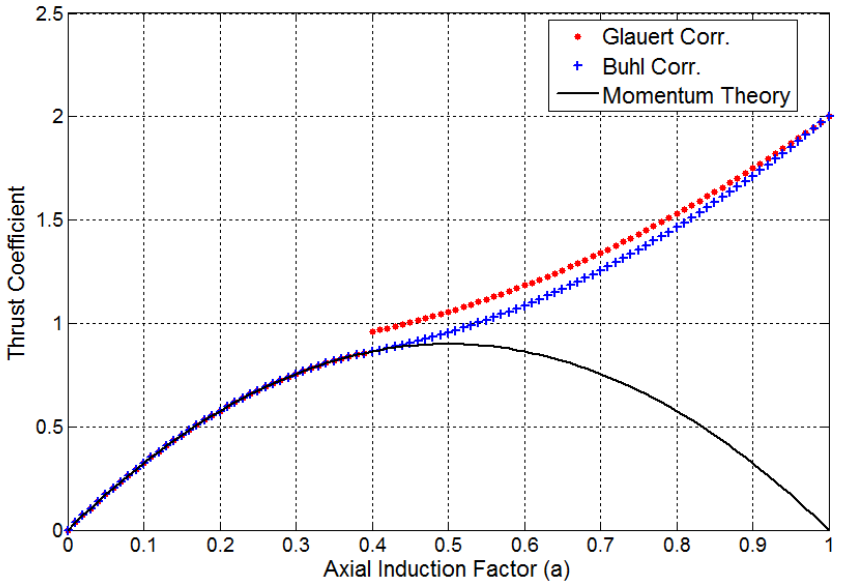

Figure 4.7: Thrust Coefficient versus Axial Induction Factor (a)

In Figure 4.7, the empirical relations are plotted with F=0.9. Lastly, this expression can be equalized with the empirical relations according to wind turbine state. Further information can be found in Refs. ([2], [11], [52], [53]). All equations are given for the BEM theory. The iteration procedure is performed to obtain axial and tangential induction parameters.

4.1.3. Optimum Blade Geometry

The blade geometry can be determined by simple calculations. Optimum blade geometry is related to chord and twist distributions. Many assumptions are applied and they are stated below [1]:

- Drag effect is neglected $C_d = 0$
- Tip losses are neglected F =1.0
- Induced velocity is a =1/3 which is the optimum value

The algorithm for the calculation of chord and twist distribution:

1. Find local tip speed ratio along the blade:

$$\lambda_r = \lambda_{Design} \frac{r}{R_{Design}} \tag{4.41}$$

2. Compute angle of relative wind, $\varphi(r)$ and convert it to degree unit:

$$\varphi_{Radian} = \tan^{-1}(\frac{2}{3\lambda_r}) \tag{4.42}$$

$$\varphi = \varphi_{Radian} \frac{180}{\pi} \tag{4.43}$$

3. Find design lift coefficient (C_{LD}) and design angle of attack (α_{Design}):

$$C_{LD} = \frac{C_l}{C_d}(\max) \Rightarrow \alpha_{Design} \tag{4.44}$$

4. Optimal twist distribution is determined by this formula:

$$\theta_p(r) = \varphi(r) - \alpha_{Design} \tag{4.45}$$

5. Find the optimal chord distribution from Betz theory:

$$c = \frac{8\pi r \sin\varphi}{3BC_l\lambda_r} \tag{4.46}$$

Alternatively, chord distribution can be computed with another formula from Schmitz theory. Further information can be found in the Ref. [54].

$$c = \frac{1}{B}\frac{16\pi r}{C_l}\sin^2\left(\frac{1}{3}\tan^{-1}\left(\frac{R}{\lambda_{Design} r}\right)\right) \tag{4.47}$$

4.1.4. Airfoil Lift and Drag Polar Generator Program

In this study, aerodynamic data is obtained at various angle of attack and Reynolds Numbers from this program. Airfoil lift and drag polar should be obtained from the wind tunnel experiments scientifically. Many experimental airfoil data can be also obtained in Ref. [55]. Another way is to perform XFOIL program which is used to find the airfoil data. Secondly, correlation method by Viterna and Corrigan is coupled with raw airfoil data to form the polar curves. Noting that, 3D effects cannot be taken into account with XFOIL and BEMT. Tangential velocity changes a lot from hub to tip. Therefore, airfoil characteristics also vary a lot from hub to tip. Consequently, they have been ignored in this study.

It is necessary to compute the airfoil data up to 90 degrees for the wind turbines. The airfoil data is precalculated according to particular Reynolds numbers. In overall, the algorithm of this program is developed according to these instructions:

1. Compute the airfoil data with XFOIL program or
   enter the experimental data of airfoil at particular Reynolds number,
2. Constitute a combined curve with two methods,
   a. If $-10 < \alpha < \alpha_{stall}$, take the raw data from Step 1,
   b. If $\alpha_{stall} < \alpha < 90$, correlate the data according to Viterna and Corrigan method,
3. Read the angle of attack (AOA),
4. Obtain the lift and drag coefficients.

XFOIL program [56] which is an open source program was developed by M.Drela. It is a potential flow solver for airfoils at subsonic range. The theory behind this code is based on Panel Method and Boundary Layer computations. Pressure distribution on the airfoil can be calculated. Therefore, lift and drag characteristics are obtained. XFOIL also have capability for inverse airfoil design but it is not used in this study. Viscous and inviscid analyses are performed with a linear-vorticity panel method. Kutta condition is utilized. The velocity distribution is acquired by Panel Method. Furthermore, the thickness of the boundary layer varies with different Reynolds number. NACA four or five digit airfoil series can be defined in this program. In addition to this feature, external airfoil profile can be also inserted. The transition factor for boundary layer computations is selected as 9 in this study. This refers to average wind tunnel situation which is in a low turbulence environment according to XFOIL descriptions [56]. Noting that, XFOIL cannot converge at all angle of attack values, especially in stall region. Therefore, following theory is utilized for post stall region.

Viterna and Corrigan correlation method is utilized to predict the aerodynamic coefficients for post stall region. This assumption which defines the rotor with zero twist angle is considered. If the maximum drag coefficient is known, it can be defined in the program. Otherwise, the maximum drag coefficient is calculated at inflow angle α=90 with the equation (4.48). Drag coefficient at this angle and aspect ratio value are enough to make this correlation. Aspect ratio can be considered as the ratio between the blade length and the sectional chord length. This theory and further information can be found in Reference ([57], [58]).

$$C_{d_{\max}} = 1.11 + 0.018 \cdot AR \tag{4.48}$$

For example, it is possible to correlate the experimental data of the used airfoil. The comparison is made for S809 between the experimental data and XFOIL results. This program also finds the best curve by using cubic spline data interpolation. Reynolds number can be selected for particular case at span 75% where the average maximum power contribution is [59]. This approach is not applied for the validation cases in this study, because the available experimental data for S809 airfoil profile is given at $1x10^6$ Reynolds number in Reference [60]. In Figure 4.8, the processed data is compared with the raw (experimental) data for S809 airfoil profile at that Reynolds number. This procedure is not applied for NREL 5MW Wind Turbine which has only 3D corrected experimental data. Airfoil coordinates are also not available [61].

Therefore, post stall characteristics of airfoil can be calculated by Airfoil Lift and Drag Polar Generator Program. To sum up, there are two options to insert the data into the program. First one is experimental data which can be provided from the literature or wind tunnel tests. Second one is XFOIL calculation which is required Reynolds numbers and the range of angle of attack values. The flowchart of the program is presented in Figure 4.9.

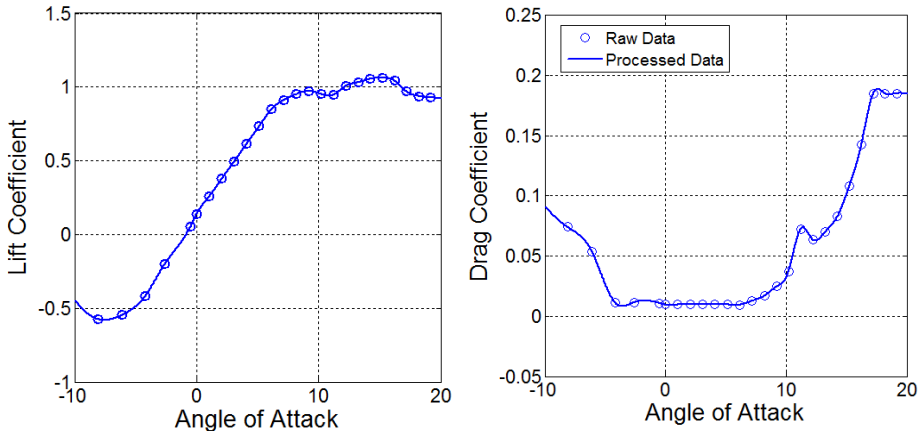

Figure 4.8: Comparison of Raw and Processed Data for S809 Airfoil at Re=1x10^6

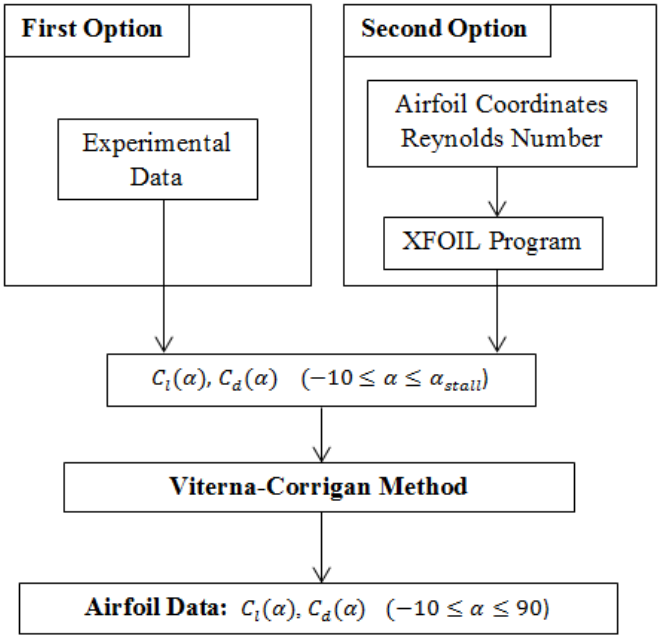

Figure 4.9: Flowchart of Airfoil Lift and Drag Polar Generator Program (α: AOA [degree])

Eventually, experimental and XFOIL data are processed in this program to obtain the necessary lift and drag polar curves. Figure 4.10 and 4.11 shows the comparison of processed experimental and XFOIL data for both coefficients. It can be observed that XFOIL agrees with the experimental data in the range of small angle of attacks because of the attached flow regime. On the other hand, the prediction is poor around the stall region because of the detached flow properties. It is tough to predict the boundary layer and separation phenomena. After this region, the predictions tend to get closer with the experimental data for both coefficients.

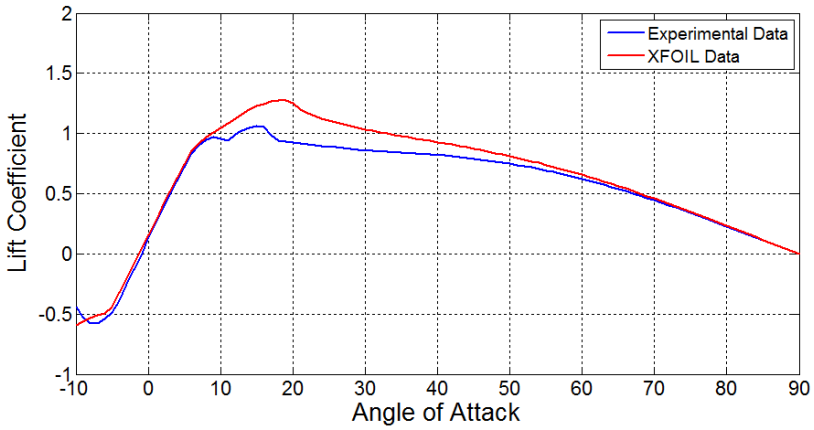

Figure 4.10: Comparison Between Experimental and XFOIL Data for Lift Coefficient for S809 Airfoil at Re=1x10^6

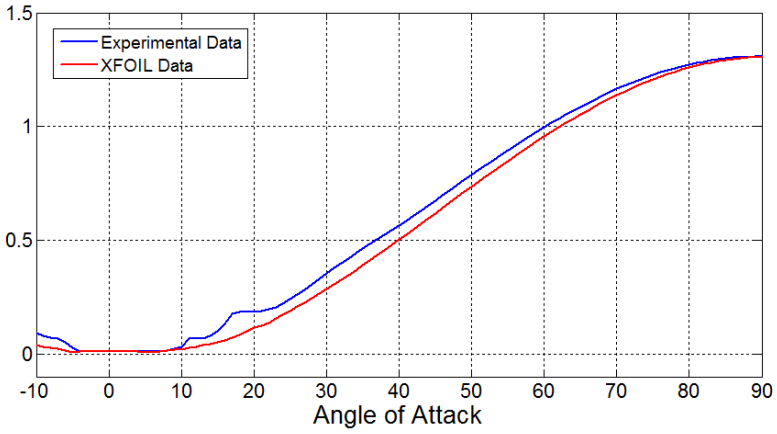

Figure 4.11: Comparison Between Experimental and XFOIL Data for Drag Coefficient for S809 Airfoil at Re=1x10^6

4.1.5. BEMT Algorithm

The validation studies and NREL 5MW Baseline Wind Turbine will be examined with the BEMT algorithm. Axial induction and tangential induction factors are computed iteratively. Two convergence histories should be checked in order to ensure the results. First one is number of sections. Second one is related to axial and tangential induction factors. The iterations are finished until the convergence occurs. The tolerance is selected as 10^{-5} in this study according to the results of sensitivity analysis. The convergence should be reached for both induction factors to proceed the thrust and power calculations. The residuals are also monitored for the divergence situations in the program.

The algorithm steps of this procedure are listed below:

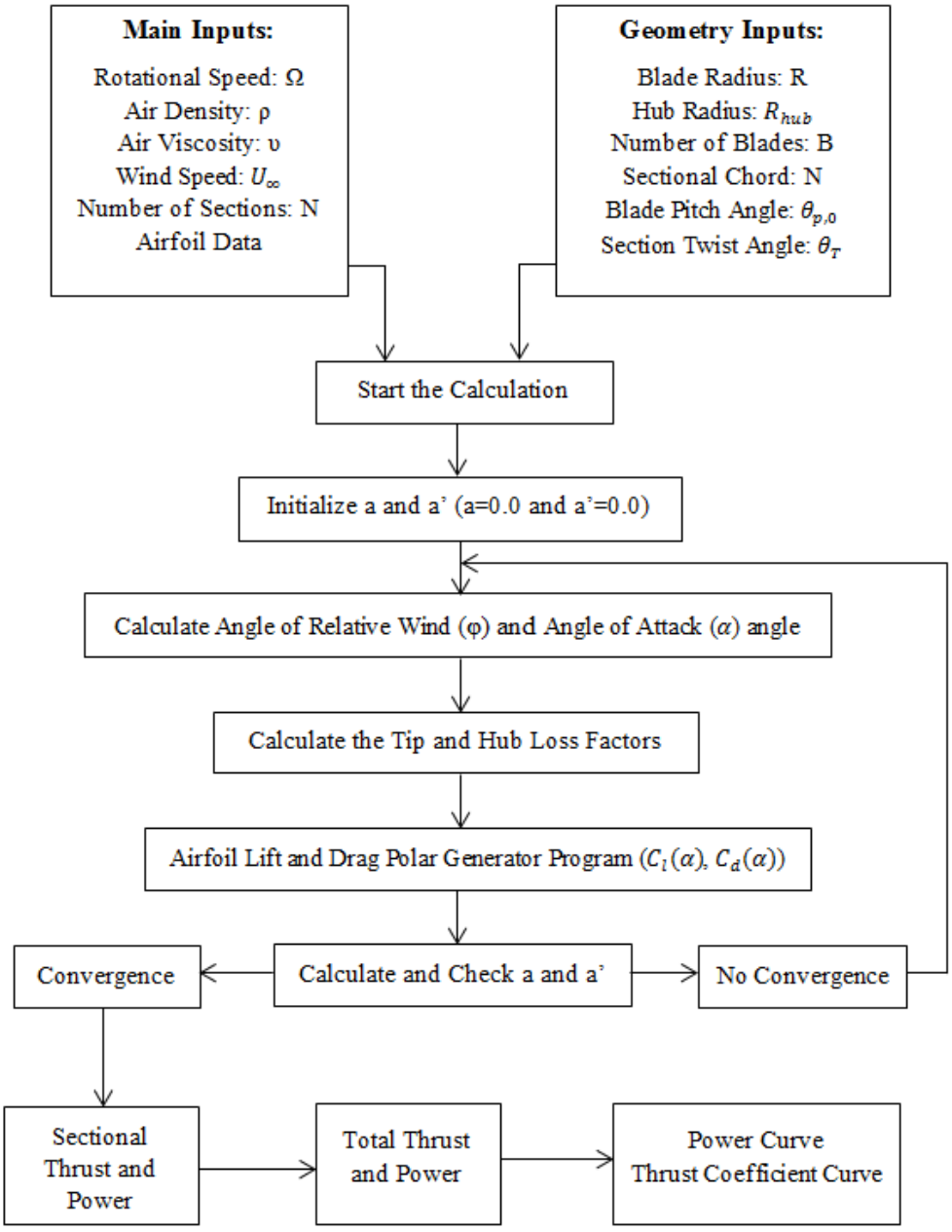

Figure 4.12: Flowchart of BEMT Algorithm

$$\Delta a = a_{new} - a_{old} \tag{4.49}$$

$$\Delta a' = a'_{new} - a'_{old} \tag{4.50}$$

4.2. Jensen Wake Model

Wind turbines extract optimum kinetic energy from the wind in order to generate electricity. While this solid-liquid interaction happens, reduction in wind speed occurs behind the wind turbine. If upwind type wind turbine is considered, lower wind speed and higher turbulence is the consequences of this event. Thus, velocity deficit causes reduction in wind energy for downwind wind turbine. Another thing is that the fatigue of downwind turbine is increased by turbulence values. However, wind speed returns to original speed after particular distance. Furthermore, when generated wake from upwind turbines encounters with the part of the downwind turbine, shadowing effect should be also computed. These processes should be taken into account to maximize the total energy in wind farm design and optimization [62].

As a rule of thumb, wake effect can be ignored 10 diameter spacing between each other. However, spacing is smaller than this value because of geographic conditions, land restrictions, cost effectiveness of system, cabling etc. Therefore, the effects should be predictable to constitute wind farm layout [63]. In this part of study, Jensen mathematical model which is widely used in wake models is explained. Shadowing effect is also added to this model to enhance the predictions. Further information can be obtained in Ref. [36]. This model is easy to code in MATLAB. This program is also favorable to couple with BEMT algorithm part of AEROWIND in-house code.

4.2.1. Single Wake Model

The main idea of this model is to expand wakes linearly. The velocity deficit depends on the distance behind the wind turbine. The conservation of momentum can be written in equation (4.51). Wake expansion is computed with wake decay coefficient (k) by equation (4.52). This coefficient can be calculated considering surface roughness by equation (4.53) [64].

$$\pi R^2 U_T + \pi (R_W{}^2 - R^2) U_\infty = \pi R_W{}^2 U_W \tag{4.51}$$

$$R_W = R + k.\,x \tag{4.52}$$

$$k = \frac{1}{2In\left(\frac{z}{z_o}\right)} \tag{4.53}$$

$$\alpha = \tan^{-1}(k) \tag{4.54}$$

The angle of deflection (α) can be computed above. Recommended values for wake decay coefficient are 0.04 for offshore turbines and 0.075 for onshore turbines in general [63]. In Figure 4.13, linear expansion of wake behind single wind turbine is illustrated. The distance from upwind turbine is denoted as x in meter.

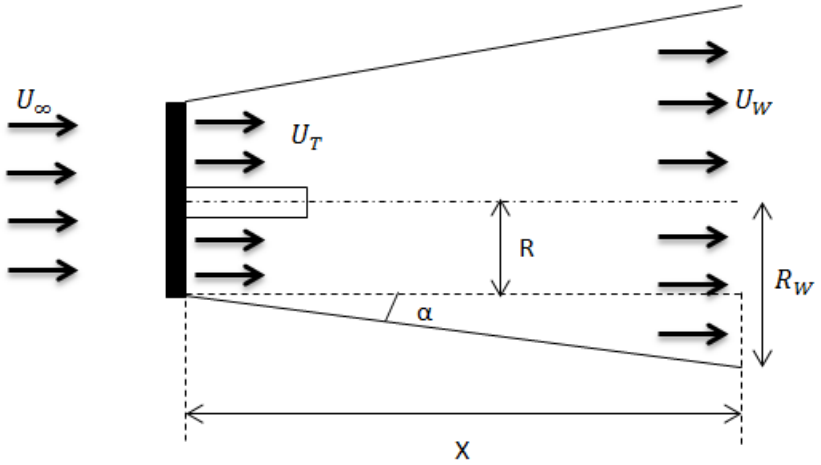

Figure 4.13: Linear Expansion of Wake behind Single Wind Turbine

The thrust coefficient can be computed in ideal conditions or it can be obtained from tables:

$$C_T = 4a(1-a) \tag{4.55}$$

The relationship between in front of and behind the wind turbine can be found:

$$\frac{U_T}{U_\infty} = 1-2a = \sqrt{1-C_T} \tag{4.56}$$

As a result, wind speed in the wake can be found in equation (4.57). Velocity deficit is plotted according to different operation conditions in Figure 4.14. According to many tabulated charts of wind turbines in WindSim, thrust coefficient values ranges from 0.80 to 0.95 at low wind speeds and they decreases to 0.10 at high wind speeds.

$$U_W = U_\infty \left(1 - \frac{2a}{\left(1 + \frac{k.x}{R}\right)^2} \right) = U_\infty \left(1 - \frac{1 - \sqrt{1 - C_T}}{\left(1 + \frac{k.x}{R}\right)^2} \right) \tag{4.57}$$

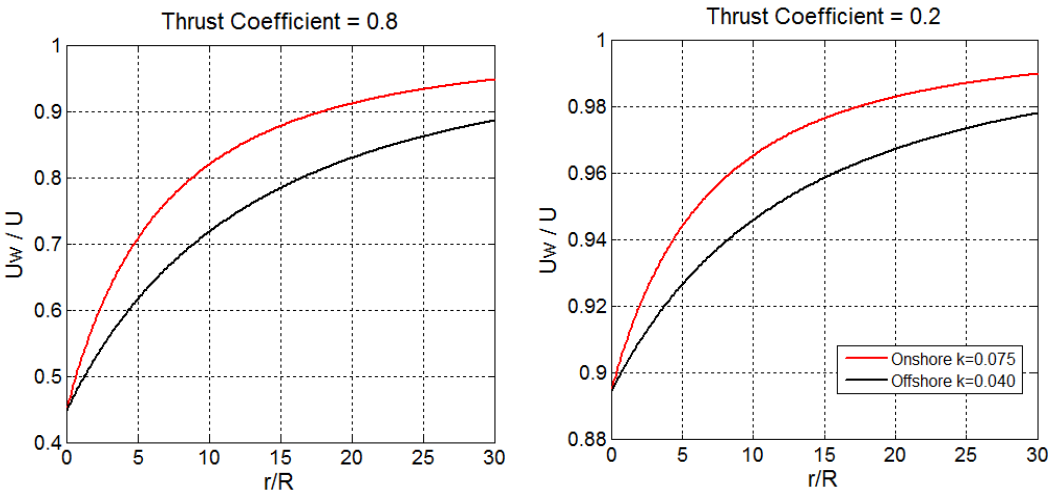

Figure 4.14: Velocity Deficit behind Wind Turbine according to Different Conditions

It can be observed in Figure 4.14, the effect of wake over velocity deficit is decreased while the distance increases between upwind side to downwind side of the wind turbine. The different patterns are found for onshore and offshore lands. Velocity deficit in offshore land is greater than onshore one. When the comparison is made for different thrust coefficients, higher thrust coefficient has more diminishing effect than lower one.

4.2.2. Multiple Wake Model

In wind farm configurations, many wind turbines are placed in selected region. The possibility of encountering several wakes increases in this type of layout. Multiple wake model is the remedy to obtain the wake effects over energy production of Wind Farm. The assumption is related to kinetic energy deficit of interacting wakes. The sum of the energy deficits is computed with every individual wakes. Example configuration is illustrated in Figure 4.15. According to notations, turbine j is affected not only from turbine i but also other turbines. If all wind turbines have same hub height and blade diameter, the swept area of upwind turbine occurs expanding wake over downwind turbine and partial shadowing occurs as illustrated in Figure 4.16 [62].

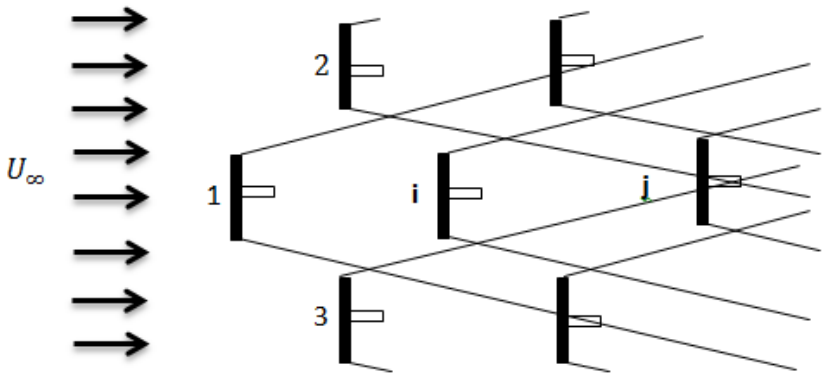

Figure 4.15: Multiple Wake Model

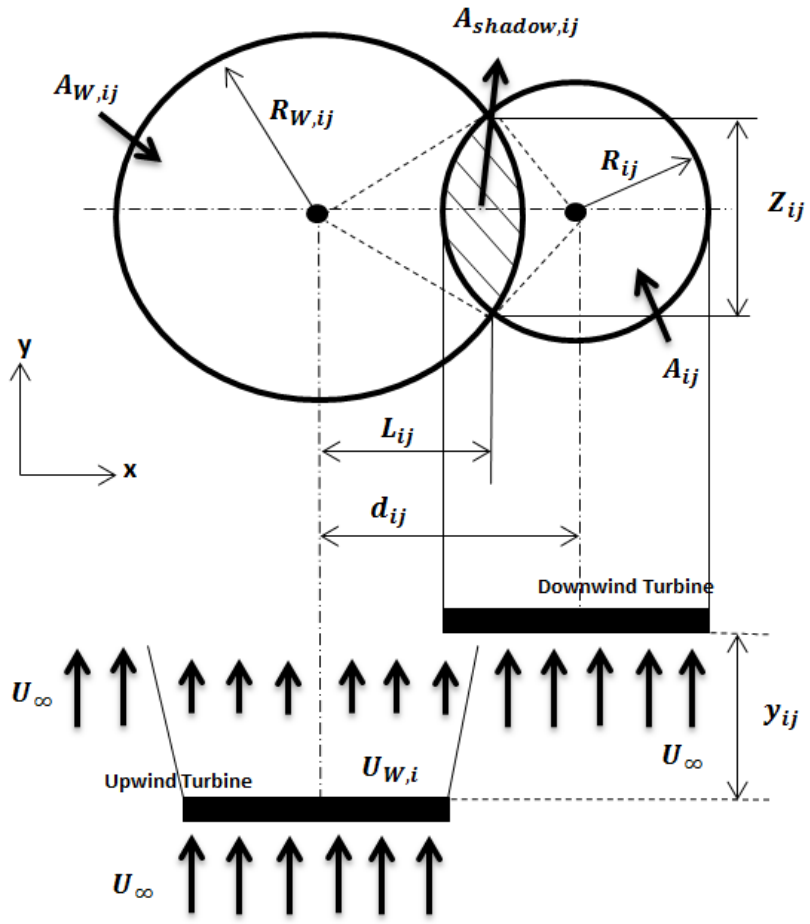

Figure 4.16: Partial Shadowing of Upwind Turbine over Downwind Turbine

$$A_{shadow,ij} = [R_{W,ij}(y_{ij})]^2 \cos^{-1}\left(\frac{L_{ij}}{R_{W,ij}(y_{ij})}\right) + R_{ij}{}^2 \cos^{-1}\left(\frac{d_{ij}-L_{ij}}{R_{W,i}(y_{ij})}\right) - d_{ij}Z_{ij} \quad (4.58)$$

$$U_j(y_{ij}) = U_i\left[1-\sum_{i=1}^{n}(1-\sqrt{1-C_T})\left(\frac{R_{ij}}{R_{W,i}(y_{ij})}\right)^2 \frac{A_{shadow,ij}}{A_{ij}}\right] \quad (4.59)$$

There are two ways to calculate wake deficits. These are stated below. The velocity deficit can be computed with the following formula [65].

$$\delta U_{ij} = U_\infty \frac{(1-\sqrt{1-C_T})}{\left(\frac{R_{W,i}}{R_{ij}}\right)^2} \quad (4.60)$$

1. Linear superposition of wake deficits

$$\delta U = \delta U_1 + \delta U_2 + ... + \delta U_n \quad (4.61)$$

2. Root-square of sum of squares of wake deficits

$$\delta U = \sqrt{\delta U_1^2 + \delta U_2^2 + ... + \delta U_n^2} \quad (4.62)$$

Main algorithm which is proposed by Chouwdhury et al. [66] is used for energy analysis in this code. However, many modifications are applied to the program in order to cover complex terrain investigations. These are related to input features of topographical and wind turbines. Different hub heights, different turbine models, altitude and wake deficit coefficients can be inserted into the program in advance. The outputs of the program are AEP and capacity factor of Wind Farm.

As presented in Figure 4.16, intersection area of two circles can be computed in analytical way. The calculation method of Jensen wake model [66] is presented in Appendix A.

4.3. Annual Energy Production and Capacity Factor

Weibull based approach is utilized for the computations. Suitable wind turbine should be selected for the site. If wind turbine is pitch-regulated type, power curve can be divided into three parts:

$$P_{curve} = \begin{cases} 0, & U < U_{cut-in} \text{ or } U_{cut-out} < U \\ P_{curve}(U), & U_{cut-in} \le U < U_{rated} \\ P_{rated}, & U_{rated} \le U < U_{cut-out} \end{cases} \quad (4.63)$$

Power production of wind turbine is computed for annual ([5], [51]):

$$E_T = Time \times \int_{U_{cut-in}}^{U_{cut-out}} P_{curve} f(U) dU \quad (4.64)$$

where ‘‘$Time$’’ term is considered as the total operation period (hours) for annual,

$$Time = 8760 \quad (4.65)$$

Therefore, total energy is the sum of two regions:

$$E_T = E_{IR} + E_{RO} \quad (4.66)$$

$$E_{IR} = Time \times \int_{U_{cut-in}}^{U_{rated}} P_{curve}(U) f(U) dU \quad (4.67)$$

$$E_{RO} = Time \times P_{rated} \int_{U_{cut-in}}^{U_{cut-out}} f(U) dU \quad (4.68)$$

Annual Energy Production is calculated as follows:

$$AEP = E_T . \eta_{\text{other}} . Availability \qquad \text{[kWh]} \tag{4.69}$$

$$\eta_{other} = (1 - Soiling\ Losses) * (1 - Array\ Losses) \tag{4.70}$$

Annual Energy Production is calculated with the consideration of availability, soiling and array losses. Soling losses are related to the lift reduction due to accumulation of insects and dirt on the leading edge of blade. The recommended value is 3.5 %. Another parameter is array losses and the recommended value is 5%. However, array losses can be selected as 0 % for this research because wake model is already used to compute the array losses. Moreover, availability can be chosen as 98% [67]. Finally, capacity factor is calculated with this formula:

$$C_F = \frac{AEP}{Time.P_R} \tag{4.71}$$

4.4. Economics

Costs of wind energy projects are divided into two parts mainly: Fixed and variable costs. Fixed costs are related to initial investment costs which are wind turbine cost and other essential components. In Figure 4.17, break up of capital cost are given for initial investment of 5MW wind energy project. Variable costs are operation and maintenance costs which can be computed as percentage of the initial investment ([5], [51]):

$$C_{OM} = mC_I \tag{4.72}$$

where $1.5 < m\ (\%) < 2$, total cost of the project can be found now:

$$C_A = C_I + C_{OM} \tag{4.73}$$

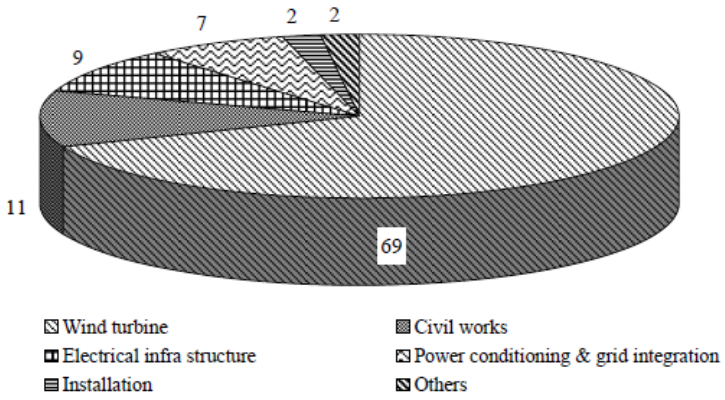

Figure 4.17: Capital Investment of 5MW Wind Energy Project [5]

Other essential component is approximately 30% of wind turbine cost. Cost of wind turbines based on the rated power can be calculated with Table 4.1 [5].

Table 4.1: Cost of Wind Turbines [5]

Size (kW)	**Cost ($/kWh)**
Up to 10	2400-3000
100	1250-2000
250 and above	700-1000

The apparent rate of escalation, corrected for inflation is as follows:

$$e_a = \{(1+e)(1+IR)\} - 1 \tag{4.74}$$

Therefore, the real rate of discount is computed for both inflation and escalation:

$$I_{real} = \frac{1+I}{1+e_a} \tag{4.75}$$

Net present value of all costs is computed as:

$$NPV(C_A)_{1-n} = C_I \left[1 + m \left[\frac{(1+I)^n - 1}{I(1+I)^n} \right] \right] \tag{4.76}$$

Cost of operation for annual is calculated with present value approach:

$$NPV(C_A) = \frac{NPV(C_A)_{1-n}}{n} \tag{4.77}$$

Cost of wind generated electricity can be computed with following equation:

$$COE = \frac{C_A}{E_T} = \frac{NPV(C_A)}{AEP} = \frac{C_I}{8760n} \frac{1}{P_{Rated} C_F} \left[1 + m \left[\frac{(1+I)^n - 1}{I(1+I)^n} \right] \right] \tag{4.78}$$

Electricity generation tariffs are important parameter to take into account in wind energy projects. The accumulated value of all benefits over the life of the project is calculated with following equation:

$$B_A = AEP \text{ x Electricity Price} \tag{4.79}$$

For sure, net present value of all benefits should be obtained:

$$NPV(B_A)_{1-n} = B_A \left[\frac{(1+I)^n - 1}{I(1+I)^n} \right] \tag{4.80}$$

Payback period is important economic criterion for every investor. Afterwards, the net present value is calculated by subtracting annual operation and maintenance costs from net present value of benefits.

$$NPV = NPV(B_A)_{1-n} - \left\{ C_I + NPV(C_A)_{1-n} \right\} \tag{4.81}$$

Benefit cost ratio can be obtained:

$$BCR = \frac{NPV(B_A)_{1-n}}{C_I + NPV(C_A)_{1-n}} \tag{4.82}$$

Additionally, payback time can be computed with:

$$n_{PayBack} = -\frac{In\left[1 - \frac{IC_I}{B_A - mC_I}\right]}{In(1+I)} \tag{4.83}$$

Eventually, internal rate of return (IRR) is the discount rate when the net present value of the project approaches to zero in years. This is the consequence of being equality for accumulated present value of all costs and the benefits. IRR can be calculated with trial and error method by this formula:

$$B_A\left[\frac{(1+IRR)^n - 1}{IRR(1+IRR)^n}\right] = C_I\left[1 + m\left(\frac{(1+IRR)^n - 1}{IRR(1+IRR)^n}\right)\right] \tag{4.84}$$

CHAPTER 5

RESULTS AND DISCUSSIONS

In the first part of this chapter, terrain and roughness map of the case study are defined in WindSim beforehand. In first part of this chapter, site survey is carried out by using WindSim. Grid dependency and influence of turbulence models are investigated by performing data analysis. Offshore and onshore sites are selected to proceed with the energy analysis.

Secondly, economic analysis is calculated in order to overview the possible economic cost models by sensitivity analysis. The methodology of present worth approach is utilized. The effects of wake loss over COE and payback period are also researched in wide range.

In the third part, BEMT and Jensen wake model algorithm parts of AEROWIND code is applied to some cases in order to ensure the functionality and employability of in-house code. Firstly, validation studies are conducted with NREL Phase II-III and NREL 5MW Baseline Wind Turbines are used. Power curve and thrust coefficient are tabulated. Secondly, Horns Rev Wind Farm is examined with Jensen wake model.

In the fourth part, Offshore and Onshore Wind Farms are investigated with parametric study. Different layouts are compared for total energy production and wake losses.

5.1. Site Selection Using WindSim

The analyses were performed with the available terrain and wind data. It should be emphasized that long term measurements, thermal measurements, more met stations and multi anemometers can improve the flow model significantly. However, the available data is enough to show the methodology of the study and to obtain the scientific results. Firstly, the grid dependency study was conducted to ensure the stability of the parameters. Secondly, the results of different turbulence models were presented and the comparisons were made. Wind Resources Module of WindSim provides necessary information to choose the site selection. Lastly, two wind farm sites are chosen according to the results of WRA study.

5.1.1. Grid Dependency Study

Four mesh types were introduced in Section 3.4. Coupled solver and k-epsilon turbulence model are used in this investigation. All settings which are recommended for complex terrain solutions are selected. Main reasons are explained in Section 3.3. Settings of numerical model in WindSim are stated in Table 5.1. The iteration numbers depend on the model. The residual values were examined in Wind Field Module. Since the cell number increases, the iteration numbers will go up. The default one is 100 iterations.

Table 5.1: Settings of Numerical Model

Boundary Conditions	
Height of the Boundary Layer	500 m
Speed Above Boundary Layer	10 m/s
Top Boundary Conditions	Fixed Pressure
Physical Models	
Potential Temperature Equation	Disregard Temperature Equation
Air Density	1.225 kg/m^3
Turbulence Model	k-epsilon model
Solver Settings	
Solver	Coupled (Algebraic Multi Grid Solver)
Iteration Numbers	Variable

This study is essential to ensure that the solution is independent from the grid size. To determine the optimum mesh type there are many ways to research the original mesh for the following investigations. The monitored parameter should be chosen properly for every CFD problem. In this study, the main flow variables can be obtained at first hand for every sector by Results Module. However, numerous comparisons can be made for grid dependency study. Besides, there is no output file for this kind of investigation in WindSim.

The computations of other variables are all related to these flow variables. This means that if there is an error, it increases according to used equation. Another monitored parameter is the vertical mean velocity profiles at selected nodes in Wind Resources Module. WindSim program gives the 2D mean velocity magnitude for all nodes in the domain. However, the accumulation of the results is utilized considering all wind sectors. Wind Resource Map is constituted by weighting the wind database against the climatology. The climatology objects considered as information source and interpolation of the inverse distance to the climatology objects forms the wind map over the terrain [38]. 2D mean velocity is calculated from the simulation results as follows:

$$\text{Mean Speed 2D} = \sqrt{U^2 + V^2} \tag{5.1}$$

Thereby, some errors can occur due to this calculation. Proving that the error percentages of velocity magnitudes along the lines are monitored among the simulations, the original mesh can be investigated in following approach. The horizontal planes are selected as 20 and 50 meters above from the terrain. Another objective is to research the variations due to height. The variations of mean velocity speed over the planes are plotted along horizontal and vertical lines. WindSim program already gives 2D Mean Velocity Magnitudes at the selected altitude from the terrain. Node-based text file data is handled by using data analysis in MATLAB. Small program is developed to find the velocity magnitudes along the horizontal or vertical lines. In order to consider the different mesh types, interpolation is made to approach main cross section. In Figure 5.1, the horizontal and vertical lines are shown. They almost intersect with the midpoint of the edges.

The coordinates are stated for both directions as:

- Horizontal Line: Y = 4102510.5
- Vertical Line: X = 530560.5

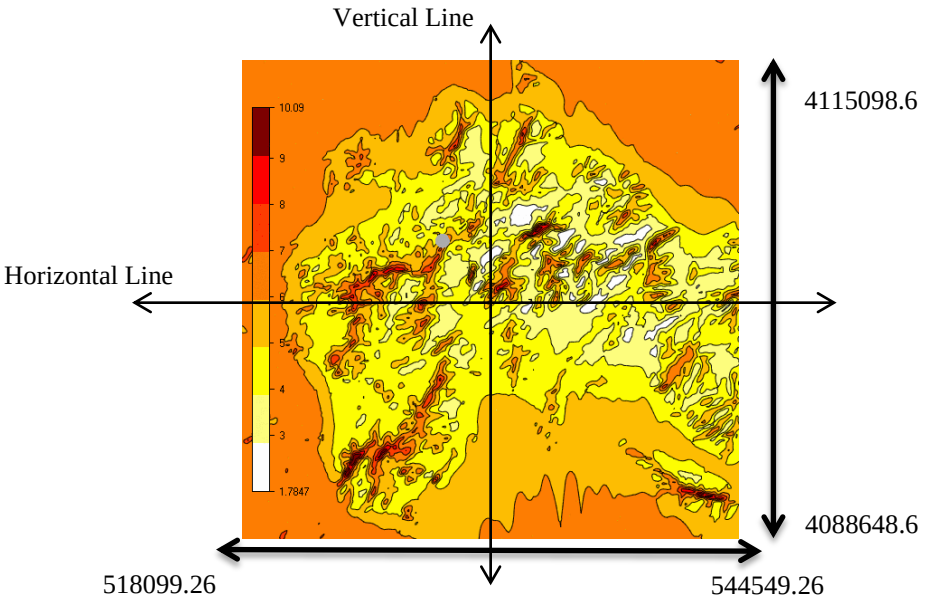

Figure 5.1: Horizontal and Vertical Lines Over the Domain

The variations of altitudes along the horizontal and vertical lines are presented in Figure 5.2 and 5.3, respectively. Noting that, the height of selected horizontal plane should be added to the values in the graphs in order to reach the altitude of the nodes. In this research, this investigation is described as line-based.

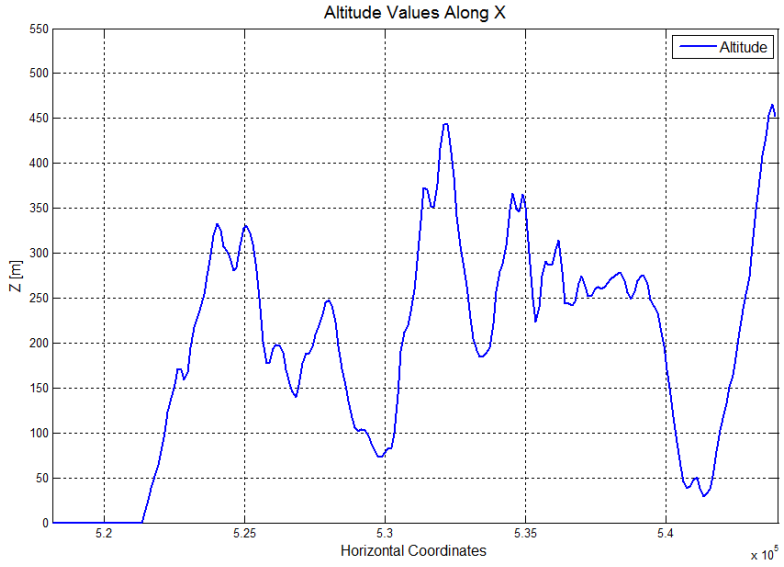

Figure 5.2: Altitudes along the Horizontal Line (West-East) just above the Terrain

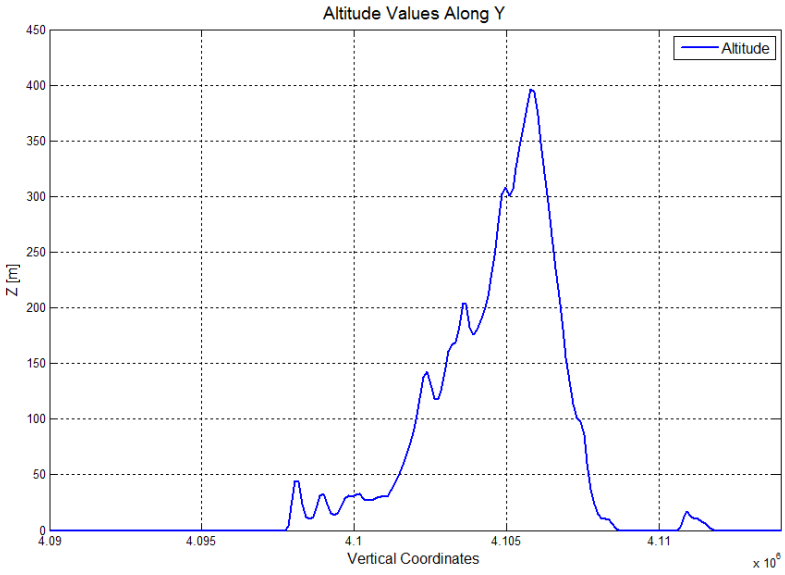

Figure 5.3: Altitudes along the Vertical Line (South-North) just above the Terrain

Following figures are related to velocity magnitudes along the horizontal and vertical line at different altitudes. Error between the mesh types can be observed easily from the following graphs. In overall, it can be deduced that Mesh 3 and 4 have almost same results along both lines.

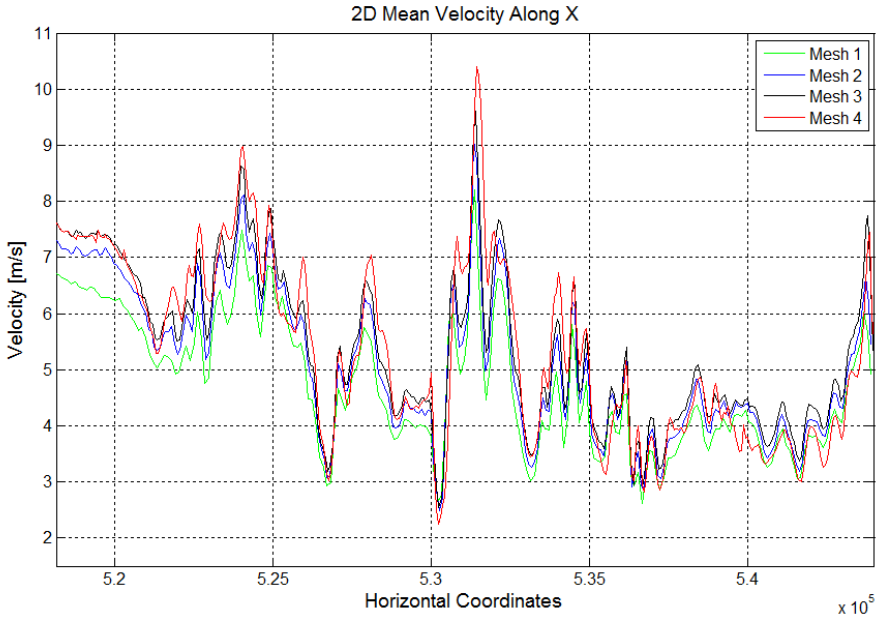

Figure 5.4: Velocity Values along the Horizontal Line at 20 m Height above the Terrain

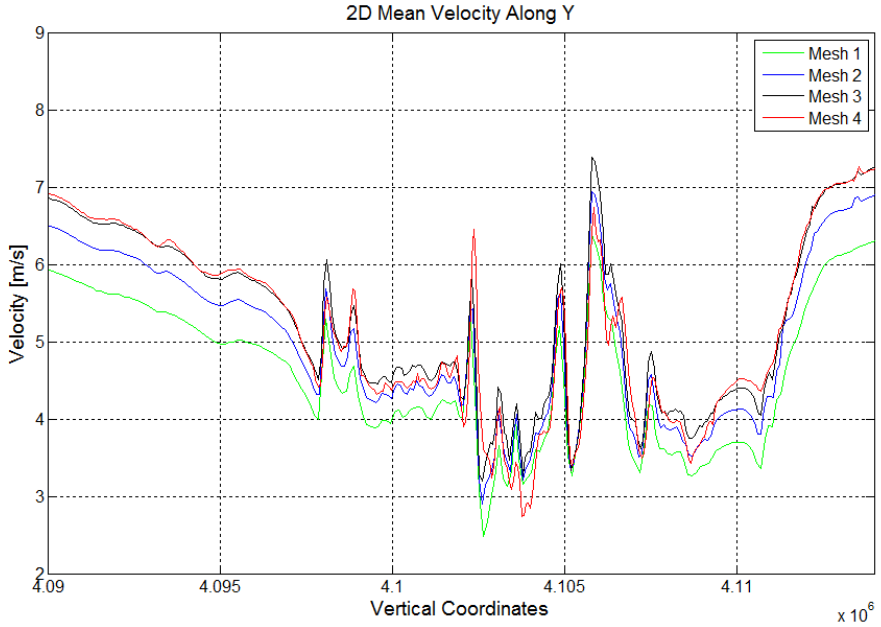

Figure 5.5: Velocity Values along the Vertical Line at 20 m Height above the Terrain

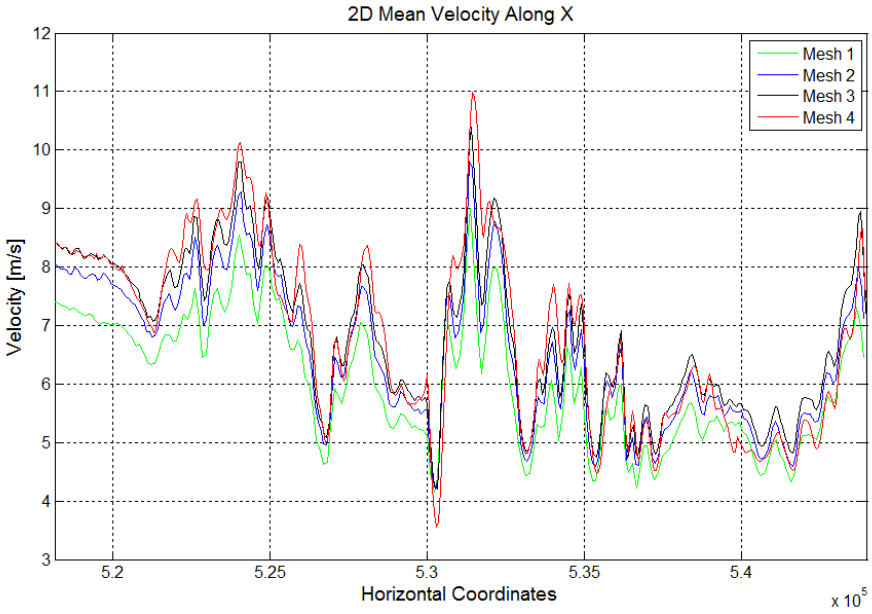

Figure 5.6: Velocity Values along the Horizontal Line at 50 m Height above the Terrain

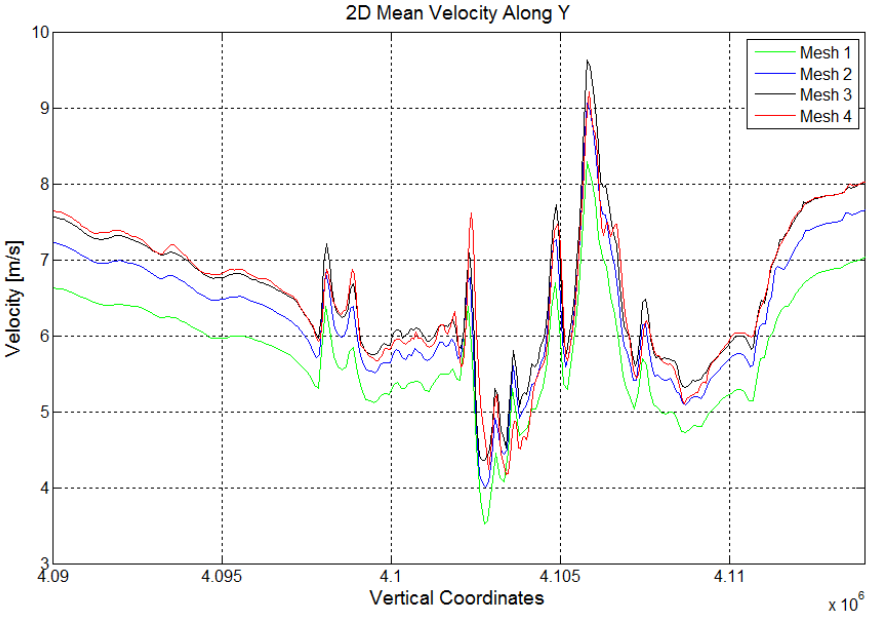

Figure 5.7: Velocity Values along the Vertical Line at 50 m Height above the Terrain

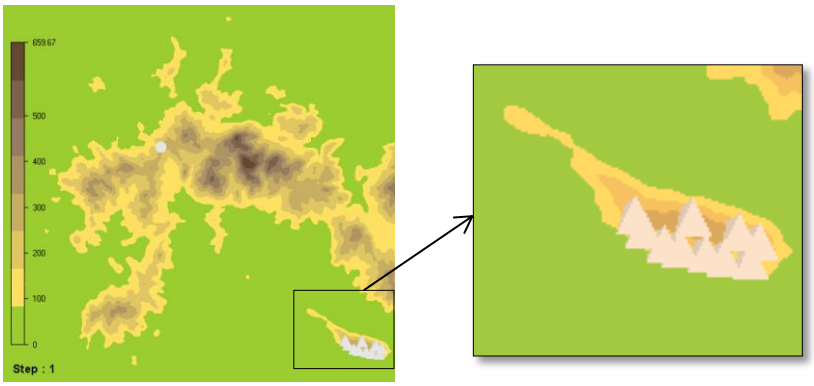

Figure 5.8: Arbitrary Wind Farm Configuration on Black Island

Secondly, an arbitrary Wind Farm configuration are arranged to investigate AEP values with simulations of the prepared grids. Wind Farm location is shown in Figure 5.8. Ten wind turbines are spread over Black Island (Kara Ada) randomly. Jensen wake model is included in the simulation. As seen in Table 5.2, the difference of estimation between Mesh 3 and Mesh 4 are within 2.9%. This error is an acceptable error to determine the original mesh in CFD [40]. It should be stressed that the grid characteristics is related to its resolution. Higher cell numbers are needed to reduce the discretization errors. If the computation time is considered, the original grid can be chosen as Mesh 3 according to all findings.

Table 5.2: AEP Values for Different Meshes

	Cell Numbers	**AEP [GWh/year]**
Mesh 1	1412190	52.793
Mesh 2	2723560	59.688
Mesh 3	4236320	63.146
Mesh 4	6493800	64.972

5.1.2. Computer Hardware and Computation Time

Computation time is an important issue for CFD projects. First of all, computer hardware is the key factor to speed up the CFD simulations. The computer hardware that is used in this research is presented in Table 5.3.

Table 5.3: Computer Hardware

Computer	Dell Precision T7400 Workstation
Processors	8 Intel Xeon CPUs - X5472 3.00 GHz
Installed RAM	16.0
Operating System	Windows 7 - 64 bit

Domain discretization, turbulence model, convergence criteria and analysis type (steady or unsteady) are the main reasons to change the computation time in CFD. As mentioned before, all the analyses are steady state in WindSim. The original grid is selected as Mesh 3 in accordance to convergence and accuracy in Section 5.1.1. The iteration number for every case is chosen manually according to spot values and convergence values in WindSim. The iteration number should be limited to reasonable margins. This criterion reduces the computing time remarkably.

An arbitrary node is chosen to monitor Speed Scalar XYZ (3D velocity) parameter in advance. This node is located in the middle of the terrain at ground level for every case in this study. To ensure the convergence of the values, spot values and convergence history are examined. Flow variables and derived variables are obtained for every iteration procedure at the selected spot node. Minimum and maximum values are scaled in the spot value monitor. Residual value monitor in WindSim is scaled according to the error (%) of the numerical solution. Spot value and residual value monitors are illustrated for particular case in Figure 5.10. Residual Root Mean Square (RMS) errors are checked in results file and it reduces to the order of magnitude of 10^{-4} for all sectorial simulations of cases. It is an acceptable value for CFD projects [40].

Lastly, the computation times for different cases are presented in Table 5.4. The simulation of Mesh 4 is the longest one among the mesh types as predicted. If a comparison is made excluding standard k-epsilon (because iteration number is not 120) among used turbulence models with Mesh 3, the simulation based on Modified k-epsilon turbulence model lasts more than others.

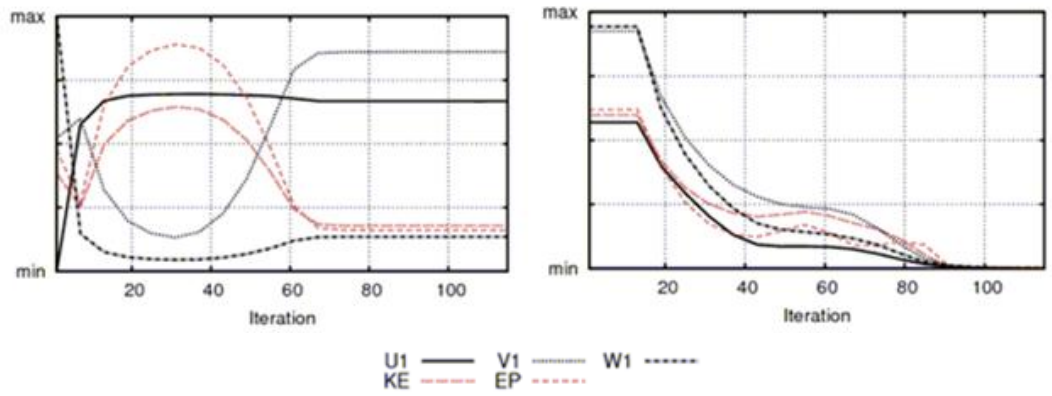

Figure 5.9: Spot Value Monitor and Residual Value Monitor for Original Mesh and Sector 0 degree

Table 5.4: Computation Times for Different Cases

Turbulence Model	Mesh Type	Iteration Number	Computation Time
Standard k-epsilon	*Mesh 1*	85	8h 24min
Standard k-epsilon	*Mesh 2*	100	19h 27min
Standard k-epsilon	*Mesh 3*	110	35h
Standard k-epsilon	*Mesh 4*	120	55h
Modified k-epsilon	*Mesh 3*	120	40h 33min
k-epsilon with Yap correction [44]	*Mesh 3*	120	37h 59min
RNG k-epsilon	*Mesh 3*	120	39h 55min

5.1.3. Comparison of Turbulence Models

Selected nodes are located as shown in Figure 5.10. In order to observe different flow characteristics, nodes are pinpointed at specific regions of the domain. Their coordinates are given respect to original mesh as stated in Table 5.5. The roughness lengths at the nodes are also given. The comparisons are conducted in two ways.

Figure 5.10: Selected Nodes in the Solution Domain

Selected nodes are located in following areas: over the sea (node 1), over the hillside (node 2), top of the hill (node 3), on the top of the island (node 4).

Table 5.5: Coordinates of the Nodes and Roughness Lengths around the Nodes

	Original Mesh (Mesh 3)			
	X	**Y**	**Z**	**Roughness Length [m]**
Node 1	522117	4091220	0	0.0001
Node 2	524691	4101438	248	0.35
Node 3	534051	4103934	658	0.75
Node 4	541305	4092156	307	0.75

The terrain with roughness model is considered for this investigation. The used turbulence models are Standard k-epsilon, Modified k-epsilon, k-epsilon with Yap correction, RNG k-epsilon.

Noting that, the resolutions of the grid are not sufficient to examine turbulence research. As discussed earlier, the computer hardware is not enough to construct finer mesh over this great extent of region. Therefore, it is not possible to detect the differences between the turbulence models. The effect of turbulence model on AEP cannot be also detected.

The expectation can be validated in the following figures. Firstly, 2D mean velocity is plotted at 20 and 50 m altitudes along the horizontal and vertical lines.

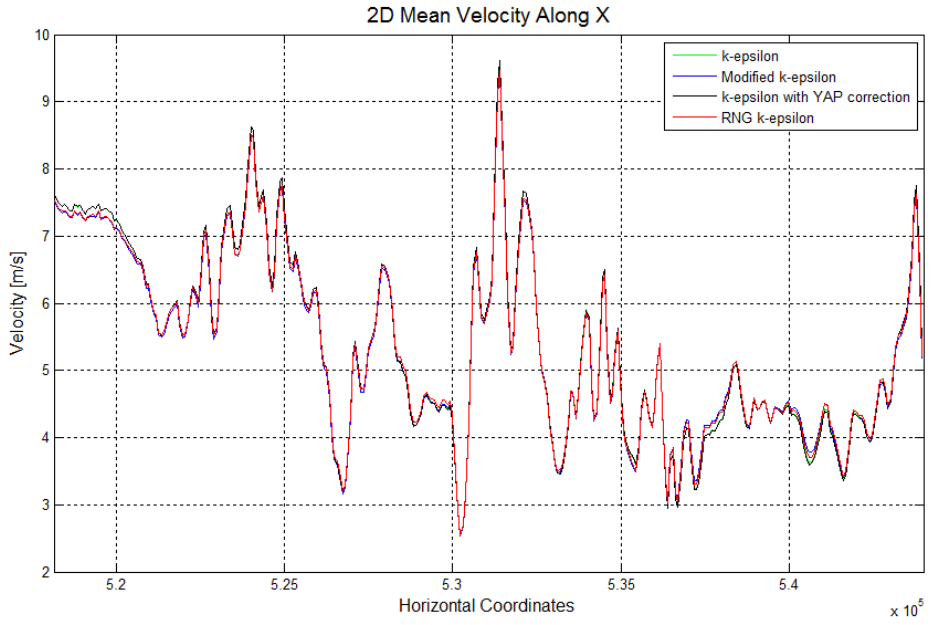

Figure 5.11: Velocity Values of Turbulence Models along the Horizontal Line at 20 m Height above the Terrain

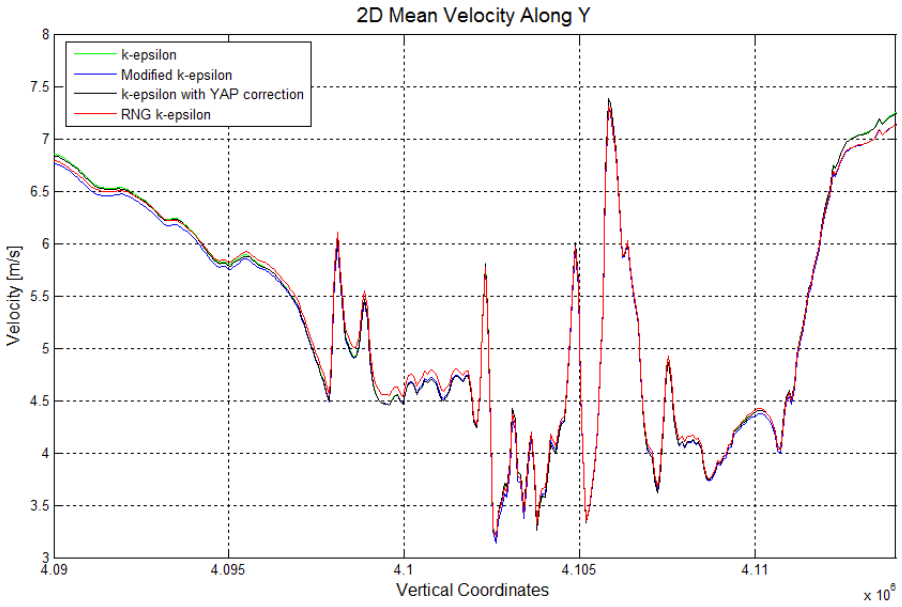

Figure 5.12: Velocity Values of Turbulence Models along the Vertical Line at 20 m Height above the Terrain

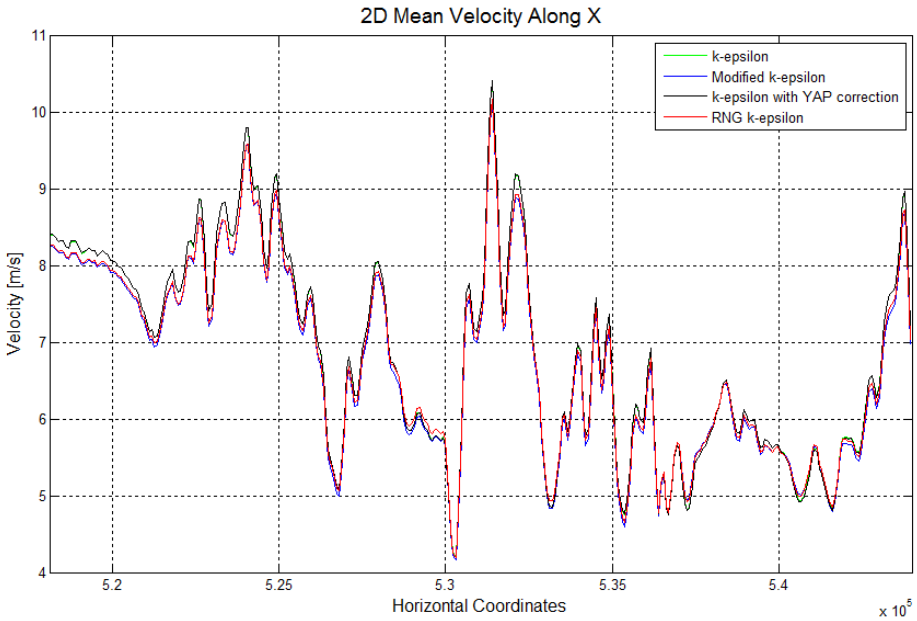

Figure 5.13: Velocity Values of Turbulence Models along the Horizontal Line at 50 m Height above the Terrain

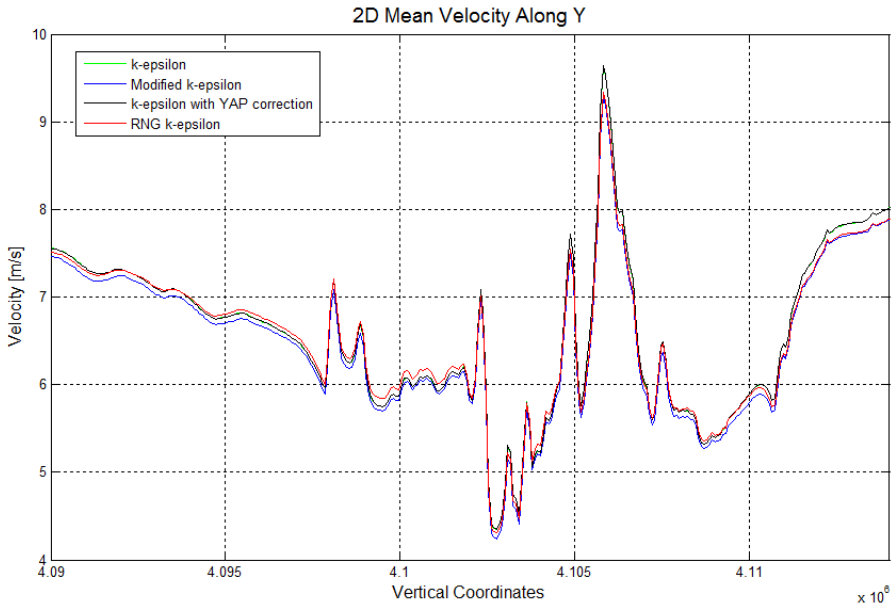

Figure 5.14: Velocity Values of Turbulence Models along the Vertical Line at 50 m Height above the Terrain

It can be deduced that k-epsilon and k-epsilon YAP correction turbulence models gives almost same results. Modified k-epsilon and RNG k-epsilon turbulence models also give similar results but some differences are observed along the lines. Furthermore, first two turbulence models predict the velocity magnitudes more than other two turbulence models. In addition to these, the tendencies of all turbulence models are very similar. There is also no significant difference according to height variations.

The mean velocity profiles are also plotted at different heights. It is not recommended to use the results of any parameter below the first computational node over the terrain in WindSim. The reason is that the program tries to interpolate the existing values linearly, but this is very rough approximation and inaccurate results can occur. Therefore, the values between 0-10 m above the terrain are not presented in this study [42]. The heights are chosen as 10, 20, 30, 40, 50, 80, 100, 120, and 150 meters from the terrain. Vertical mean velocity for different nodes varies with height as shown in Figure 5.15.

The node based research shows the similar inferences about the turbulence models. The difference between first and second group models increases with the height variation. In overall, the differences are not very significant.

Nevertheless the differences cannot be detected in this research, the methodology can be applied to finer meshes in order to make a comparison among the turbulence models.

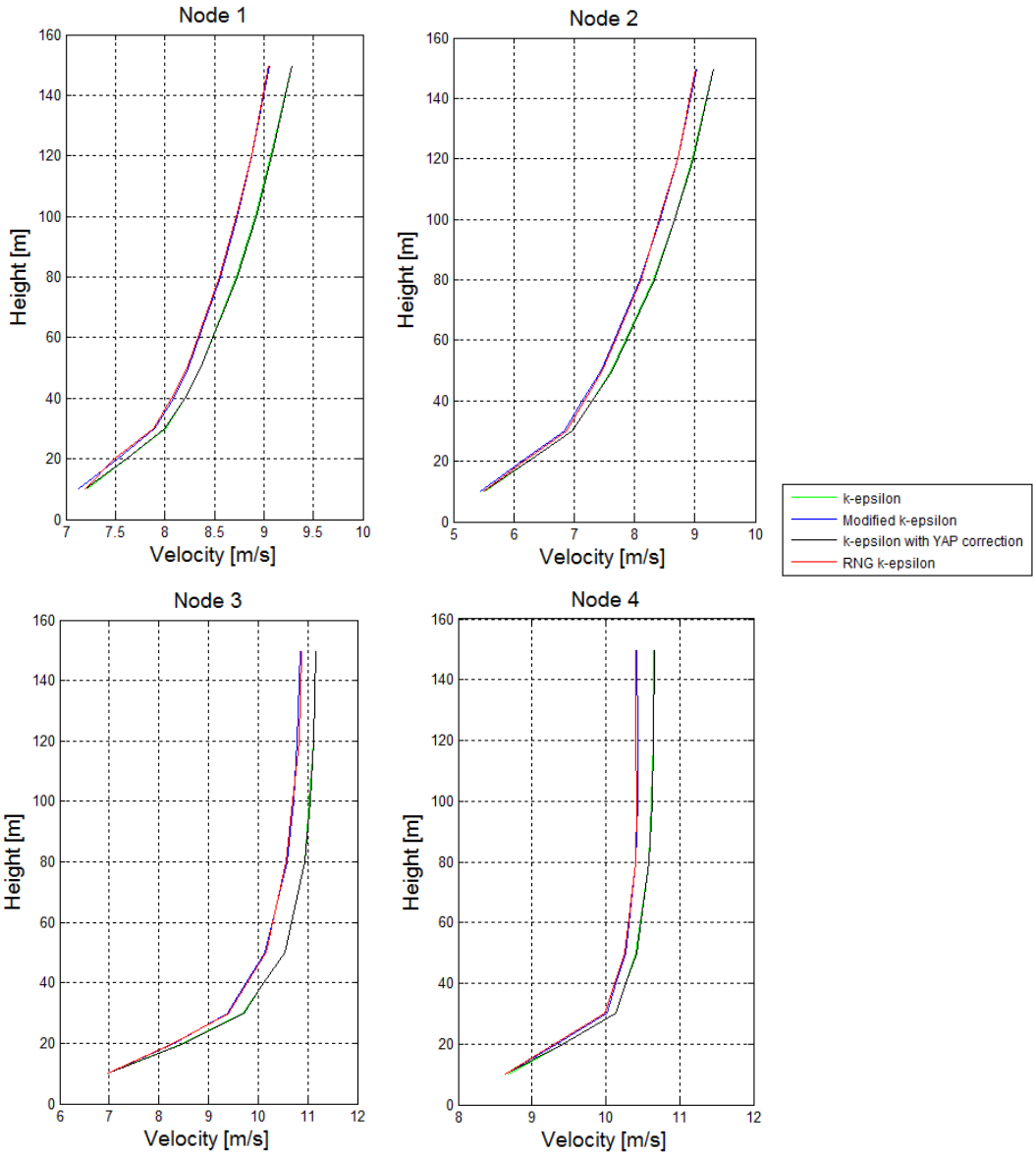

Figure 5.15: Variations of Vertical 2D Mean Velocity Values at Specific Nodes

5.1.4. Wind Resource Assessment Study and Site Selection

Wind Resource Module gives the 2D mean velocity over the terrain at particular heights. This module has a tool for area classification. The areas are classified according to the wind speed and size. In Figure 5.16, wind resource map at particular heights are presented. The wind energy potential can be investigated with these maps. Wind Farm can be established in the area which has high velocity values and stable vertical 2D mean velocity profile. The reference attitude can be selected for the hub height of the designed wind turbine.

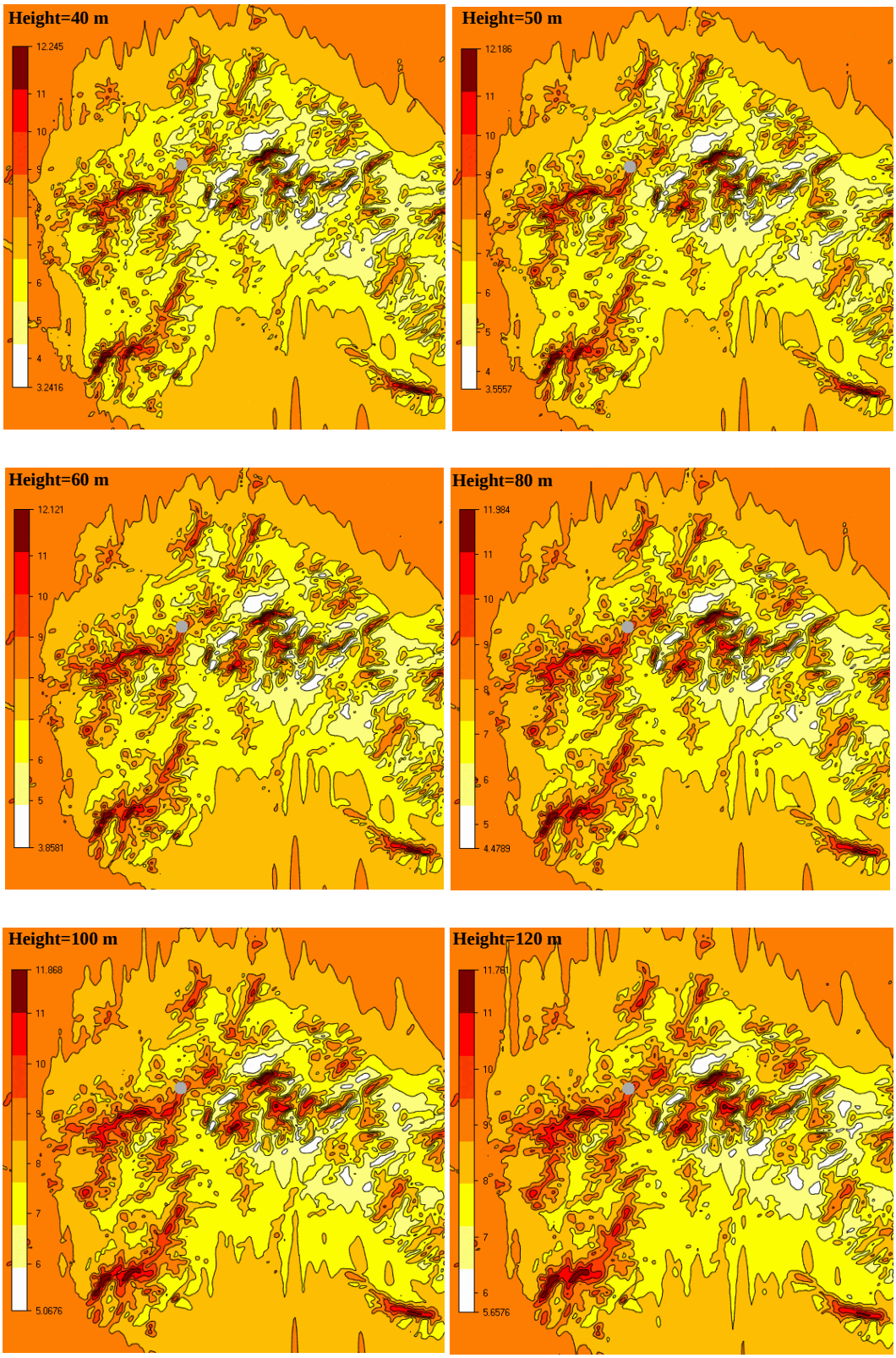

Figure 5.16: Wind Resource Maps at Particular Heights (40, 50, 60, 80, 100, 120 m)

Site selection is the following procedure after wind resource assessment study. Hub height is selected as 100 meters above the terrain in this study. The wind farm locations are determined as shown in Figure 5.17 and 5.18. First site is offshore and second one is onshore site. The priority is not to select highest wind energy potential region in this study. First site is Offshore and second one is Onshore Wind Farm. NREL 5MW Baseline Wind Turbine is selected as wind turbine type in wind farms. Wind farms are assumed to consist of nine wind turbines and the total installed capacity is taken to be 45MW as a case study.

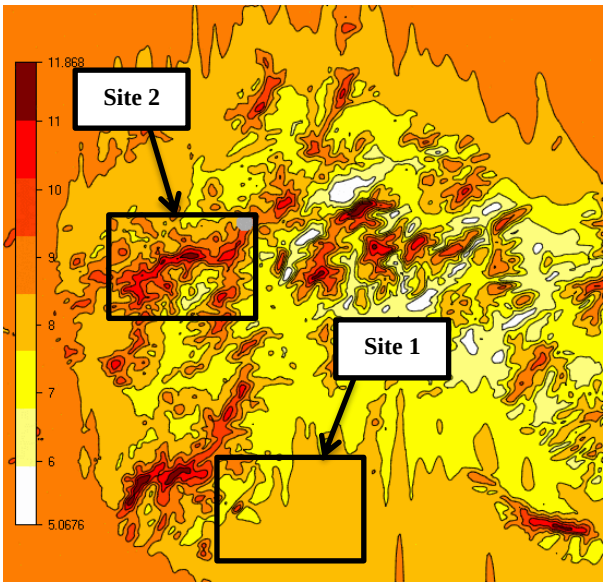

Figure 5.17: Wind Farm Sites on WindSim

Figure 5.18: Wind Farm Sites on Google Earth

5.2. Economic Analysis

Economic analysis is conducted with sensitivity approach to cover all WindSim simulations in Section 5.4. The algorithm is based on present worth approach [5]. Economics part of the code is straightforward, thus validation is not presented here. Before the economic analysis, AEP is calculated over total energy production considering capacity factor. Wind speed distribution, wake losses, soiling losses and availability have impact on AEP calculation as discussed in Chapter 4. Wake losses are assumed as 6 % for the first economic cost model. Other essential inputs for economic analyses are assumed as listed in Table 5.6. Outputs of the economic tab are given in Table 5.7.

Table 5.6: Inputs for Economics Tab

Total Power Capacity of Wind Farm:	45000 kW
Availability:	90 %
Soiling Losses:	3.5 %
Wake Losses:	6 %
Total Energy Production (excluding wake losses):	160000 MWh/year
Cost per kW:	1000 $
Interest Rate (discount):	10 %
Local Inflation Rate:	8.88 %
Escalation Rate:	2 %
Local Electricity Selling Price:	0.073 $/kWh
Wind Turbine Economic Life:	20 years
Operation and Maintenance Cost Factor:	2 %

Table 5.7: Outputs of Economics Tab

AEP:	130620 MWh/year
Capacity Factor:	33.2 %
Initial Investment:	65217391 $
Operation and Maintenance Costs:	1304348 $
Total Cost of the Project:	66521738 $
Net Present Value of All Costs (NPV):	117080589 $
Yearly Cost of Operation:	5854029 $ / year
Cost of Generated Electricity (COE):	0.036 $/kWh
Payback Period:	7.60 years
Internal Rate of Return (IRR):	11.08 %

The outputs of Economics Tab are assumed as the first economic model. The influence of many parameters can be examined with sensitivity analysis. The uncertainty of input parameters causes certain level of risk in every project. NPV, IRR, COE and payback period are the monitored parameters for this study. The variation of these parameters can be determined whether the project is robust or not.

Following parameters are tuned in both decreasing and increasing directions. The percentage of the variation of the parameters is chosen as 20 % in this study. Each parameter is taken into account separately.

1. Initial Investment Cost
2. Operation and Maintenance Costs
3. Interest Rate
4. Total Energy Production (excluding wake losses)
5. Local Electricity Selling Price
6. Wake Losses
7. Wind Turbine Economic Life

The variations of parameters influence other variables differently. This study investigates the parameter and the impacts of its dependent variables. Especially, the effects of wake loss are examined closer. The sensitivity analyses are presented with following figures.

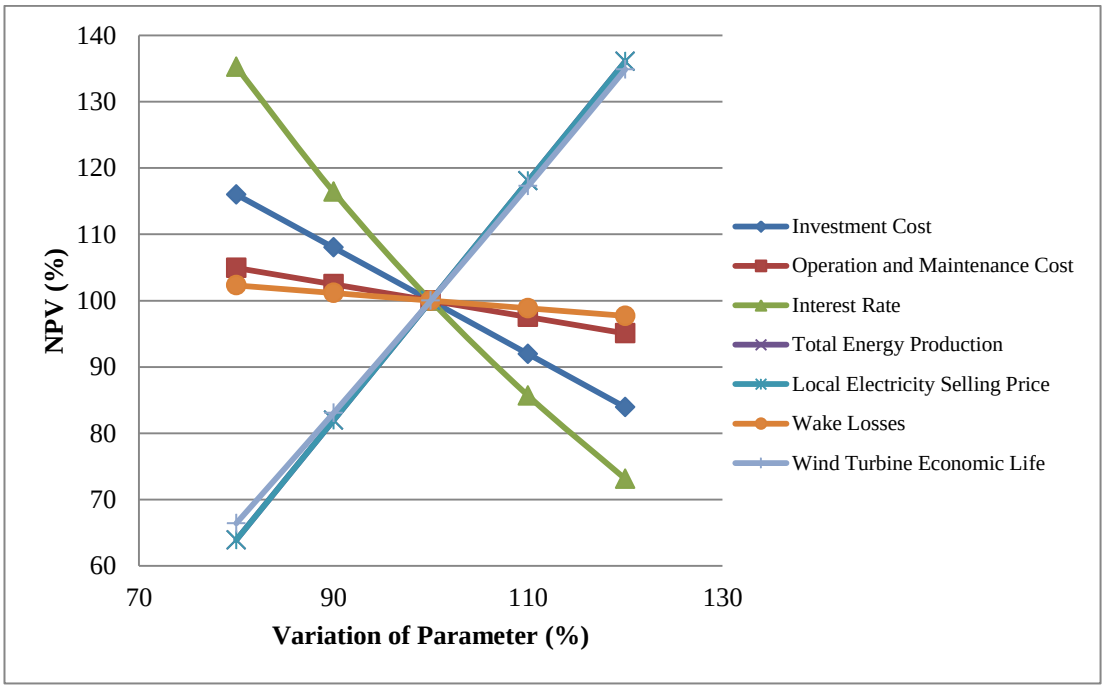

Figure 5.19: Sensitivity Analysis for NPV

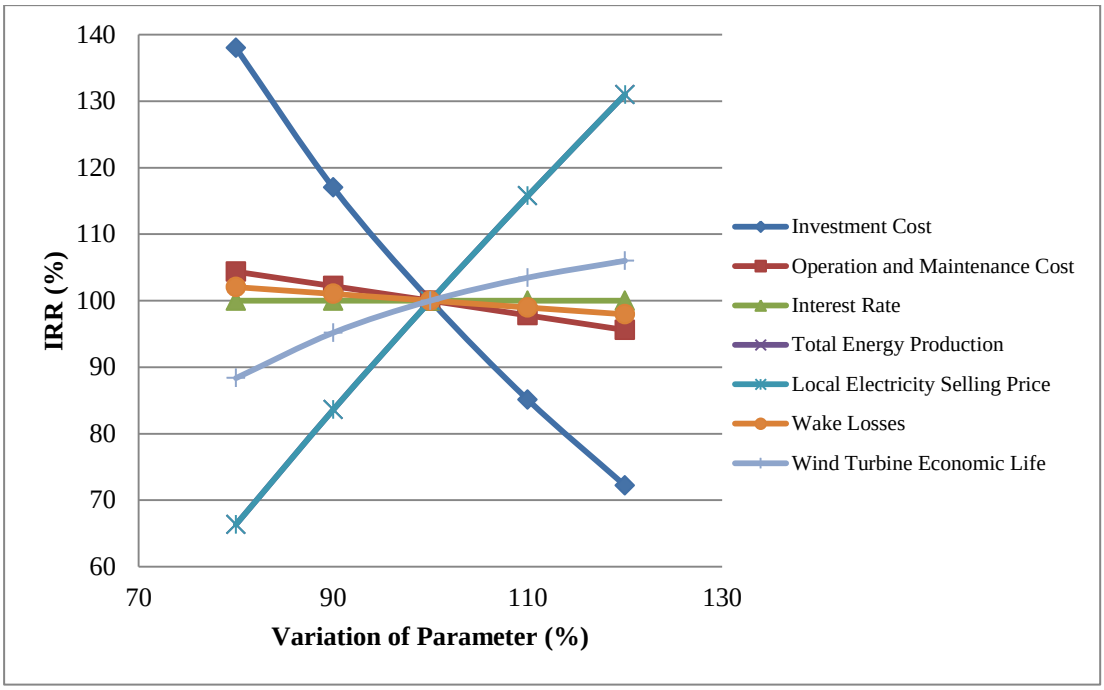

Figure 5.20: Sensitivity Analysis for IRR

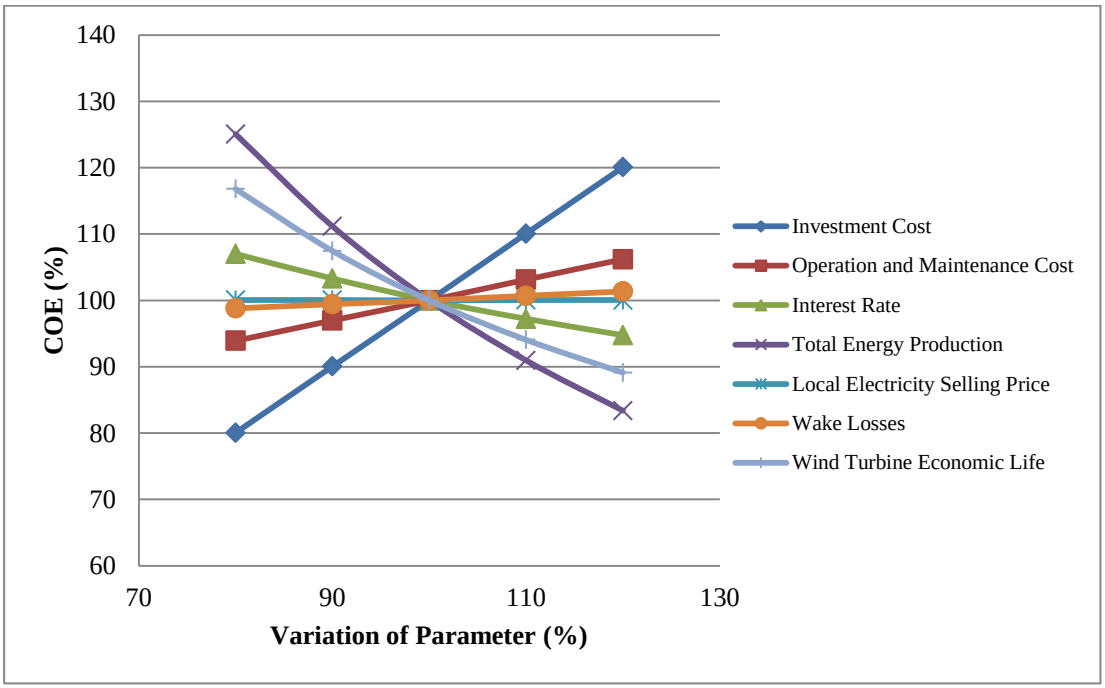

Figure 5.21: Sensitivity Analysis for COE

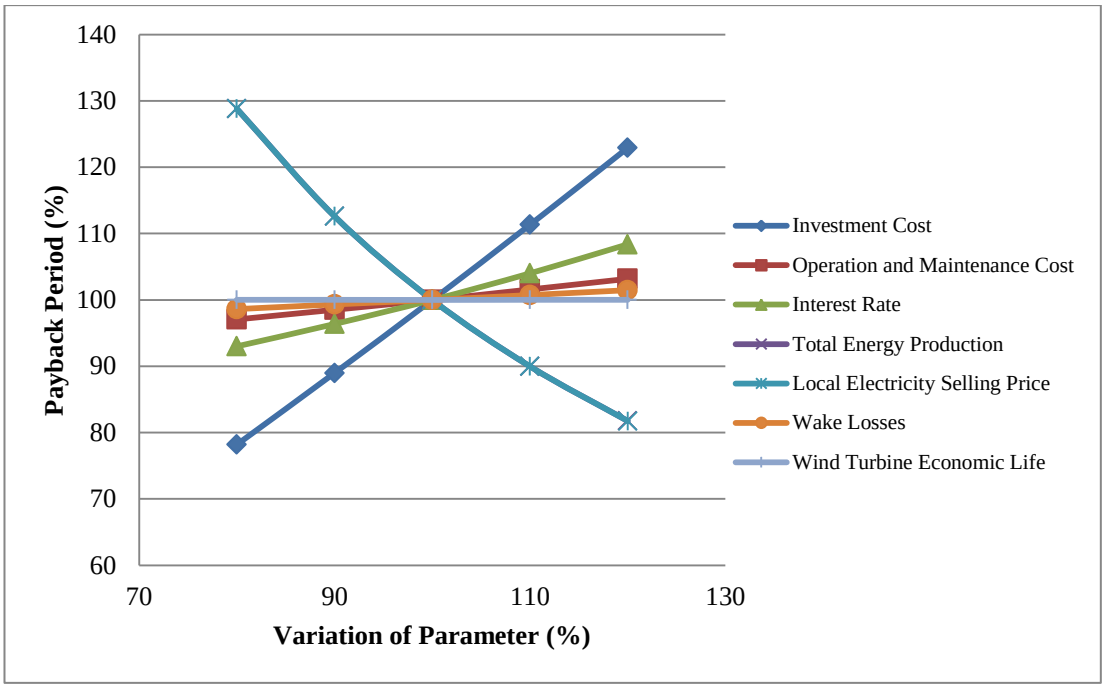

Figure 5.22: Sensitivity Analysis for Payback Period

At the end of the study, it is obtained that variables have different effects to each other. The effects change in direct or inverse proportion. This study also summarizes the dependency of variables to each other. Some important remarks are stated below:

- Local electricity selling price and total energy production have same percentage values for NPV, IRR and Payback period. Besides, they have huge impact on these parameters comparing to other variables. However, local electricity selling price has no impact on COE but total energy production varies in inverse proportion to COE. Therefore, COE can be minimized if the site has higher mean wind speeds.
- Local electricity selling price is quite related to support and incentives of local government. The project can be more profitable if the local electricity selling price increases.
- Interest rate has important effect on NPV. They vary each other in inverse proportion. Another parameter is wind turbine lifetime which has positive effect for NPV.
- Investment cost has also significant effect on all monitored parameters. Especially its influence on IRR is noteworthy.
- Wake losses have less effect over the monitored parameters than others.

Additionally, the variations of cost of generated electricity and payback period can be investigated in wide range according to different capacity factors and wake losses. In Figure 5.23 and 5.24, the effect of the parameters can be seen for the economic model.

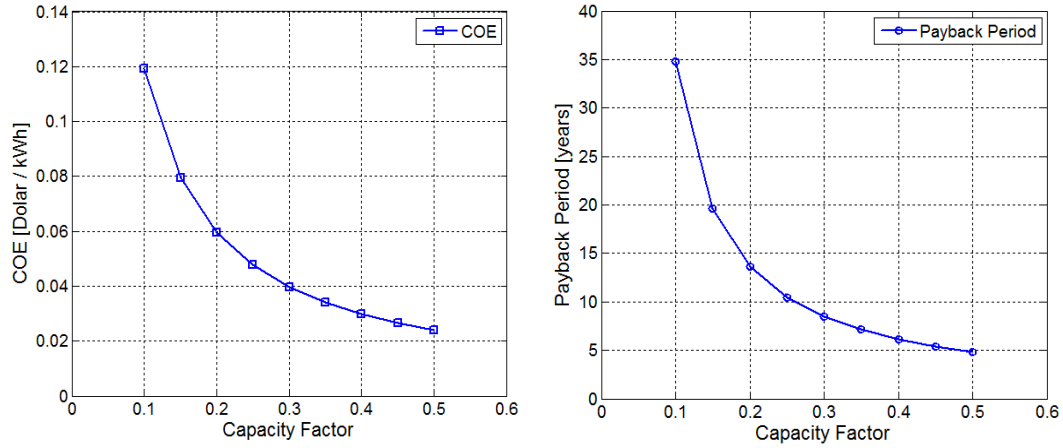

Figure 5.23: Effect of Capacity Factor on COE and Payback Period

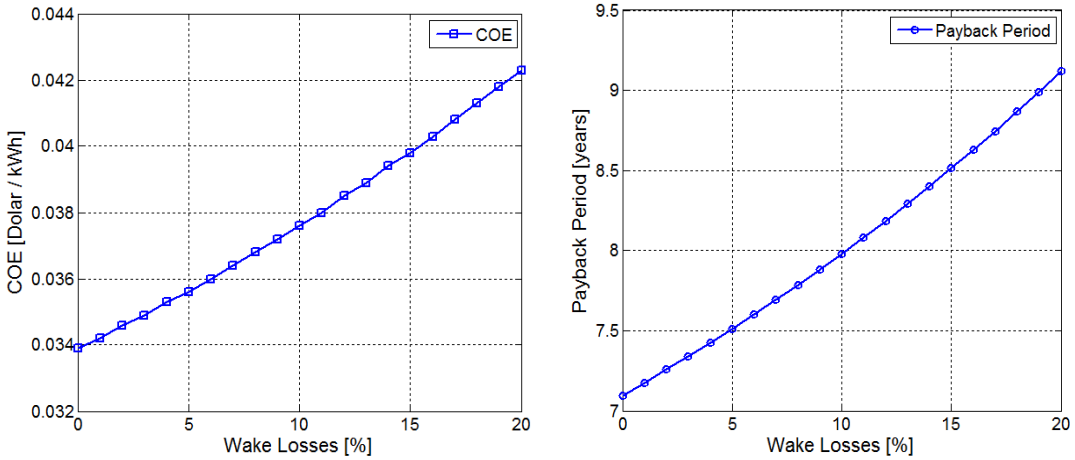

Figure 5.24: Effect of Wake Loss on COE and Payback Period

It can be observed in Figure 5.23 that COE and payback period decreases while capacity factor values increases (See Eq. 4.71). Therefore, the project can be more favorable for the investors if the efficiency of wind farm has higher capacity factor values. On the other hand, when wake losses increase the repayment period and COE goes up at particular amount. For sure, the effect of wake losses is lower than the effect of capacity factor for both parameters. However, it is crucial to minimize the wake losses in order to enhance the efficiency of the system. The program does not taken into account the fatigue effect of wake losses. This effect can decrease the economic lifetime and increase the maintenance costs of the wind turbine. Owing to the enhancements, COE and repayment period can decrease remarkably. Based on an engineer's view, designing more efficient wind turbines and minimizing wake losses are the main objectives in order to achieve higher total energy production and capacity factor. Therefore, AEROWIND program is mainly based on these research areas.

5.3. AEROWIND Code Validation

AEROWIND code is written and compiled in MATLAB program. In this section, validation of BEMT is investigated at first. Afterwards, NREL 5MW Reference Wind Turbine is examined with this tool to utilize in Wind Farm configuration. At the end of this analyses, power and thrust coefficient curves are obtained. Lastly, Jensen wake model is validated with Horns Rev Wind Farm case.

5.3.1. Validation of BEMT Code

Aerodynamics Tab of AEROWIND is based on BEMT code. The validation study is applied to NREL Phase II and III wind turbines [60]. The functionality is tested with the substantial data. They are designed for experimental studies in National Renewable Energy Laboratory (NREL). First one is NREL Phase II and it has untwisted and untapered blades. Other characteristics of this turbine are stated below in Table 5.8.

Table 5.8: NREL Phase II Wind Turbine Specifications [60]

Blade Numbers:	3
Diameter:	10.06 m
Rotational Speed:	71.3 RPM
Hub Radius:	0.723 m
Chord Length:	0.4572 m
Twist Angle:	0º
Blade Pitch Angle:	12º (constant)
Airfoil:	S809
Power Regulation:	Stall
Mechanical Power Output:	19.8 kW
Gearbox + Generator Efficiency:	78 % (approximately)
Air Density:	0.9793 kg/m^3

BEMT code is performed for different wind speeds. The algorithm divides the blade into 20 equal sections. Power production is very poor from the root to 20% span. It can be observed for both tested turbines in Figure 5.25. Therefore, the calculations are ignored in this region. Noting that, there can be occurred numerical instabilities at the maximum tip section. Thus, this section is also ignored. Prandtl tip and hub corrections are included in the calculations. Experimental data and the BEMT tool results are compared for power curve in Figure 5.26. BEMT tool is performed with the experimental data and XFOIL results for S809 airfoil profile.

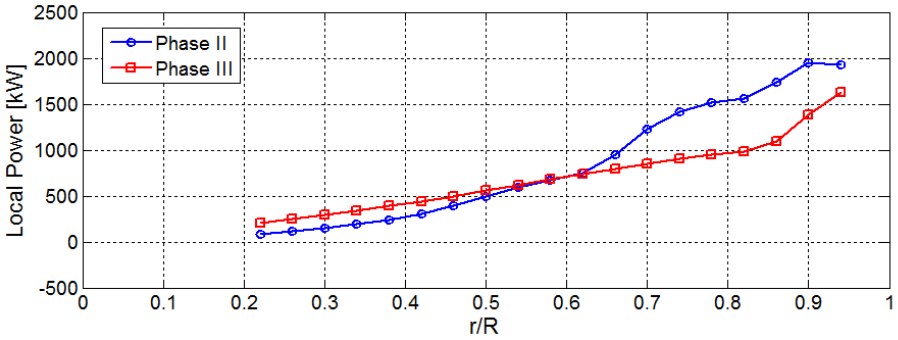

Figure 5.25: Local Power Production versus Non Dimensional Radius at 15 m/s Wind Speed with AEROWIND code

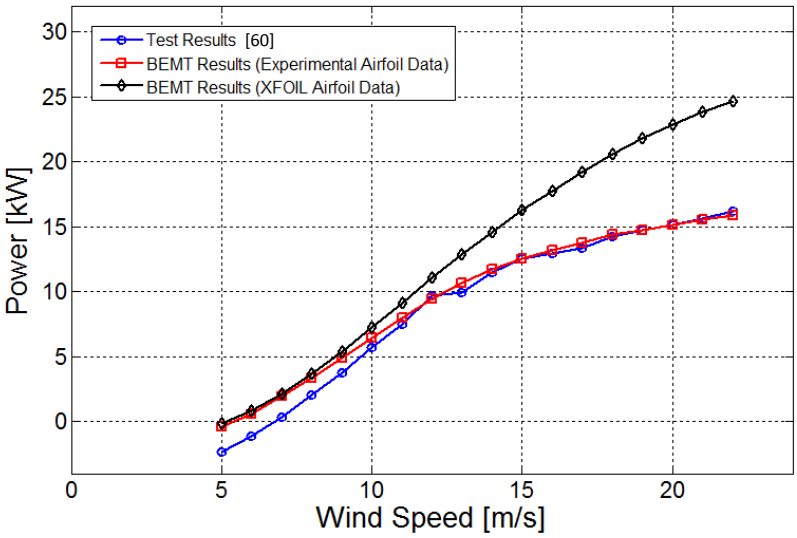

Figure 5.26: Comparison between Test [60] and AEROWIND Results for NREL Phase II

It can be observed from the figure, BEMT code agrees well with NREL Phase II experimental data by using airfoil data from experimental data. The trends of all curves are very similar with the experimental data at small wind speeds. However, the airfoil data from XFOIL gives remarkable difference at higher wind speeds. As presented earlier, XFOIL over predicts lift coefficients in post stall region. In contrast, XFOIL predicts less drag coefficient than the experimental data in that region. It is known from the equations that the negative contribution of drag coefficient to the power production increases with the wind speed. Besides, lift coefficient has positive effect on power production. Therefore, the power prediction diverges. XFOIL data gives higher power predictions. The reason is related to increments of local angle of attack values at high wind speeds. These differences are all related to local angle of attack values and resulting lift and drag coefficients. As shown in Figure 5.25, the effective region of power production is located near the tip of the blade. The

angle of attack values attains high magnitudes with wind speed gradually. As presented in Figure 5.27, local angle of attack magnitudes are below the stall region for Phase II.

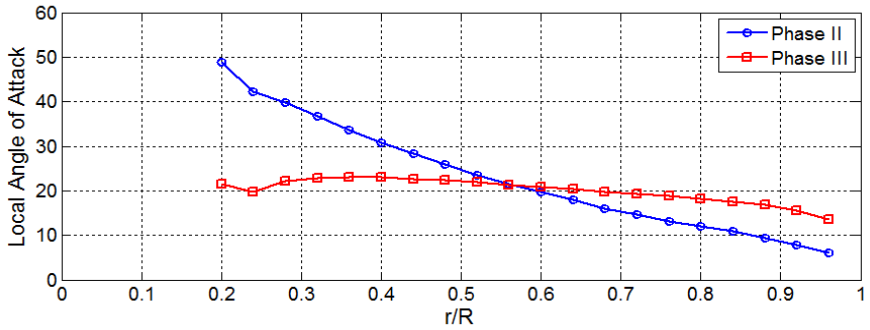

Figure 5.27: Local Angle of Attack versus Non Dimensional Radius at 15 m/s Wind Speed with AEROWIND code

Second validation case is NREL Phase III and it has twisted and untapered blades. The twist angle distribution is presented in Figure 5.28. Other characteristics of this turbine are stated below in Table 5.9.

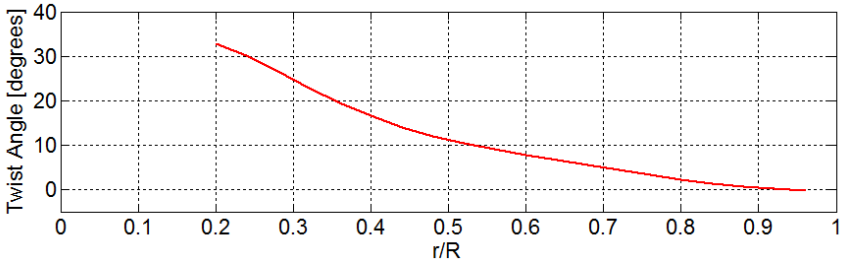

Figure 5.28: Twist Angle Distribution of NREL Phase III Wind Turbine

Table 5.9: NREL Phase III Wind Turbine Specifications [60]

Blade Numbers:	3
Diameter:	10.06 m
Rotational Speed:	71.3 RPM
Hub Radius:	0.723 m
Chord Length:	0.4572 m
Blade Pitch Angle:	3° (constant)
Airfoil:	S809
Power Regulation:	Stall
Mechanical Power Output:	19.8 kW
Gearbox + Generator Efficiency:	78 % (approximately)
Air Density:	0.9793 kg/m^3

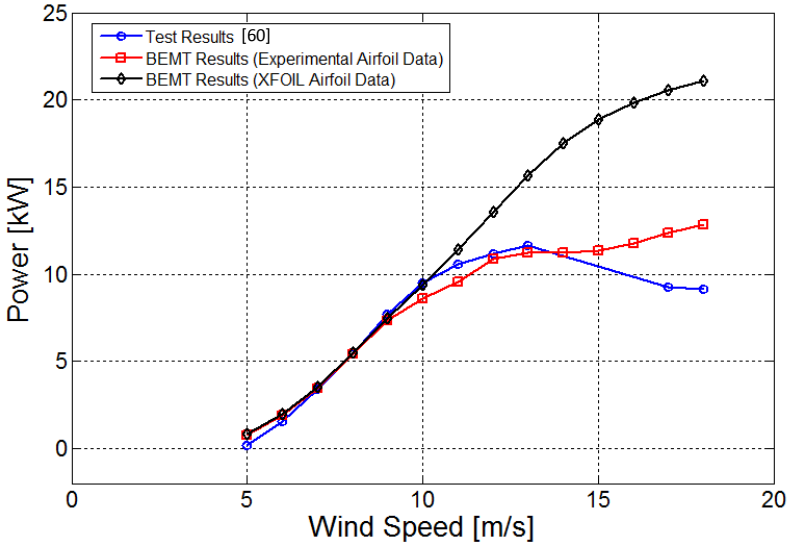

Figure 5.29: Comparison between Test [60] and AEROWIND Results for NREL Phase III

It can be deduced from the Figure 5.29 that the trends are similar with NREL Phase III Wind Turbine results. At small wind speeds the predictions are better because of the consistency of local angle of attack along the blade. In contrast, the predictions are poor at high wind speeds especially in post stall region. As observed in 5.27, local angle of attack magnitudes are higher than stall angle of the airfoil for Phase III. This is the main reason of the differences. Moreover, experimental airfoil data is more reliable than the XFOIL data. Lastly, there are 3D effects which are not included for BEMT results with XFOIL data. The best way to reduce the errors for solutions with XFOIL, airfoil data should be covered all Reynolds numbers along the wind blade in order to make the prediction more accurate. In addition, correction methods which are present in literature can be implemented.

5.3.2. NREL 5 MW Baseline Wind Turbine

Turbine design is detailed study and it is not investigated in this study. Instead of designing a new turbine, NREL 5MW Baseline Wind Turbine is selected as wind turbine model. The available data is obtained from Ref. [61]. It has 5MW power output at nominal wind speed. This case is also researched with the BEMT algorithm of AEROWIND code. The main specifications are showed in Table 5.10. Besides, DU and NACA64 profiles are used in this turbine. Airfoil coordinates are not available, thus lift and drag coefficients are not computed in XFOIL program. In the report, lift and drag coefficients are given and they are already corrected for rotational delay. Besides, interpolation method is also used for high angle of attack values by Viterna and Corrigan method. Airfoil data, blade geometry and other parameters are given in Appendix B [61].

Table 5.10: Main Specifications of NREL 5MW Baseline Turbine [61]

Blade Numbers:	3
Rotor Diameter/ Hub Diameter:	126 / 3 m
Hub Height:	90 m
Rotor Orientation:	Upwind
Cut-in Speed:	3 m/s
Cut-out Speed:	25 m/s
Nominal Power Output:	5 MW
Nominal Wind Speed	11.4 m/s
Minimum/ Maximum Rotor Speed:	6.9 / 12.1 RPM
Power Regulation:	Variable Control - Pitch
Air Density:	1.225 kg/m^3

Chord and twist distribution along the blade are given in Figure 5.30.

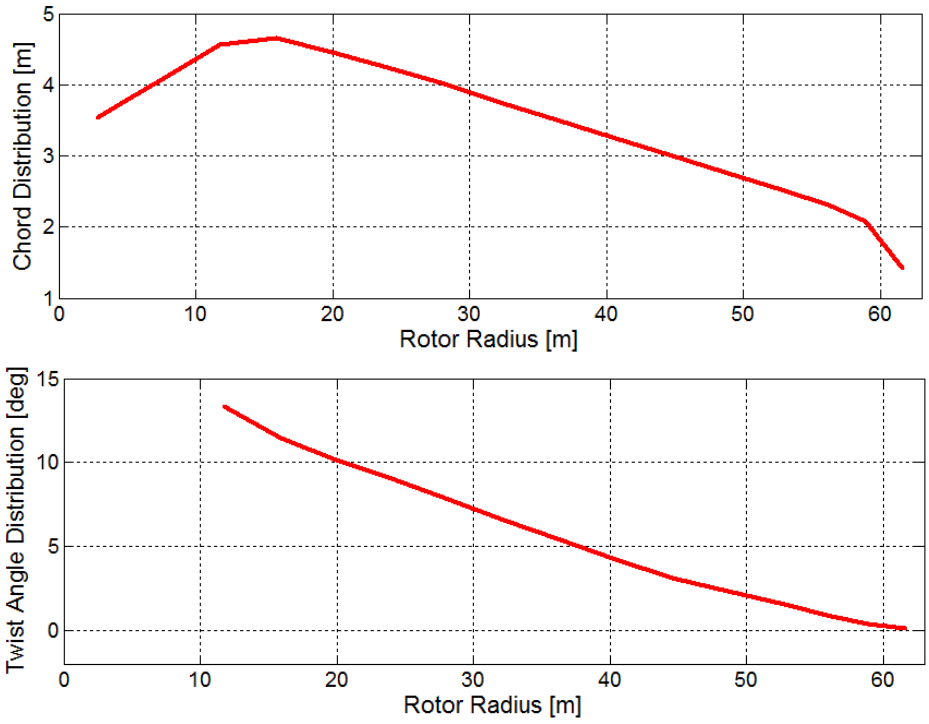

Figure 5.30: Chord and Twist Angle Distribution of NREL 5MW Wind Turbine

Mechanical power comparison is given in Figure 5.31. Power and thrust coefficient curves are obtained to use in wake modeling code at the end of this study. They are presented in Figure 5.32. Sectional airfoil profile, pitch angle and rotational speed variations should be inserted into BEMT code in advance.

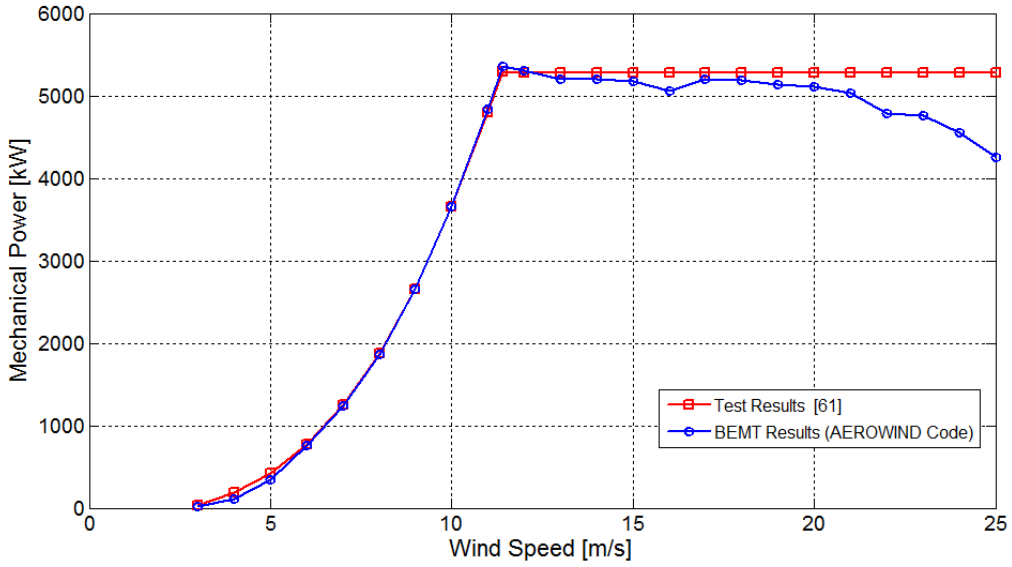

Figure 5.25: Power Curve of NREL 5MW Baseline Wind Turbine

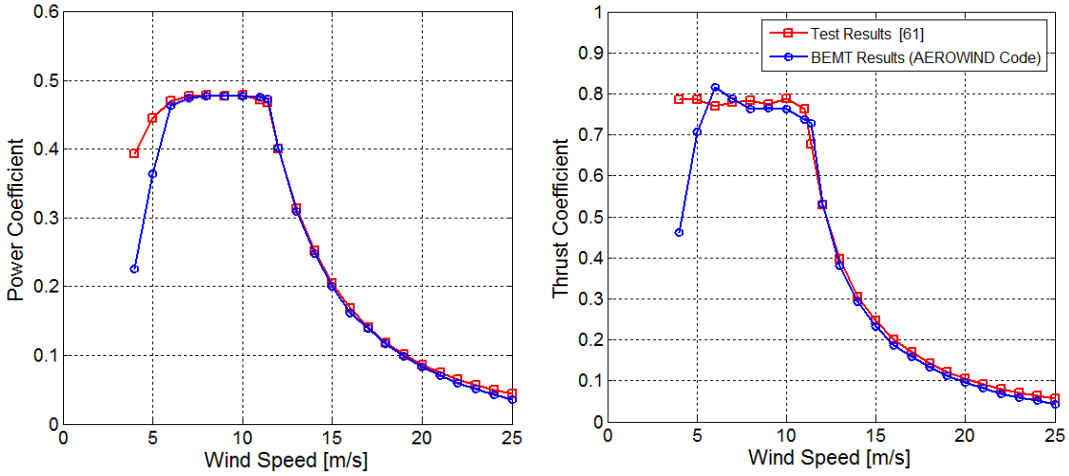

Figure 5.32: Power and Thrust Coefficient Curves of NREL 5MW Baseline Wind Turbine

Sensitivity analysis is conducted for section numbers. Afterwards, blade is divided into 100 sections in order to find converged values. The calculations last 7 minutes approximately. At the end of the analysis, it can be deduced that results are well matched until in the 15-20 m/s band. Over that speed, BEMT code underestimates the mechanical power. Trends of power and thrust coefficients are similar. It can be seen that some errors occur for mechanical power predictions at small wind speeds. Besides, some reading errors can be occurred because these values are taken from graphs by marking the points.

5.3.3. Validation of Wake Model Code

The validation study is conducted for Horns Rev Offshore Wind Farm where is located 13 km far from Danish coastline. 80 identical wind turbines are spread over the sea. This case is suitable to test AEROWIND code, because there are no wake-terrain interactions. The specifications of this wind farm are listed in Table 5.11. The configuration is given according to diameter unit along both directions in Figure 5.33. Power curves and thrust coefficients of turbine are also available in Ref. [68].

Table 5.11: Main Specifications of Horns Rev Wind Farm

Rows and Columns	8 x 10
Turbines:	Vestas 2 MW
Hub Height:	70 m
Rotor Diameter:	80 m
Turbine Spacing:	7 Diameters
Type:	Offshore
Vertical Alignment Angle of Layout:	7.2º

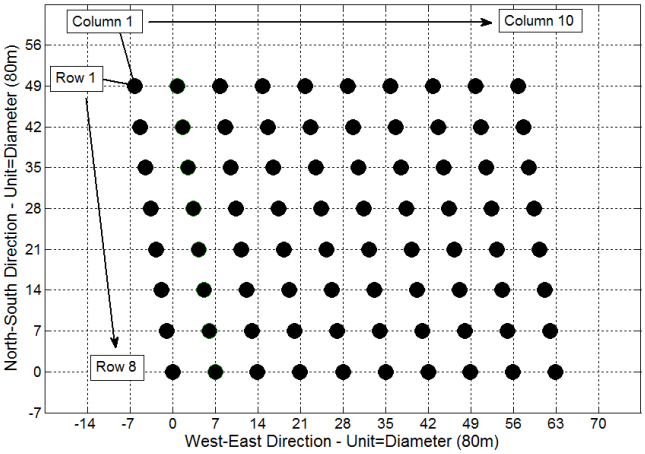

Figure 5.33: Horns Rev Wind Farm Configuration

Wind Farm layout is arranged and wake deficit coefficient is found as 0.037 according to Eq. (4.53). Jensen wake model is used for all cases in AEROWIND. Besides, different wake models in WindSim were performed to compute wake deficit in Ref. [65] as well. This data is used for comparisons. Power curves and thrust coefficients are computed according to available data. The wind speeds were monitored at particular time in this experiment, and the validation cases are listed in Table 5.12 [68]. The alignment of observed turbines was arranged according to wind direction in this experiment. Wind directions are illustrated in Figure 5.34.

Table 5.12: Validations Cases for Horns Rev Wind Farm

CASES:	Wind Speed at Hub Height [m/s]			Wind Direction [degree]	Monitored Turbine Numbers:
1	6	8	10	222	5
2	6	8	10	270	8
3	6	8	10	312	5

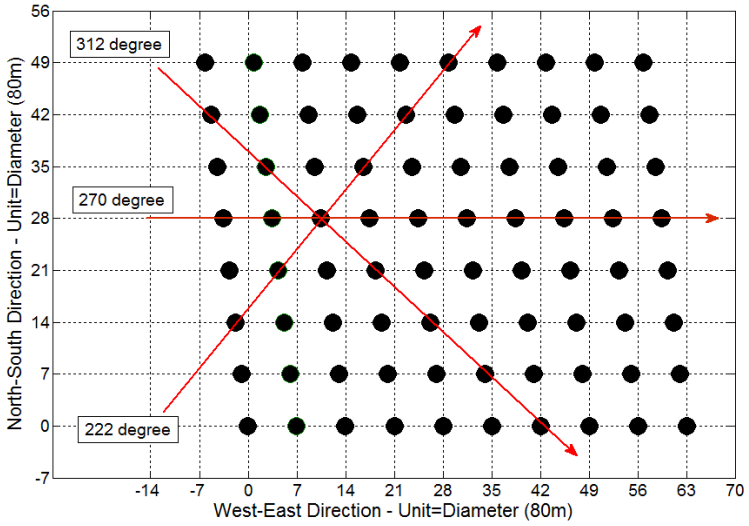

Figure 5.34: Wind Directions over Horns Rev Wind Farm

Many abbreviations are made on the following figures. Experimental cases are named on the figures as given in Ref. [65] (For instance, Case 2.6.2, Case 2.8.1, Case 2.10.1 and etc.). WindSim simulation results of Ref. [65] are named as 'WS'. Linear superposition of wake deficits is called as 'LS'. Root square of sum of square of wake deficits are referred as 'RSS'.

The results of validation cases are plotted in following figures. It can be observed that AEROWIND code and WindSim have similar results for Jensen Model [65] in all figures. The difference can be arisen from wake deficit coefficient, thrust coefficient or shadowing calculation method. In the reference, these values are not revealed for WindSim solution. Error of LS of wake deficits is greater than other models at high column numbers. It is better to use the method which is RSS of wake deficits. Another inference is that RSS method is converged after 4 columns for all wake models. Lastly, the closest result to test cases is observed as WindSim result with Larsen wake model among other wake models. However, the deviations of all wake models are too much. As given in Chapter 4, the velocity deficits are calculated in wake interactions. Apparently, the cube of velocity gives more errors. Turbulence model and mesh resolution should be also deeply investigated. Besides, the inconsistent predictions of the wake losses affect the economics a lot (see Fig. 5.24).

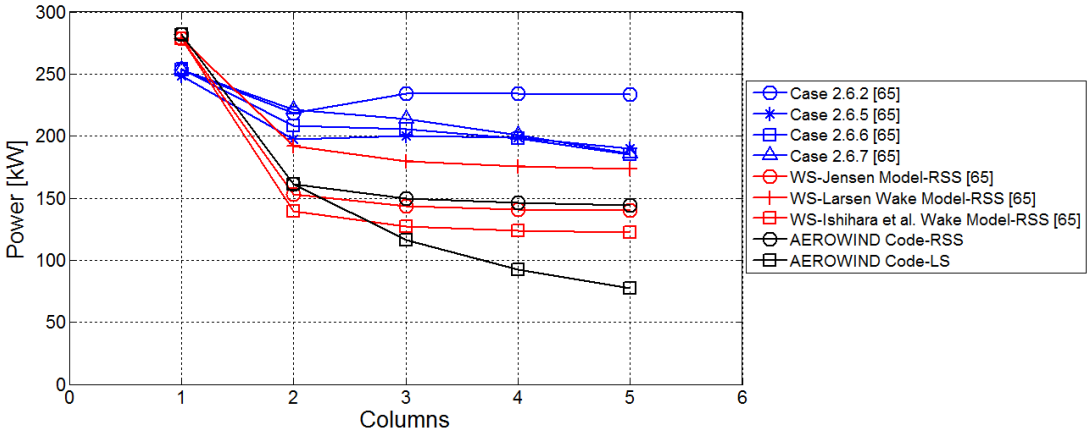

Figure 5.35: Power Deficits (Wind Direction=222, U=6m/s)

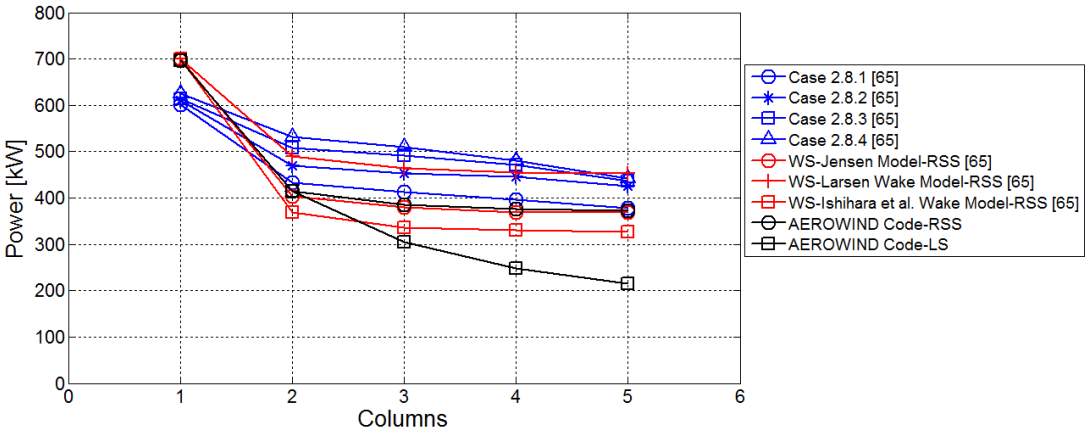

Figure 5.36: Power Deficits (Wind Direction=222, U=8m/s)

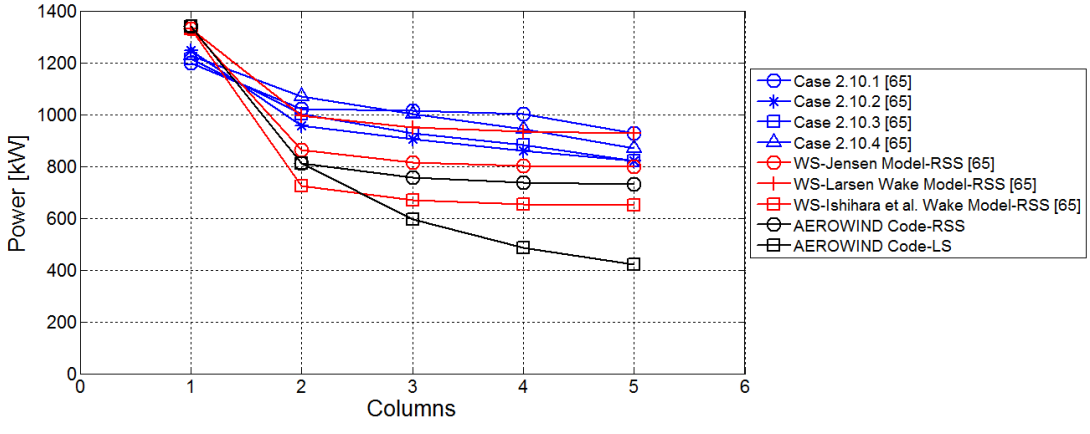

Figure 5.37: Power Deficits (Wind Direction=222, U=10m/s)

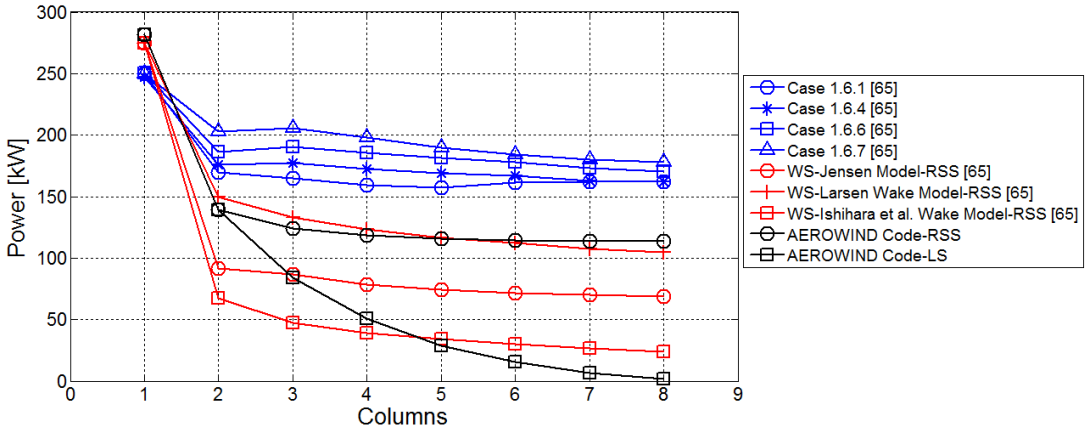

Figure 5.38: Power Deficits (Wind Direction=270, U=6m/s)

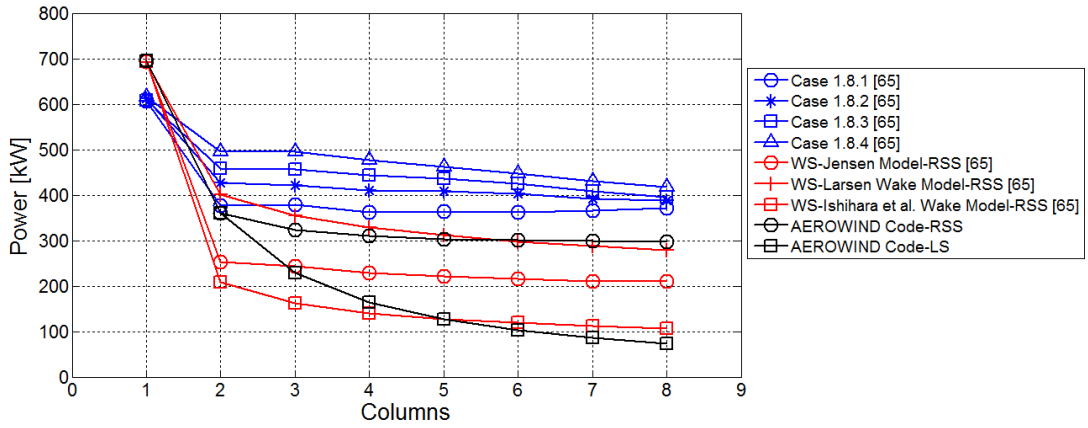

Figure 5.39: Power Deficits (Wind Direction=270, U=8m/s)

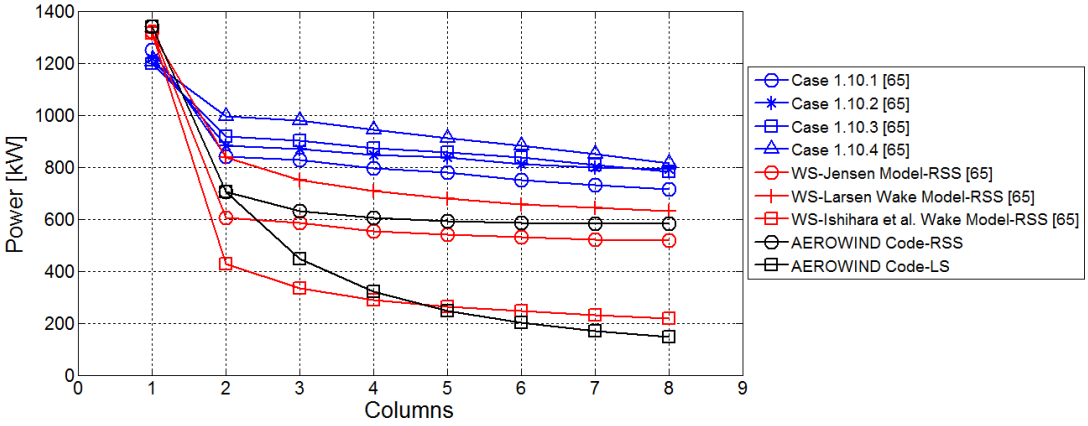

Figure 5.40: Power Deficits (Wind Direction=270, U=10m/s)

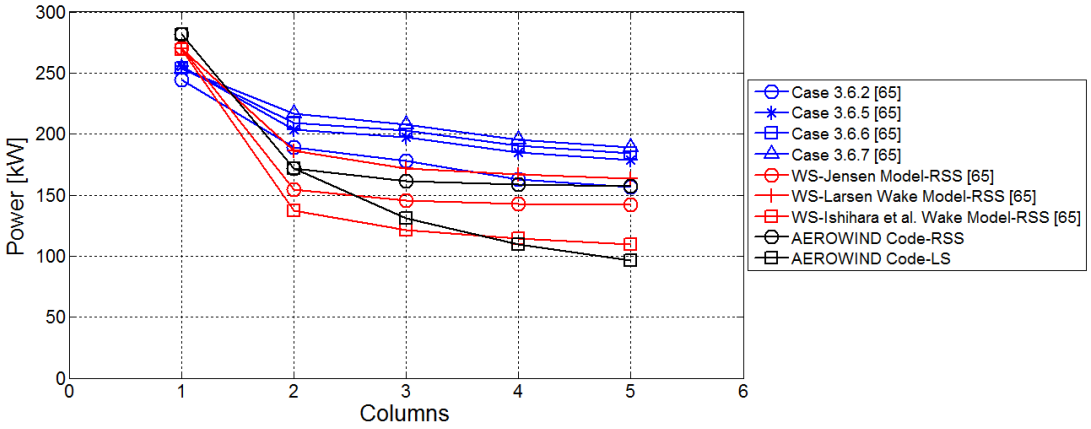

Figure 5.41: Power Deficits (Wind Direction=312, U=6m/s)

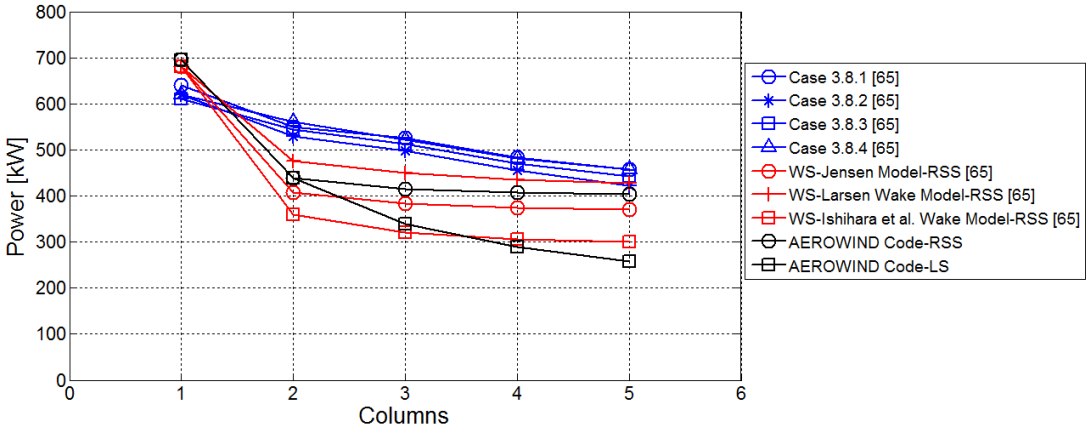

Figure 5.42: Power Deficits (Wind Direction=312, U=8m/s)

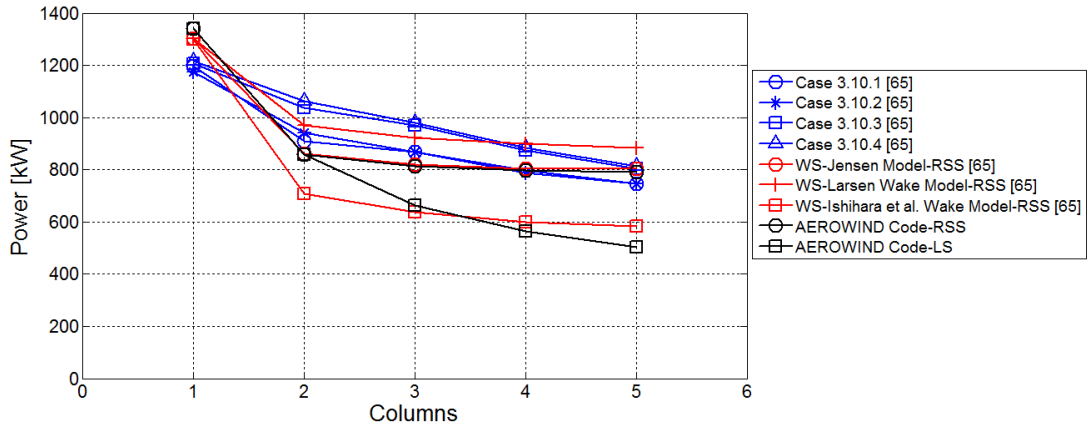

Figure 5.43: Power Deficits (Wind Direction=312, U=10m/s)

5.4. Energy Analysis in WindSim

Two scenarios are investigated in WindSim program. They are Offshore and Onshore Wind Farms over Bodrum region. Locations of sites were presented in Section 5.1.4. Limited climatology data is available as discussed in Chapter 3. Therefore, WindSim program aids to gather wind data referring to original data. That is called as 'Transferred Climatology' in WindSim. Some other assumptions are also stated below for all cases:

1. Orientations of Wind Farms are aligned with prevailing wind direction according to wind data distribution. Turbine Nacelle is usually controlled so the rotor can be oriented perpendicularly to the wind direction.
2. Turbines are already chosen as 5MW NREL Baseline Wind Turbine. Generator and gearbox efficiency is included to tabulate the power curve.
3. Distances between turbines are calculated from hub locations (will be given in diameter unit = D). The layout distribution is considered as matrix array.
4. Rows and columns are selected as 3 (9 Turbines), so that Installed Power Capacity of Wind Farms is 45 MW.
5. Air density is constant and it is selected as 1.225 kg/m^3.

Turbulent intensity decreases energy production when the turbines are very close to each other. Sufficient spacing reduces interactions, turbulence and hazardous loads on the turbine. Studies showed that wind turbines in a wind farm are typically placed 5 rotor diameters apart perpendicular to the prevailing wind (crosswind spacing), and 8-10 rotor diameters apart parallel to the prevailing wind (downwind spacing) [1]. The depiction is shown in Figure 5.44. In this research, different cases are investigated. These are firstly related to crosswind and downwind spacing in order to observe wake deficits. As shown in Table 5.13, Case 1.2.4 means Offshore Wind Farm layout with crosswind spacing of 2 diameter lengths and downwind spacing of 4 diameter lengths. At the end of the study, 36 cases will have performed. Both spacing parameters are specified in diameter unit for all cases.

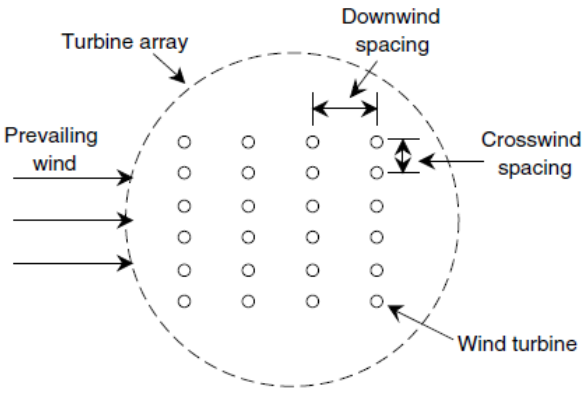

Figure 5.44: Wind Farm Array [1]

Table 5.13: Case Denotation for WindSim Simulations

Case Denotation:	A: Case Number:	B: Crosswind Spacing: [in Diameter unit]	C: Downwind Spacing: [in Diameter unit]
Case A.B.C	1: Offshore 2: Onshore	2-3-4	2-3-4-5-6-8

5.4.1. Wind Farm Layouts for Bodrum Region

Prevailing wind direction should be investigated beforehand. It is applied to WindSim program by pinpointing many transferred climatologies over the site region. Wind rose and Weibull parameters are obtained from WindSim program for both scenarios. Wind roses and climatology characteristics at 100 m height are presented in Figure 5.45 and Table 5.14.

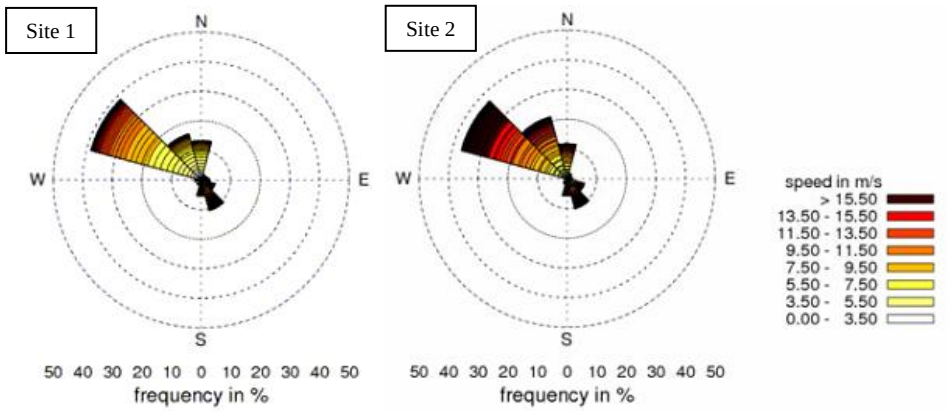

Figure 5.45: Wind Rose Presentations for Sites at 100 m Height

Table 5.14: Climatology Characteristics of Sites at 100 m Height

Offshore Wind Farm													
Sector Midpoint	**All**	**0º**	**30º**	**60º**	**90º**	**120º**	**150º**	**180º**	**210º**	**240º**	**270º**	**300º**	**330º**
k	**1.31**	1.86	1.47	1.02	1.17	1.19	1.45	1.35	1.61	1.30	2.05	2.11	1.87
A	**8.04**	5.95	1.97	2.55	8.24	8.85	13.47	12.25	6.07	4.29	8.20	8.44	6.00
freq	**-**	13.40	1.90	1.90	2.80	4.80	10.70	5.50	1.90	0.60	2.10	38.40	16.00
mean	**7.43**	5.33	1.74	2.53	8.05	8.71	12.57	11.58	5.13	4.00	7.20	7.50	5.40
Onshore Wind Farm													
Sector Midpoint	**All**	**0º**	**30º**	**60º**	**90º**	**120º**	**150º**	**180º**	**210º**	**240º**	**270º**	**300º**	**330º**
k	**1.53**	1.85	1.51	1.3	1.05	1.19	1.45	1.36	1.61	1.48	1.57	2.15	1.88
A	**11.7**	9.21	2.96	3.21	7.55	9.96	16.2	14.73	6.82	4.83	3.76	13.03	10.04
freq	**-**	11.8	2	1.4	1.8	6	10.4	5.8	1.8	0.5	0.2	36.9	21.5
mean	**10.5**	8.18	2.56	2.89	7.78	9.79	15.17	13.8	5.75	4.28	3.13	11.51	8.97

In Figure 5.45, it can be observed that Site 2 has high wind potential when comparing to Site 1. According to these findings, prevailing wind direction is 300 degrees for both cases. The orientation is aligned to 300 degrees. It is essential to select the starting point for first Wind Turbine in the layout. They are presented in Table 5.15. Firstly, Wind Farm layouts are prepared. Coordinates of each wind turbine are transferred to WindSim subsequently. For example, layout of Case 1.2.4 and Case 2.2.4 can be observed in Figure 5.46.

Table 5.15: Coordinates for First Wind Turbine without Hub Height

Coordinates	Offshore Wind Farm	Onshore Wind Farm
X	530215	522860
Y	4092990	4102200
Z	0	132.7

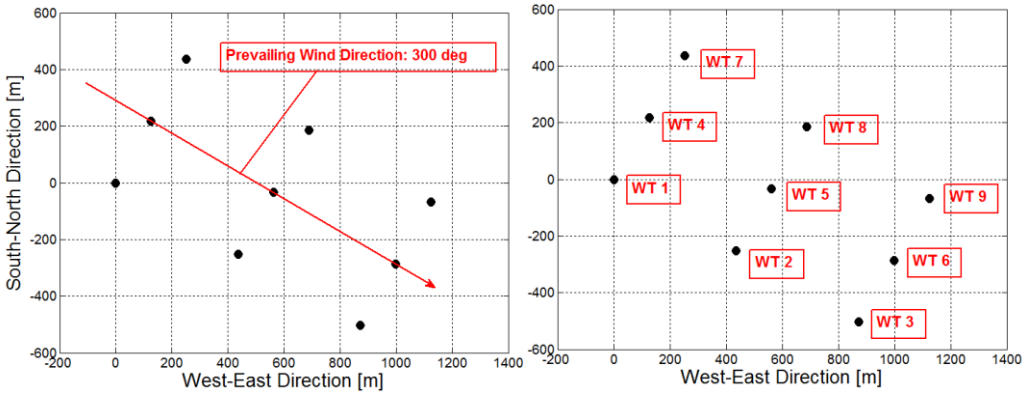

Figure 5.46: Wind Farm Layout for Case 1.2.4 and 2.2.4

5.4.2. Case 1 Results: Offshore Wind Farm

Case 1.2.4 is set up in object module of WindSim as shown in Figure 5.47. Likewise, other cases are prepared and started to simulate in WindSim. The wake model is applied only between one to ten diameters towards downstream of wind turbine in WindSim [65].

AEP and wake losses are calculated with RSS method. It is better to select this method, because LS of Wake Deficits can give more power deficits in comparison with RSS. Noting that, climatology information is also variable for every turbine over the terrain in WindSim. No wake deficits condition can be taken as reference for this variation. Besides, speed up correction which is captured by CFD method to compute inclination angles until the separation occurs is also included in WindSim. Simulations based on Weibull distribution are presented in sequence.

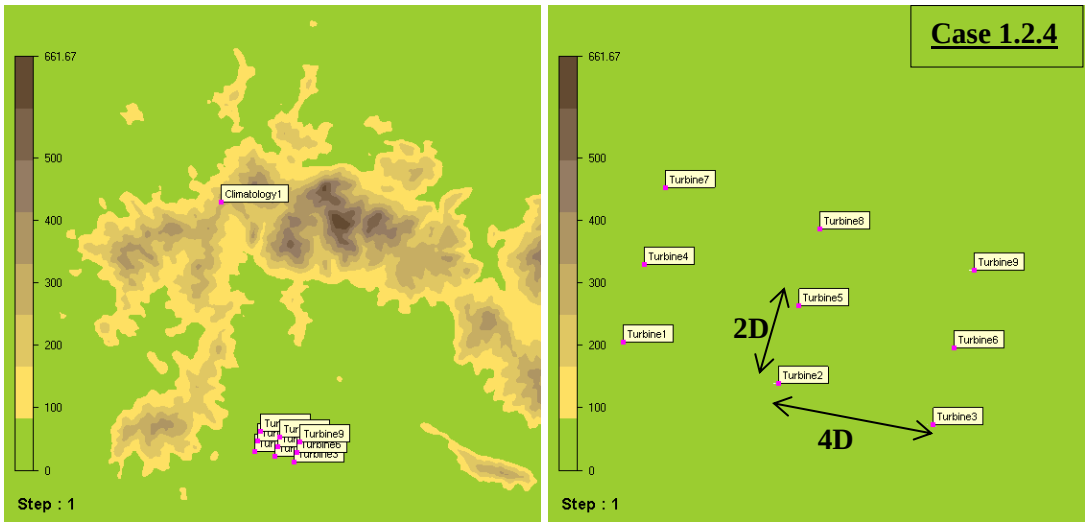

Figure 5.47: Object Module for Offshore Wind Farm in WindSim

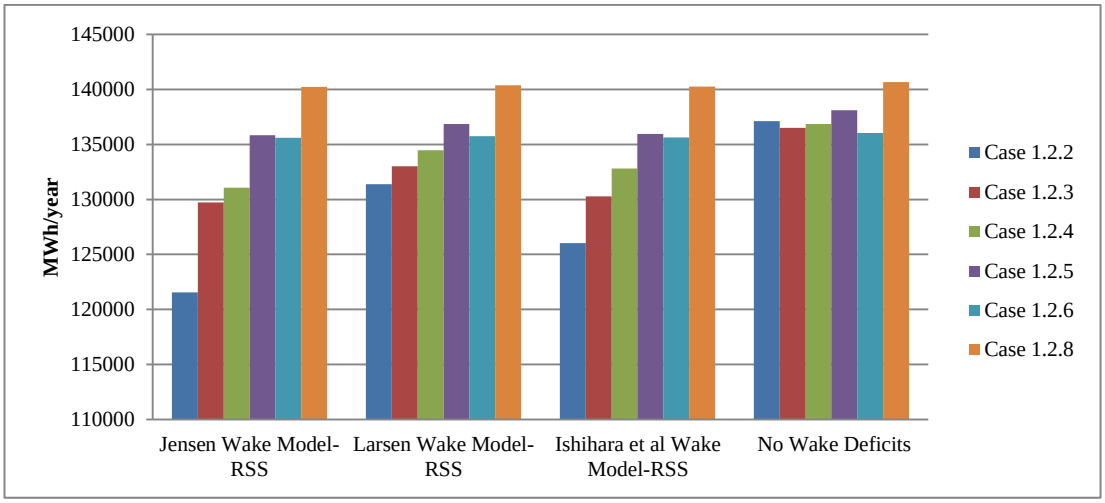

Figure 5.48: Total AEP Values for Case 1.2.X

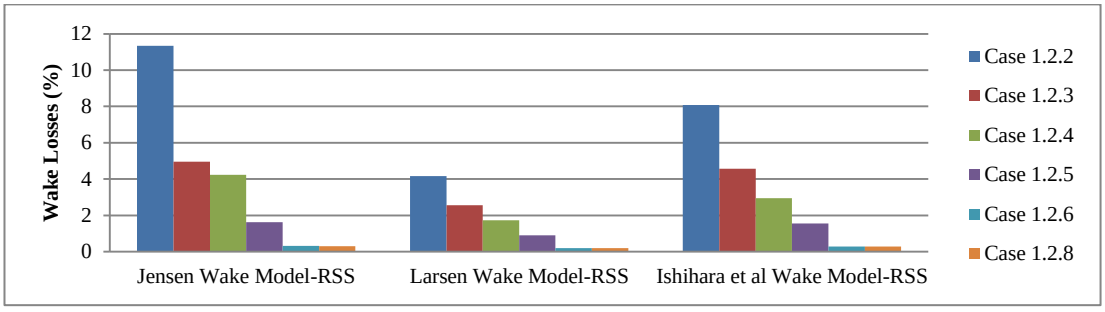

Figure 5.49: Total Wake Losses (%) for Case 1.2.X

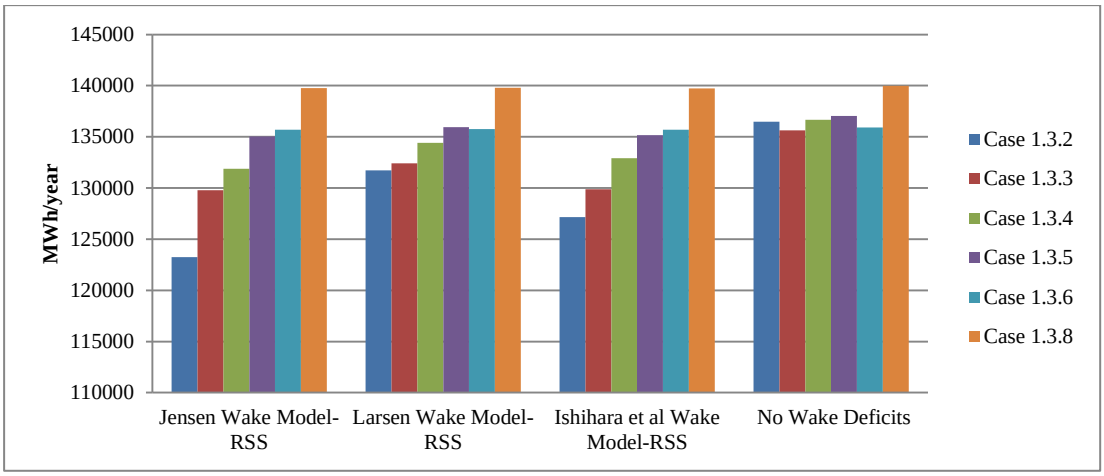

Figure 5.50: Total AEP Values for Case 1.3.X

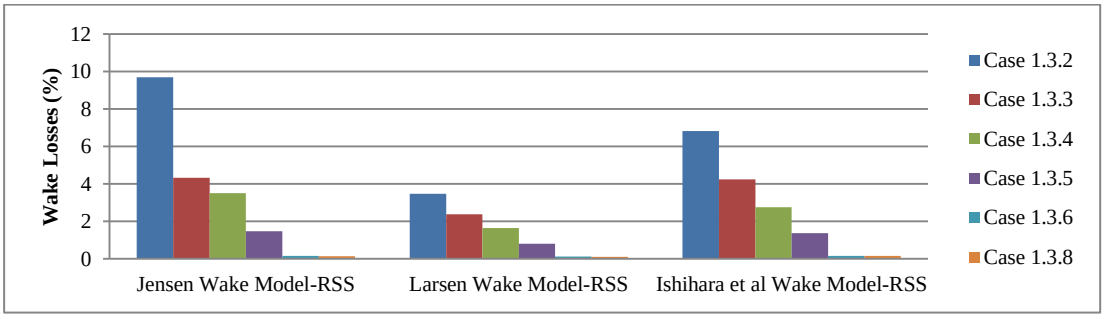

Figure 5.51: Total Wake Losses (%) for Case 1.3.X

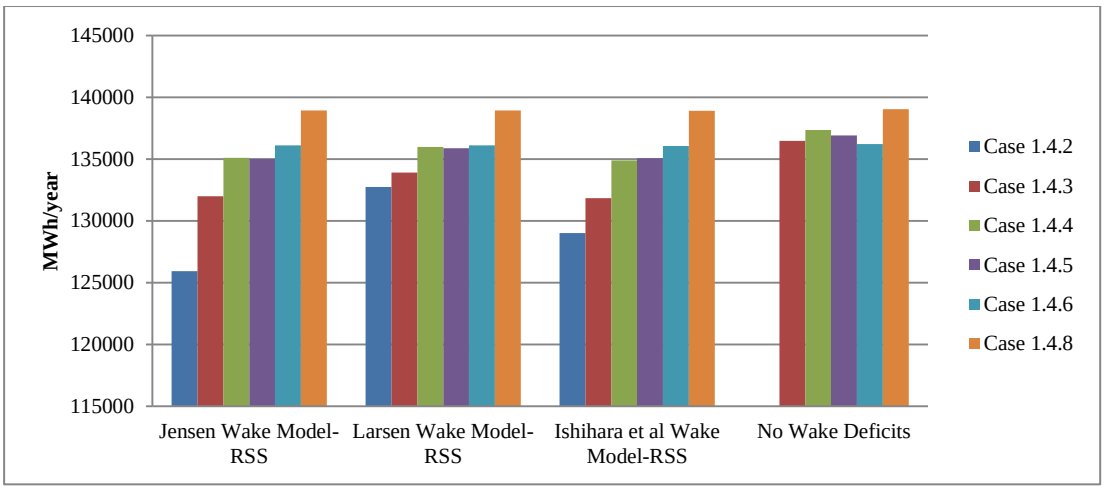

Figure 5.52: Total AEP Values for Case 1.4.X

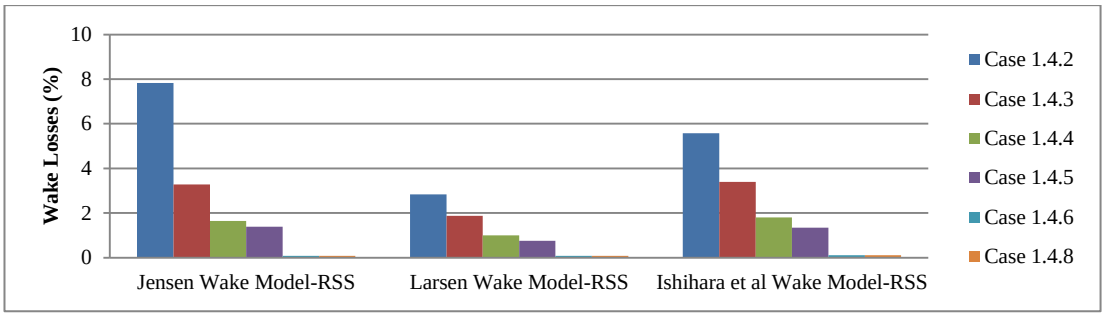

Figure 5.53: Total Wake Losses (%) for Case 1.4.X

First of all, it should be emphasized that Offshore Wind Farm is favorable to observe the wake effects. There are no terrain-wake interactions and climatology does not change much in overall. No wake condition bars show the maximum AEP for particular case. It can be seen from the graphs that once distances between turbines increase, wake losses decrease remarkably.

The wake losses are almost ignorable after 6D downwind spacing. Likewise, increase of crosswind spacing results in reduction for wake loss. Jensen wake model estimates more power deficits for all layouts of Case 1. Larsen wake model predicts lower wake losses for all layouts of Case 1.

Consequently, Case 1.2.8 can be determined as the best layout for this survey. The total wind farm area (land cover) of this layout is lower than Case 1.3.8 which is a wanted situation for wind farm design. Maximum energy production (MWh) is achieved and wake losses (%) are also minimized for this layout.

5.4.3. Case 2 Results: Onshore Wind Farm

Case 2 is Onshore Wind Farm and it is located over complex terrain. Wind potential is higher than Case 1. Therefore, it is expected that total energy production values should be higher. Wake-wake and wake-terrain interactions should be taken into account for this case. Altitudes and roughness classes of all turbines are variable for all layouts. In Figure 5.54, wind turbines are pinpointed over the terrain for Case 2.2.4. The results are presented in following figures in sequence.

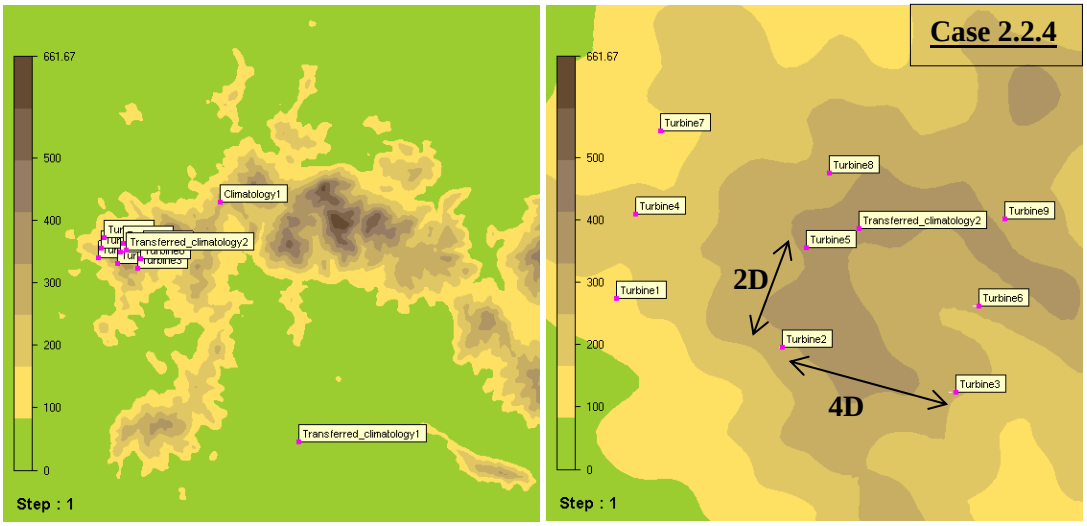

Figure 5.54: Object Module for Onshore Wind Farm in WindSim

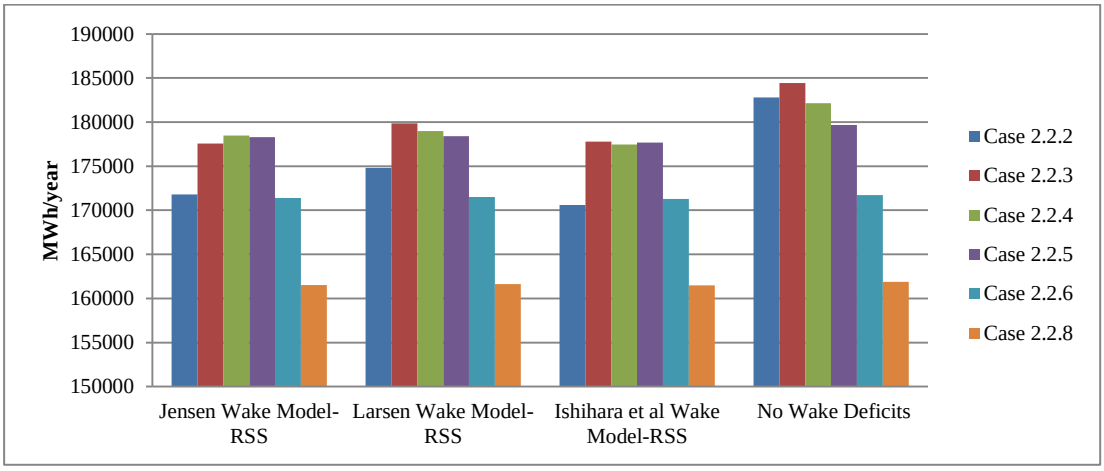

Figure 5.55: Total AEP Values for Case 2.2.X

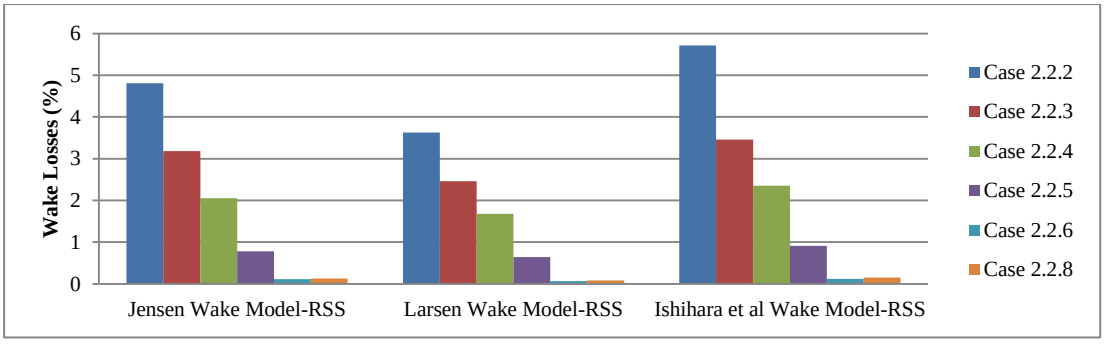

Figure 5.56: Total Wake Losses (%) for Case 2.2.X

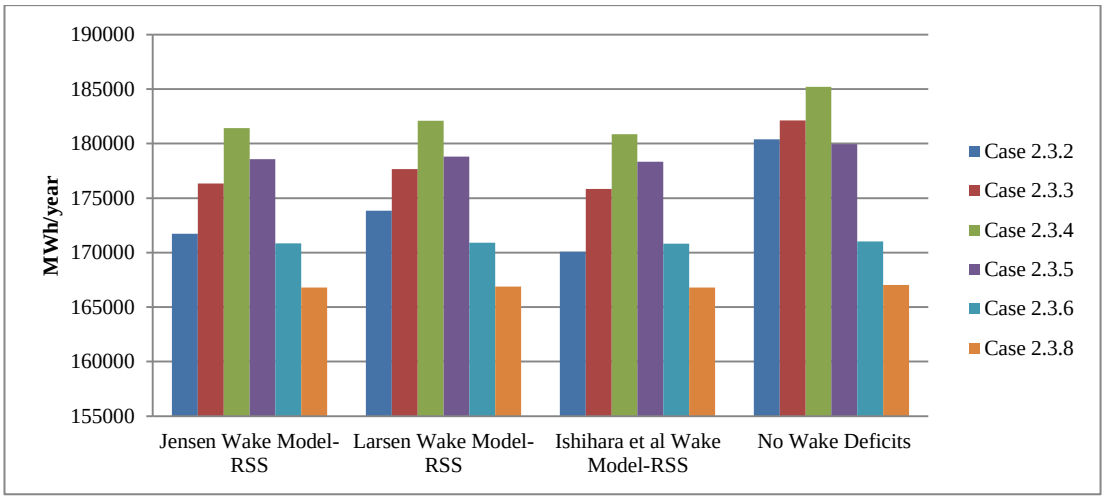

Figure 5.57: Total AEP Values for Case 2.3.X

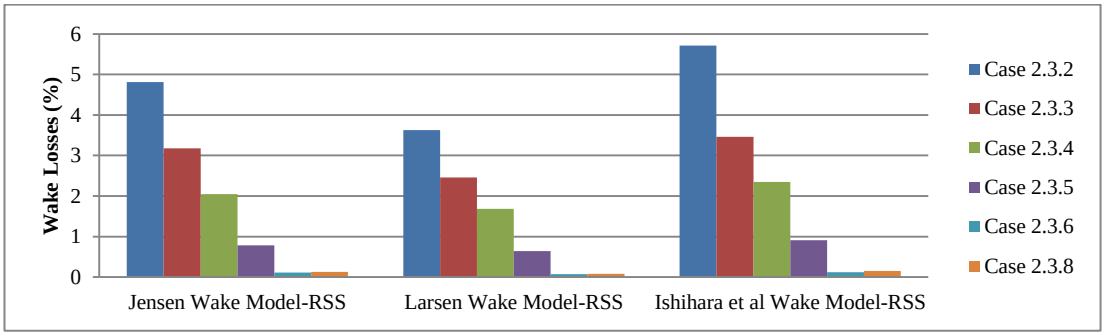

Figure 5.58: Total Wake Losses (%) for Case 2.3.X

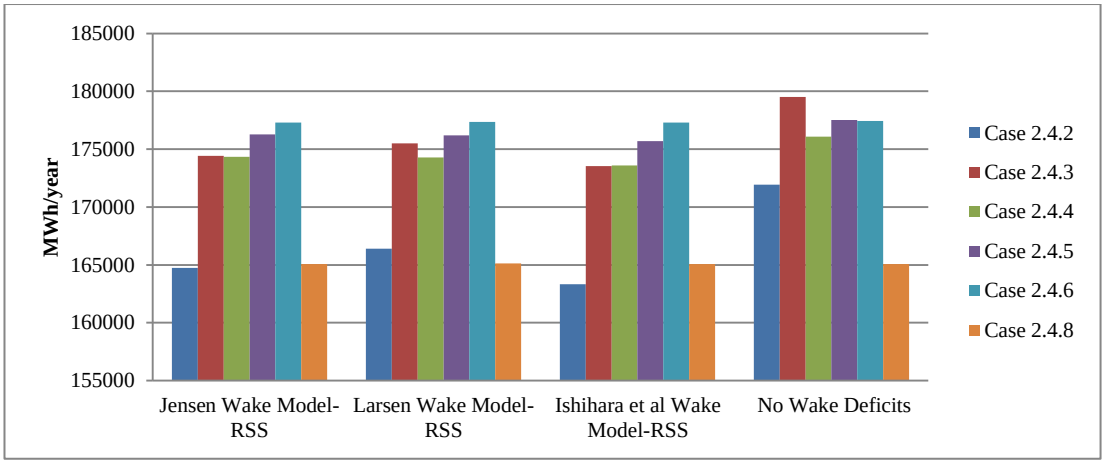

Figure 5.59: Total AEP Values for Case 2.4.X

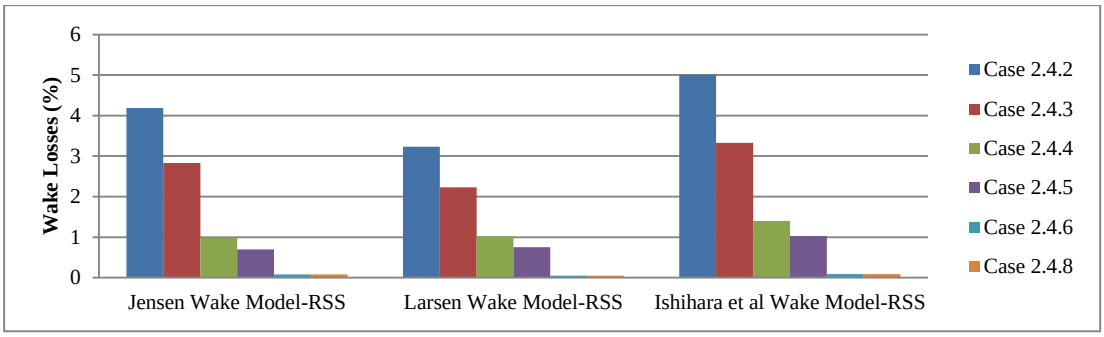

Figure 5.60: Total Wake Losses (%) for Case 2.4.X

Similar inferences can be observed for Case 2. Wake losses are lower than Case 1, because the interaction mechanism between turbines is different in this layout. Terrain slope is also important parameter to consider not only shadowing but also speed up effects in WindSim. Many turbines may have different wake interaction because of this reason.

Moreover, the variations of AEP can be seen clearly due to different Weibull distributions of turbines if no wake condition is considered. The reason is that climatology changes are prominent for complex terrain.

At the end of the survey, Case 2.3.4 has maximum energy production (MWh) and reasonable wake loss (%) among the all layouts due to roughness and orography of the onshore land.

CHAPTER 6

CONCLUSIONS

In this research, the methodologies of Wind Resource Assessment and Wind Farm Modeling are examined by using CFD tool. This investigation ranged from wind data analysis to wind farm layout design and AEP calculations. Moreover, AEROWIND in-house code is developed to calculate many essential parameters which are used to estimate annual energy yield in theoretical manner. Necessary theoretical framework of the developed code is given in Chapter 4. It can be concluded that this code can be coupled with any research tool (such as WindSim) or can be performed single-handed in future work.

First of all, WindSim program which solves RANS equations by using finite volume method used as a CFD tool. This program also facilitates many operations to research WRA and Wind Farm Modeling. It is utilized to investigate the proper locations of wind turbines in prospected areas. Terrain and roughness map are coupled to insert into the program in advance.

Data analysis program is developed to survey the grid dependency study and comparison of turbulence models in WindSim. Coordinates are already available and 2D mean speed values can be obtained at any altitude in Wind Resources module of WindSim program. Thereby, 2D velocity mean profiles are plotted along the South-North and West-East directions by using the data analysis program (Line-based investigations).

Furthermore, domain discretization is constructed by structured mesh. Grid dependency study and aspect ratios of solution model are researched to ensure the solution of the model. Line-based investigation showed that Mesh 3 can be selected as the optimum grid among four mesh types. Additionally, AEP values for arbitrary wind farm are computed to validate this inference. At the end of this study, converged solution is achieved for the monitored parameter which is AEP value.

Moreover, turbulence models have led to quite similar results according to line-based and node-based investigations. However, the resolution is not sufficient to capture the differences according to mesh specifications. Therefore, this type of research is not suitable for prepared grids. The reason is the limitation of available computer hardware. The given method can be utilized to investigate the differences between the turbulence models by performing the simulations with finer mesh.

Consequently, wind resource map is obtained and it can be deduced that Bodrum Peninsula have high wind energy potential for many territories. The locations of Offshore and Onshore Wind Farms are chosen. Onshore site has high wind potential according to transferred climatology option of WindSim. Moreover, NREL 5MW Baseline Wind Turbine is selected as wind turbine type that used in wind farm layouts. Nine wind turbines are pinpointed over both regions considering the distances between each other.

In the following investigation, the Economic Tab of AEROWIND is investigated with sensitivity analyses. These analyses are carried out for NPV, IRR, COE and payback time parameters. The interactions of different parameters are discussed. The effects of capacity factor and wake loss over COE and payback time are also scoped in wide range. Ultimately, aerodynamics of wind turbine and energy analysis with wake modeling are essential engineering tools to succeed higher energy production and less wake interactions in wind farm layouts. The predictions of these parameters should be accurate to construct the economic model of the system. Therefore, the wake interactions are monitored to compare energy yield throughout the year in WindSim program by using three wake models.

In this respect, total wake losses for the layouts are obtained with the energy module of WindSim program. Different wake models are performed and the results are compared. As observed in analyses of Offshore and Onshore Wind Farm, wake losses decrease with the increment of crosswind and downwind spacing. If multiple wind turbines are placed too close to one another, the efficiency of the turbines will be reduced. Each wind turbine extracts some energy from the wind, so that winds will be slower and more turbulent for downwind turbine. Therefore, wake models are essential to be taken into account in this type of studies.

Furthermore, AEP values can be variable due to climatology changes in Onshore Wind Farm. The optimal layout for site can be determined considering high AEP, minimum wake interactions and minimum land cover with this type of study. At the end of the simulations, the optimal layouts for Offshore and Onshore Wind Farm can be determined as shown for Case 1.2.8 and 2.3.4 respectively.

In this progress, AEROWIND in-house code is envisioned in order to cover many areas while operating the WindSim program. It consists of site information, aerodynamics, energy and economy analyses. It is compiled in MATLAB program. In Site Information Tab, theory based on maximum likelihood method is utilized to handle wind data. Weibull distribution and wind rose of the data is acquired by the algorithm. In Aerodynamics Tab, BEMT algorithm is coupled with Airfoil Lift and Drag Polar Generator Program in order to compute aerodynamic performance of the selected wind turbine. This program is utilized to obtain power and thrust coefficient curves of wind turbine. The program also computes many important parameters of the rotor theoretically. NREL Phase II-III and NREL 5 MW Baseline Wind Turbines are examined to validate the algorithm. The results are satisfactory with the experimental data. Some important inferences are stated below about BEMT algorithm and Airfoil Lift and Drag Polar Generator Program:

- XFOIL program overestimates lift coefficients and underestimates drag coefficients at particular range of angle of attacks. These values ranged from -10 to stall angle of the airfoil in general.
- In order to increase the accuracy of XFOIL predictions, some correction methods are available for aerodynamic coefficients in the literature. This approach will be implemented into this algorithm in future work.
- XFOIL cannot converge at post stall region of the airfoil.
- Viterna and Corrigan method employs well to cover corresponding lift and drag coefficients at post stall region of the airfoil.
- Any interpolation method for reading the airfoil data is highly recommended in order to reduce the errors in predictions. For example, cubic interpolation method is suitable for this approach.
- Prediction with XFOIL is poor at high wind speeds, whereas prediction with experimental airfoil data agrees well with all ranges.
- Wind tunnel tests can be carried out to obtain experimental data of airfoil. CFD method can be also utilized to obtain aerodynamic performance of airfoil.
- Local angle of attack values have significant effect on wind turbine energy calculations due to the connection with airfoil performance data.
- New airfoil profiles can be designed by using inverse airfoil design techniques.
- In future work, optimization tool will be added to design a specified wind turbine for concentrated wind site.

In Energy Analysis Tab of AEROWIND code, Jensen wake model is studied to compute wake losses for any layout of wind farm. Horns Rev Wind Farm ([65], [68]) is utilized to validate the algorithm. At particular wind speed and direction, wind turbine power deficits are calculated and compared with experimental and WindSim data. WindSim and AEROWIND have similar results for Jensen wake model-RSS at the end of the analysis. Additionally, error of Jensen wake model-LS increases with the increment of columns. There should be more validation cases, but it can be deduced that AEROWIND code employs well for this case. In addition to all findings, the deviations of the wake models can be observed clearly in reference to power production of wind turbines. In overall, the results of this study showed that the predictions of wake deficits are too much for both WindSim program and AEROWIND code. One reason can be related to the sequence of computing the power deficits. The velocity deficits are calculated in advance to proceed the power equation.

Wake-wake interaction is only considered phenomena for the AEROWIND code, because it is theoretical tool. Thus, terrain-wake interaction is not covered. Terrain slope can be small or zero in order to compute wake-wake interactions in this program. Noting that, wind turbine types, hub heights and roughness lengths can be inserted to program. These features can be examined in future work. Therefore, it is not useful for complex areas now. However, this program can be coupled with CFD tool (such as WindSim, OpenFoam, Fluent and etc.) to improve the investigation of the wake modeling in future work. Thus, necessary information can be transferred from CFD tool.

This thesis has showed that the written algorithm helps to design a Wind Farm layout (Offshore or Onshore) which will be more efficient in both technical and economic aspects. Site Information Tab prepares the necessary wind speed distribution for site. BEMT examines the wind turbine type in order to select the suitable one according to the results of Site Information Tab. Energy and Economic Analysis Tabs can be performed to obtain the best solution simultaneously. Therefore, not only technical but also economical parameters are examined to construct objective function of optimization tool.

In future work, optimization tool will be arranged with the genetic algorithm. This procedure can reduce the design time of Wind Farm layout. Suitable specifications can be also optimized for wind turbines according to any topographical land and wind distribution.

In addition to mentioned future work, others can improve this study and can be listed as:

- Wind resource analysis can be improved by adding Rayleigh distribution to Site Information tab.
- Unsteady BEMT theory can be utilized to estimate more accurate AEP values for current Wind Farms with the aid of wind data in real time.
- Other disciplines can be added to BEMT program such as aero elasticity, control and electrical topics.
- Different wake models can be researched in literature. Therefore, new wake models can be implemented into AEROWIND code.
- New wake models can be developed with conducting experiments by using sophisticated wind tunnel and high quality equipment.
- Cost of wind farm can be investigated in detail.

REFERENCES

[1] Manwell, A., *Wind Energy Explained - Theory, Design and Application*, Second Edition, September 2002.

[2] Hansen, M., McGowan, J.G., Rogers, A.L., *Aerodynamics of Wind Turbines*, Second Edition, 2008.

[3] Hau, E., *Wind Turbines - Fundamentals, Technologies, Application, Economics*, 2006

[4] Spera, D., *Wind Turbine Technology-Fundamental Concepts in Wind Turbine Engineering*, Second Edition, 2009

[5] Mathew, S., *Wind Energy - Fundamentals, Resource Analysis and Economics*, Netherlands, 2006

[6] Wikipedia, http://en.wikipedia.org/wiki/Wind_power_by_country, as accurate of July 2013

[7] GWEC - Global Wind Energy Council, *Global Wind Report – Annual Market Update*, 2012

[8] TÜREB – Turkish Wind Energy Association, *Turkish Wind Energy Statistics Report*, February 2012

[9] Burton, T., Sharpe, D., Jenkins, N., Bossan, E., *Wind Energy Handbook*, John Wiley & Sons, 2001.

[10] AWS Truepower, *Wind Resource Assessment Handbook – Final Report*, New York State Energy Research and Development Authority, New York, April 2010.

[11] Spera, D. A., *Wind Turbine Technology: Fundamental Concepts of Wind Turbine Engineering*, ASME Press, New York, 1994.

[12] Leblebici, E., *Terrain Modeling and Atmospheric Turbulent Flow Solutions Based On Meteorological Weather Forecast Data*, MSc Thesis, Middle East Technical University, Ankara, January 2012

[13] Manwell, J.F., *An Offshore Wind Resource Assessment Study for New England*, Renewable Energy 27 ,175–187, 2002

[14] Fallo, D., *Wind Energy Resource Evaluation in a Site of Central Italy by CFD Simulations*, Master of Science Thesis, Universita degli Studi di Cagliari, Italy, 2008

[15] Wallbank, T., *WindSim Validation Study, CFD Validation in complex terrain*, 2008

[16] Taylor, P.A. and Teunissen, H.W., *The Askervein Hill Project: Overview and Background data, Boundary-Layer Meteorology*, 39, 15-39, 2010

[17] Berg, J., Mann, J., Bechmann, A., Courtney, M.S., Jørgensen, H.E, *The Bolund experiment, Part I:Flow over a steep, three-dimensional hill*. Boundary-Layer Meteorol., 141(2):219–243, 2011. doi: 10.1007/s10546-011-9636-y.

[18] Bechmann, A., Sørensen, N.N., Berg, J., Mann, J., and et al., *The Bolund experiment, Part II: Blind comparison of microscale flow models*. Boundary-Layer Meteorol., 141(2):245–271, 2011. doi: 10.1007/s10546-011-9637.

[19] Weir, D. E., Gravdahl, A.R., *WindSim: Micrositing with Numerical Simulations: a Simple Approach*, NZ Wind Energy Conference and Exhibition, Wellington, 2011.
[20] Murakami, S., *Current Status and Future Trends in Computational Wind Engineering*, Journal of Wind Engineering and Industrial Aerodynamics, 67-68, p. 3-34J, 1997.
[21] Kim, S.E., Boysan, F., *Application of CFD to environmental flows, Journal of Wind Engineering and Industrial Aerodynamics*, 81, p. 145-158, 1999.
[22] Ehrhard, I.A., Khatib, C., Winkler, R. Kunz, N., Moussiopoulos, G.E., *The microscale model MIMO: development and assessmen*t, Journal of Wind Engineering and Industrial Aerodynamics, 85, p. 163-176, 2000.
[23] Castino, F., Rusca, L., Solari, G., *Wind climate micro-zoning: A pilot application to Liguria Region (North-Western Italy)*, Journal of Wind Engineering and Industrial Aerodynamics 91, 1353–1375, 2003.
[24] Lange, B., Larsen, S., Højstrup, J., Barthelmie, R., *Importance of thermal effects and sea surface roughness for offshore wind resource assessment*, Journal of Wind Engineering and Industrial Aerodynamics, Volume 92, Issue 11, pp959-988, 2004.
[25] Tapia, X.P., *Modelling of Wind Flow Over Complex Terrain Using OpenFoam*, Master of Science Thesis, Department of Technology and Built Environment, University of Gavle, June 2009.
[26] Özdede, S., Kurtuluş, D.F., Kurtuluş, B., *Bodrum Bölgesinin Rüzgar Kaynakları Araştırılması Neticesinde Rüzgar Türbinlerinin Muhtemel Yerlerinin Belirlenmesi ve Yerleştirilmesi*, UHUK 2012, IV. National Aerospace Conference, Air Force Academy, Istanbul, 2012.
[27] Stathopoulos, T., *Computational wind engineering: Past achievements and future challenges*, Wind Eng. Ind. Aerodyn. 67&68 (1997) 509 532.
[28] Gosman, A.D., *Developments in CFD for Industrial an environmental application in wind engineering*, Journal of Wind Engineering and Industrial Aerodynamics, 81, p. 21-39, 1999.
[29] Ayotte, K.W., *Computational modeling for wind energy assessment,* J. Wind Eng. Ind. Aerodyn., 96, p. 1571–1590, 2008.
[30] Leroy, J., *Wind field simulations at Askervein hill*, Technical Report, Vector AS, 1999.
[31] Gravdahl, A.R., *The Sensitivity on Numerical Field Modeling,*WindSim AS, Wind Power Exhibition, Los Angeles, 2007.
[32] Gravdahl, A.R., *Power Prediction and Siting – When the terrain gets rough,* WindSim AS, Wind Power Exhibition, Los Angeles, 2007.
[33] Simisiroglou, N., *Wind Resource Assessment Comparison on a Complex Terrain Employing WindPro and WindSim*, Graduate Study, Gotland University, June 2012.
[34] Castellani, F., Franceschini G., *A new technique to improve expected AEP estimation in very complex terrain*, Department of Industrial Engineering, University of Perugia, 43rd AIAA Aerospace Sciences Meeting and Exhibit, Reno, Nevada, January 2005.
[35] Gravdahl, A.R., Crasto, G., Castellani, F., Piccioni, E., *Wake Modeling with the Actuator Disc Concept*, WindSim AS, Deep Sea Offshore Wind Power, Trondheim, 2012.
[36] Katic, I., Højstrup, J., Jensen, N.O., *A Simple Model for Cluster Efficiency*, EWEC Proceedings, Rome, Italy, 7-9 October 1986, Rome.

[37] Larsen, C.G., *A Simple Wake Calculation Procedure*, Risø-M-2760, Risø National Laboratory, Denmark, December 1988.
[38] Ishihara, T., Yamaguchi, A., Fujino, Y., *Development of a New Wake Model Based on a Wind Tunnel Experiment*, The University of Tokyo, Global Wind Power, 2004.
[39] Meissner, C., *Park Optimization Using IEC Constraints for Wind Quality*, WindSim AS, Brussels, Belguim, EWEA 2011.
[40] Versteeg, H. K., Malalasekera, W., *An Introduction to Computational Fluid Dynamics: The Finite Volume Method, 2nd ed.*, Pearson Education Limited, Harlow, Essex, United Kingdom, 2007.
[41] Meissner, C., *WindSim 5 Getting Started*, 5th Edition, WindSim AS, Norway, October 2010.
[42] WindSim 5.10 User Manual, WindSim AS, Norway (2010).
[43] Gravdahl, A.R., *Meso Scale Modeling with a Reynolds Averaged Navier Stokes Solver, Assessment of Wind Resources along the Norwegian Coast*, Vector AS, Norway, October 1998.
[44] Yap, C. J., *Turbulent Heat and Momentum Transfer in Recirculating and Impinging Flows*, PhD Thesis, Faculty of Technology, University of Manchester, United Kingdom, 1987.
[45] Yakhot, V., Orszag, S.A., Thangam, S., Gatski, T.B. & Speziale, C.G., *Development of turbulence models for shear flows by a double expansion technique*, Physics of Fluids A, Vol. 4, No. 7, pp1510-1520, 1992.
[46] Global Mapper 11 User Manual, Blue Marble Geopraphics, USA, 2009.
[47] WAsP 9 User Manual, Risø National Laboratory, Technical University of Denmark, Denmark, 2007.
[48] Silva, J., Ribeiro, C., Guedes, R., *Roughness Length Classification of Corine Land Cover Classes*, MEGAJOULE Consultants, Portugal, 2000.
[49] Grand Symphonie Wind Measurement System User Manual, NRG Systems, USA 2013.
[50] Windographer Help Version 3, Mistaya Engineering, Canada, 2013.
[51] Türkyılmaz, U., *Wind Energy Technologies; Preliminary Design Code Development*, Master of Science Thesis, Istanbul Technical University, Faculty of Aeronautics and Astronautics, Istanbul, 2007.
[52] Buhl M., *A New Empirical Relationship between Thrust Coefficient and Induction Factor for the Turbulent Windmill State*, NREL/TP-500-36834, National Renewable Energy Laboratory, USA, 2005.
[53] Leishman, J. G., *Principles of Helicopter Aerodynamics*, Second edition, Cambridge University Press, 2002.
[54] Gundtoft, S., *Wind Turbines*, Mechanical Engineering, University College of Aarhus, June 2009.
[55] Abbott, I., Doenho, A., *Theory of Wing Sections*, 1959.
[56] Drela, M., XFOIL, http://web.mit.edu/drela/Public/web/xfoil/, as accurate of September 2009.
[57] *Guidelines for Design of Wind Turbines*, Wind Energy Department, RISO, Second Edition, 2002.

[58] Viterna, L. A., Janetzke, D.C., *Theoretical and Experimental Power from Large Horizontal-Axis Wind Turbine*, Technical Report N82-33830, NASA Lewis Research Centre, 1982.

[59] Ceyhan, Ö., *Aerodynamic Design and Optimization of Horizontal Axis Wind Turbines by Using Bemt and Genetic Algotithm*, Aerospace Engineering, Middle East Technical University, 2008.

[60] Schepers, J.G., Brand, A.J., *Final Report of IEA Annex XVIII Enhanced Field Rotor Aerodynamics Database*, ECN-C-02-016, 2002.

[61] Jonkman, J., Butterfield, S., Musial, W., Scott, G., *Definition of a 5-MW Reference Wind Turbine for Offshore System Development*, National Renewable Energy Laboratory Golden, CO, 2009.

[62] Gonzalez, F., Wall, R., Terzija, V., *Wake effect in wind farm performance: Steady-state and dynamic behavior*, Renewable Energy, 2011.

[63] Renkema, D.J., *Validation of Wind Turbine Wake Models*, Master of Science, TU Delft, 2007.

[64] Choi, J., Shan, M., *Advancement of Jensen Wake Model*, Fraunhofer-IWES, EWEA Conference, Wien, 2013.

[65] Crasto, G., Gravdahl, A.R., *Validation of Wake Analytical Models of WindSim in Neutral Conditions in Offshore Wind Farm*, WindSim AS, Euromech Colloquium 508, Madrid, 2009.

[66] Chowdhury, S., Zhang, J., Messac, A., Castillo, L., *Unrestricted Wind Farm Layout Optimization (UWFLO): Investigating Key Factors Influencing the Maximum Power Generation*, Renewable Energy, 38(1):16 – 30, 2012.

[67] L. Fingersh, M. H., *Wind Turbine Design Cost and Scaling Model*, NREL/TP-500-40566, National Renewable Energy Laboratory, USA, 2006.

[68] Barthelmie, R.J., *Flow and Wakes in Large Wind Farms: Final Report for Upwind WP8*, National Laboratory for Sustainable Energy, RISO DTU, Denmark, February 2011.

[69] Wikipedia, http://en.wikipedia.org/wiki/REpower_Systems, as accurate of August 2013.

APPENDIX A

JENSEN WAKE MODEL CALCULATION METHOD

The algorithm has five steps for Jensen wake model calculation which is proposed by Chowdhury et al. [66]. In the current study, small changes can be observed for the alignment of wind direction. Instead of positive x axis, positive y axis is selected as wind direction.

Step 1: Wind Farm layout is arranged in fixed coordinate system. This system is transformed into another coordinate system. Therefore, positive y direction is aligned with the wind direction. This is the transformation formula:

$$\begin{bmatrix} x_i \\ y_i \end{bmatrix} = \begin{bmatrix} \cos\theta & -\sin\theta \\ \sin\theta & \cos\theta \end{bmatrix} \begin{bmatrix} X_i \\ Y_i \end{bmatrix} \tag{A.1}$$

In this equation, θ angle is the angle made by the wind direction with X-axis when measured clockwise. The distances between the turbines in both directions can be calculated as:

$$\Delta x_{ij} = x_i - x_j, \quad \Delta y_{ij} = y_i - y_j \tag{A.2}$$

Step 2: The influence of the wake over a turbine should be identified and matrix M is created to perform this operation.

$$M_{ij} = \begin{cases} +1 & \text{if Turbine-i inflences Turbine-j} \\ -1 & \text{if Turbine-j inflences Turbine-i} \\ 0 & \text{if there is not mutual influence} \end{cases} \tag{A.3}$$

Where Turbine-j is in the influence of the wake created by Turbine-I if and only if:

$$\Delta y_{ij} < 0 \quad \& \quad |\Delta x_{ij}| - \frac{D_j}{2} < \frac{D_{wake,ij}}{2} \tag{A.4}$$

Step 3: Turbines can be ranked in increasing order of their position in the wind farm layout. In this thesis, position of the turbines are monitored from their specified numbers (WT1, WT2, WT3,…., WTN) in MATLAB workspace.

Step 4: Power production of each turbine is computed in sequence considering shadowing effect. This method checks that the influence of the wakes from the turbines properly taken into account. Turbine-j can be partially or completely in the wakes of other turbines. The wake of each turbine (called as Turbine-k) is mapped onto Turbine-j (if $M_{kj} = 1$) as:

- If Turbine-j is influenced completely by Turbine-k:

$$A_{kj} = A_j, \quad A_j = \frac{\pi D_j^2}{4} \tag{A.5}$$

- If Turbine-j is influenced partially by Turbine-k:

$$A_{kj} = r_k^2 \cos^{-1}\left(\frac{d_{kj}^2 + R_k^2 - R_{wake,j}^2}{2 d_{kj} R_k}\right) + R_{wake,j}^2 \cos^{-1}\left(\frac{d_{kj}^2 + R_{wake,k}^2 - R_j^2}{2 d_{kj} R_{wake,j}}\right) - \frac{1}{2}\sqrt{\left(-d_{kj} + R_k + R_{wake,j}\right)\left(d_{kj} + R_k + R_{wake,j}\right)\left(d_{kj} + R_k - R_{wake,j}\right)\left(d_{kj} + R_k + R_{wake,j}\right)} \tag{A.6}$$

A_{kj} is the effective area of the influence of the wake from Turbine-k to Turbine-j. $R_{wake,j}$ is the wake radius and R_k is the radius of wind turbine. d_{kj} is the distance between the center of circles as showed in Figure 4.16. The wake contribution of each upwind Turbine-k toward the net kinetic energy approaching Turbine-j per unit time is calculated by:

$$P_{kj} = \frac{A_{kj}}{A_j} U_{kj}^2 \tag{A.7}$$

The effective deficit is calculated by RSS method.

$$U_j = U_\infty - \sqrt{\sum_k \frac{A_{kj}}{A_j} \left(U_\infty - U_{kj}\right)^2} \tag{A.8}$$

Step 5: The total power of the wind farm is computed by the algebraic sum of the power generated by each wind turbines:

$$P_{farm} = \sum_{j=1}^{N} P_j \tag{A.9}$$

APPENDIX B

NREL 5MW BASELINE WIND TURBINE DATA

Blade geometry of the turbine is given in Table B.1. It is tabulated from Ref. [61].

Table B.1: Blade Geometry of NREL 5MW Baseline Wind Turbine

Node	Local Radius [m]	Twist Angle [deg]	Δr for Blade Elements [m]	Chord Length [m]	Airfoil Data
1	2.8667	13.308	2.7333	3.542	Cylinder1
2	5.6000	13.308	2.7333	3.854	Cylinder1
3	8.3333	13.308	2.7333	4.167	Cylinder2
4	11.7500	13.308	4.1000	4.557	DU40_A17
5	15.8500	11.480	4.1000	4.652	DU35_A17
6	19.9500	10.162	4.1000	4.458	DU35_A17
7	24.0500	9.011	4.1000	4.249	DU30_A17
8	28.1500	7.795	4.1000	4.007	DU25_A17
9	32.2500	6.544	4.1000	3.748	DU25_A17
10	36.3500	5.361	4.1000	3.502	DU21_A17
11	40.4500	4.188	4.1000	3.256	DU21_A17
12	44.4500	3.125	4.1000	3.010	NACA64_A17
13	48.6500	2.319	4.1000	2.764	NACA64_A17
14	52.7500	1.526	4.1000	2.518	NACA64_A17
15	56.1667	0.863	2.7300	2.313	NACA64_A17
16	58.9000	0.370	2.7300	2.086	NACA64_A17
17	61.6333	0.106	2.7300	1.419	NACA64_A17

Airfoil data of the wind turbine are plotted in following figures. Raw data is processed with cubic interpolation method in MATLAB program (Fig. B.1 – Fig. B.6).

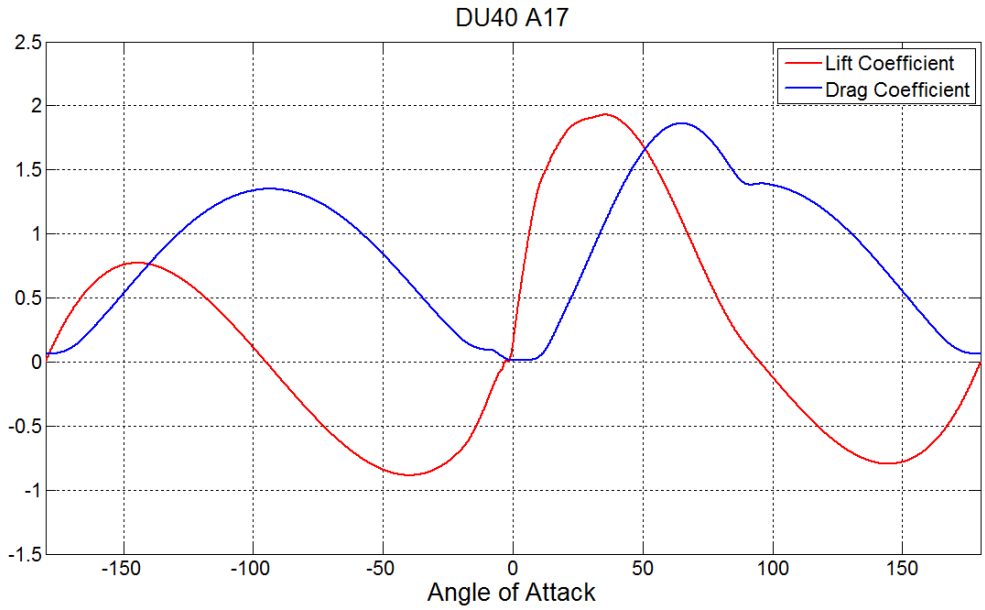

Figure B.1: Airfoil Data of DU40_A17

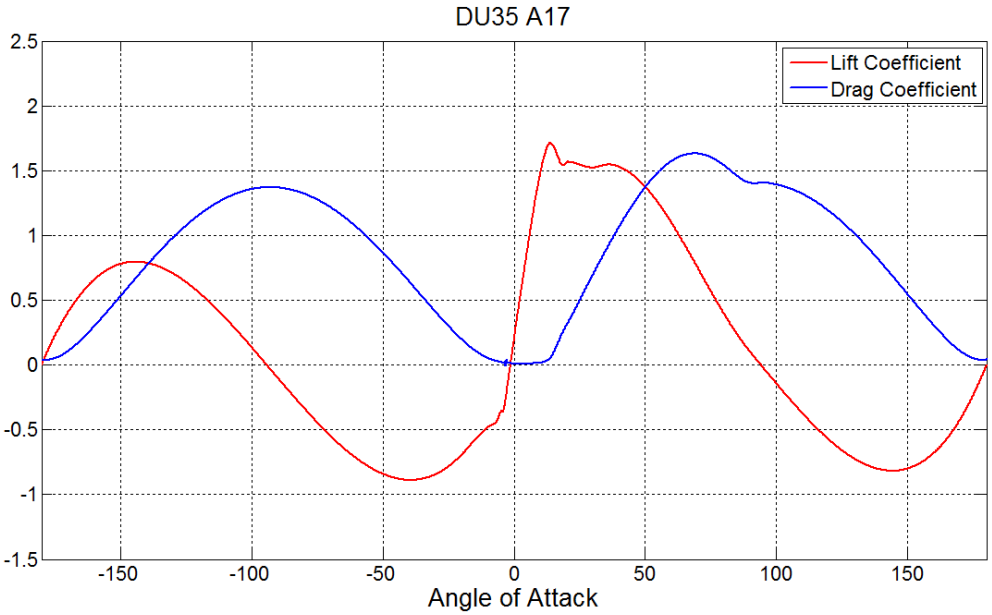

Figure B.2: Airfoil Data of DU35_A17

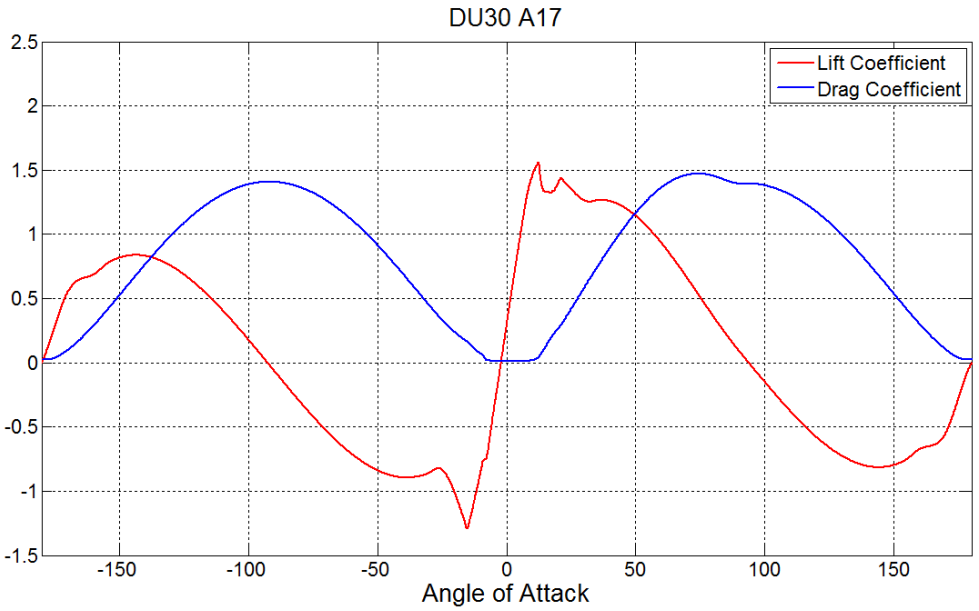

Figure B.3: Airfoil Data of DU30_A17

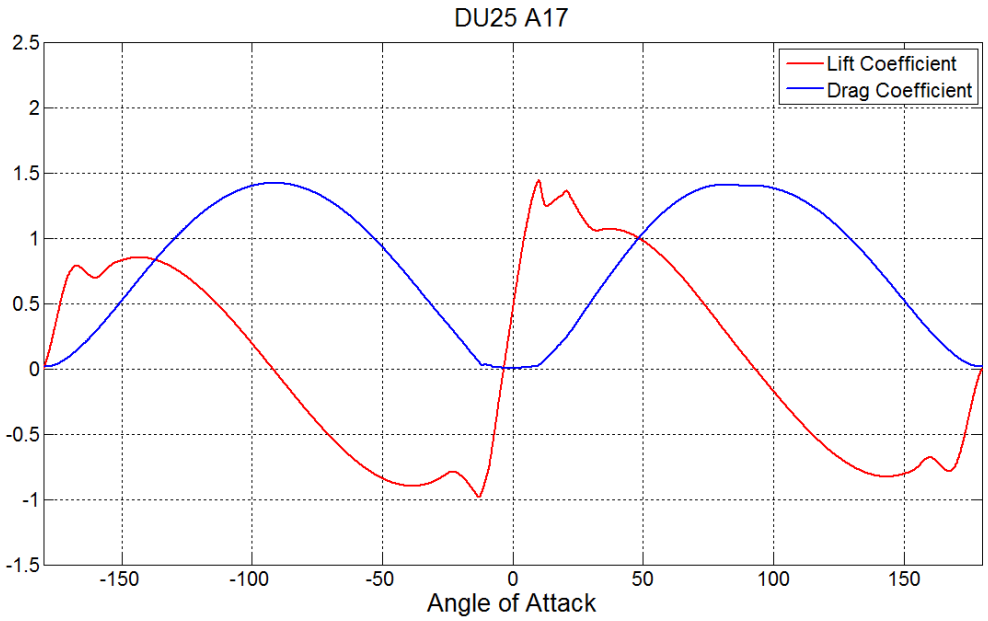

Figure B.4: Airfoil Data of DU25_A17

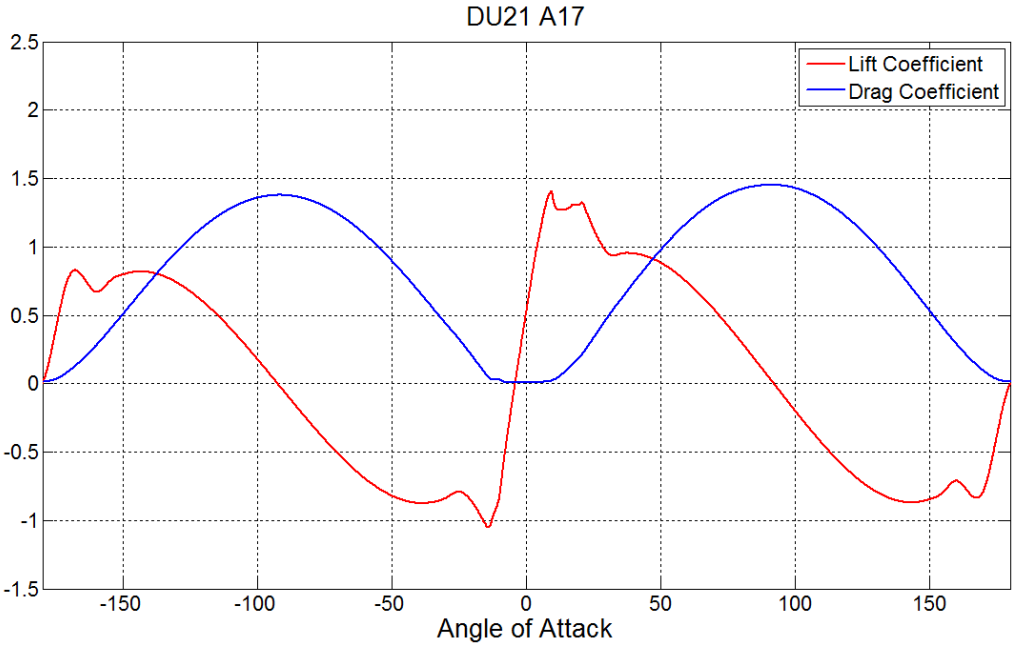

Figure B.5: Airfoil Data of DU21_A17

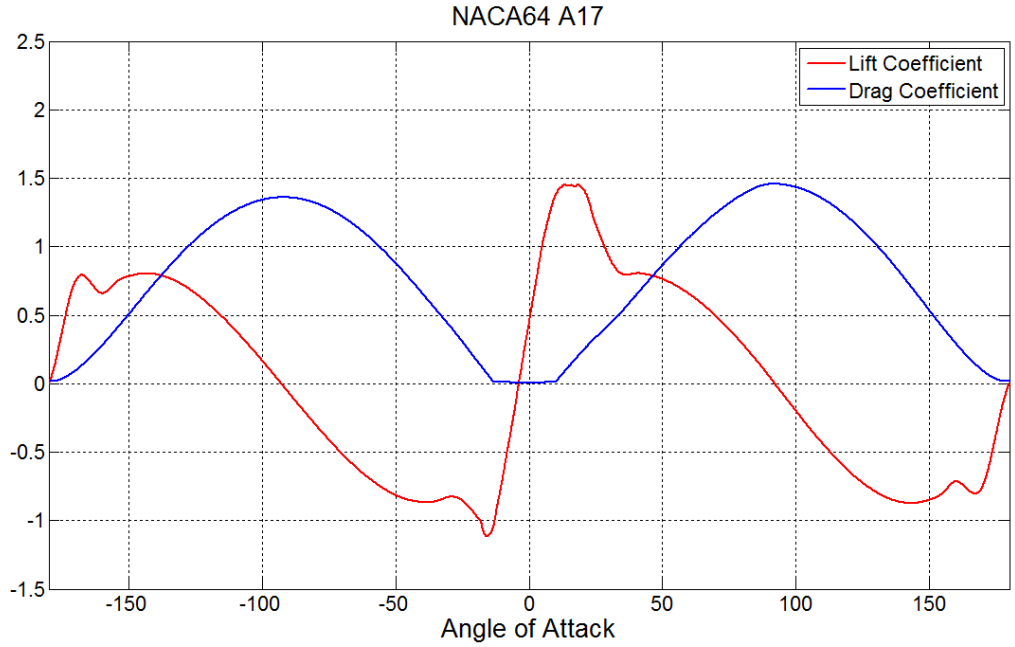

Figure B.6: Airfoil Data of NACA64_A17

Other important parameters of 5MW Baseline Wind Turbine can be observed in Figure B.7.

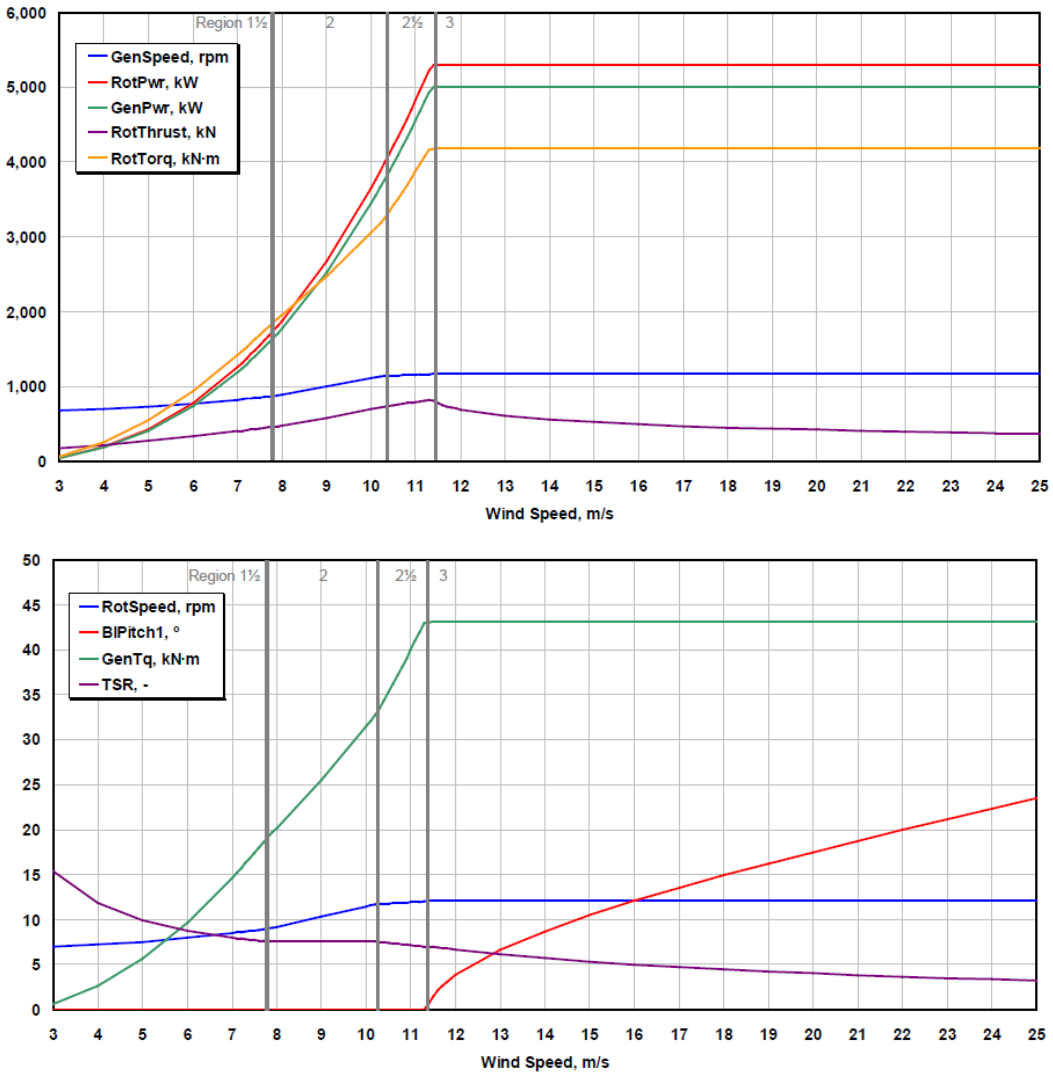

Figure B.7: Steady State Responses as a Function of Wind Speed [61]

Figure B.8: NREL 5MW Baseline Wind Turbine [69]